December 20, 2002 *CBN 02/13*

CONVERSION SYSTEM FOR OBTAINING POLARIZED ELECTRONS AND POSITRONS AT HIGH ENERGY
Translation

A.A. Mikhailichenko

Cornell University, LEPP, Ithaca, NY 14853

PREFACE

By publishing translation of my Dissertation I am carrying out promises I gave during years to many people around the world. As the interest for polarized positron production is growing at SLAC now, I decide to make quick translation.

This is a translation, not a new publication so I have neither right to upgrade neither any subject to the latest developments [which are reflected in, say, CLNS 01/1758, represented at Snowmass 2001], nor a phrase even. Results represented in this Dissertation still interesting and valid for these times however. Moreover, they become even more valuable due to impending decision about Next Linear Collider.

The conversion system was proposed in mid 1979, when W's and Z were not discovered yet [CERN, 1983]. The concept of spin, remaining a mystery, introduced by two clairvoyants - G.E.Uhlenbeck and S.A.Goudsmit [Naturwissenschaften, 13, (1925), p.953] was interesting to me at all times, however.

During 1979-1986 I was busy with other important components of Linear Collider –RF generator and Damping ring.

The Figures was just scanned from the last exemplar I have. Numeration of pages and content of every page kept the same as in original.

ACADEMY OF SCIENCE USSR
SIBERIAN DIVISION

Institute of Nuclear Physics

Manuscript
UDK 539.122.13

MIKHAILICHENKO ALEXANDER ALEXEEVICH

CONVERSION SYSTEM FOR OBTAINING POLARIZED ELECTRONS AND POSITRONS AT HIGH ENERGY

(01.04.20- Physics of charged particles and Accelerator Technique)

Dissertation on Scientific Degree c.p.-m.s. -
" Candidate of Physical-Mathematician Sciences"

Scientific advisors-

Senior Scientific Associate, c.p.-m.s.
Balakin Vladimir Egorovich

Senior Scientific Associate, c.p.-m.s.
Sil'vestrov Grigory Ivanovich

NOVOSIBIRSK
1986

CONTENTS

INTRODUCTION

Investigation of properties of Matter under large transferring momentum with colliding beams became traditional in arsenal of contemporary physical methods. Experiments with *polarized* particles carried out in storage rings have its important place there. The phenomena of self-polarization in the damping ring, caused by synchrotron radiation predicted in [19], is broadly in use in storage rings installations worldwide including the Institute of Nuclear Physics Siberian Division Academy of Science USSR.

Here we would like to mention experimental confirmation of existence of self–polarization in the VEPP-2M storage ring and method of resonance depolarization, which makes possible absolute calibration of energy while investigating the resonance [15].

At the storage ring complex VEPP-4 with the help of this method, precise measurements of masses of narrow resonances in e^+, e^- reactions were done [37].

Significant experience with obtaining, handling and operation with polarization was build up while working with polarized beams [56].

In addition to this service role, polarization was in use during measurements of azimuthal anisotropy of muons in the process $e^+e^- \to \mu^+\mu^-$ also, where conservation of polarization in interaction of colliding electron-positron beams was proved [11].

Polarization acquires unique role at high energy of colliding beams.

Impressive results of the last years, namely discovery of predicted $W^{\pm}$ and Z^0 bosons, inspired a hope to get more interesting results with organizing high–energy collisions with polarized particles.

The structure of weak interaction –parity non-conserving –one of the central problem planned for study with colliding e^+, e^- beams having energy around multi–hundred *GeV*.

Around this level of energy, the cross section of electromagnetic and weak interaction becomes comparable and with polarized colliding particles it is possible to separate effects from the weak-non conserving parity- and electromagnetic interactions.

At present times the following e^+, e^- high-energy colliders are under construction:

SLC	2×50 *GeV*	SLAC (Stanford)
LEP(2)	$2\times 55(130)$ *GeV*	CERN
VLEPP	$2\times$ 200 *GeV*	INP (Project)

With these installations more accurate testing of predictions made with Standard model will be carried together with investigation of new phenomena described by Standard model in part only. New accelerator technique will be under investigation too [1].

The scale of LEP can be characterized by its perimeter ~27 *km*. 15 MW from all acquired power (at 55 *GeV*, first stage) is going for compensation the losses caused by SR [2].

SLC is an intermediate system, where the linear accelerator SLAC with forced RF supply of accelerating structures used for acceleration, and further on the large radius bending magnets used for arrangements of collisions at IP [3].

Obtaining polarized particles at high energy is a peculiar problem itself [1].

At the same time the beams with polarization allow to get much more detailed information about neutral Z^0 bosons and theirs interaction with Fermions, establish the values of vector and axial constants in the Weinberg-Salam model, allowing easier search of the right charged currents.

More important role polarization takes in distinguishing between the models with few Z^0 bosons, where the number of independent constants are bigger, that in Standard model [4].

The difficulties with obtaining polarized particles at high energy are the following.

For *polarization by natural process* with synchrotron radiation– it is a long polarization time $\sim H^{-3}\gamma^{-2}$. Small values of magnetic field in bending magnets H defined by acceptable value of losses by Synchrotron radiation. For example the time of natural polarization in LEP

$$t_p^{-1} = \frac{5\sqrt{3}}{8\hbar^2 c^8}\left(\frac{e}{m}\right)^5 H^3\gamma^2$$

goes for E=50 GeV (first stage) ~5 hours. The last forces usage additional snakes with magnetic field, which yield even higher losses by SR. In addition the energy scale of this storage ring is overlapped by spin–depolarizing resonances, where it is impossible to have any polarization at all [42].

Acceleration of polarized particles, obtained at low energy, in cyclic accelerators requires passage over numerous spin resonances

with wide variety of theirs power and frequencies of precession. The last adds difficulties in wide interval of energy tune.

In addition, intensive souses of polarized positrons are not existing.

At SLC the only electron bunch will be polarized with the help of photocathod, irradiated by polarized light. Further on the bunch will be accelerated in a linac. Average degree of polarization is planned to be 40% in the first stage [5]. In addition, the photocathod with limiting lifetime requires special care [55].
The only one polarized bunch reduces luminosity in half however.

Summing up, the task of positron generation in amounts required for experiments looks extremely difficult.

Positrons can be obtained usually during conversion of initial electrons inside a target having high atomic number. High energy primary beam generates the shower, which is a mixture of γ's , $e^{\pm}$'s. It is been known that maximal number of the particles occurs to be at the depth which is $\tau_{\max} \cong \frac{\ln(\varepsilon_0 / \varepsilon_{cr})}{\ln 2}$ in terms of radiational length, where $\varepsilon_{cr} \cong \frac{600}{Z}[MeV]$–is so called critical energy, ε_0 is initial energy of electron. This number occurs to be $\cong \exp(\tau_{\max} \ln 2) \cong \frac{\varepsilon_0}{\varepsilon_{cr}}$ per each initial particle [6]. Extrapolated conversion coefficient (ratio N_+ / N_0) at the energy ~50 *GeV* becomes of the order of unity, and optimal thickness of the target grows, as one can see, logarithmically while the energy is growing. Average power of energy deposition in the target goes to a few kilowatt levels.

Accelerating complex VLEPP (Colliding Linear Electron-Positron Beams) has no problems with energy losses by synchrotron radiation

[7]. As the bunches used here only once, there is a vital necessity to regenerate both electron and positron bunches every time before next run of acceleration, however.

In principle, it is possible to reach this with usual conversion scheme. Polarization of particles is not conserved here however.
To have self-polarization in a separate damping ring is not possible here as the time of polarization is too long at low energy. All this yields a low repetition rate in general.

So for successful operation of the VLEPP, it is necessary to regenerate the beams of $e^{\pm}$ every pulse while repetition rate goes to 10 *Hz* and higher. So that it is why it was necessary to develop the new type of source of polarized e^{-} and, especially, e^{+}.

As it seems now that the next energy scale can be explored only with linear colliders [27], the problems, appeared during design of the VLEPP conversion system, look to be common for all other projects of this type in a future.

In *Dissertation* the conversion system allowing obtaining both polarized positrons and electrons with efficiency (defined as a ratio of the positron number to the initial number of the particles) not less than one is proposed [8, 26, 32, 53, and 54].

The problem solved by usage of undulator radiation directed to the thin, $\sim 0.5X_0$, target made from material with high *Z*. With the primary beam energy being around hundred *GeV*, radiation generated in undulator goes to the 20-30 *MeV* level for undulator having period 0.5-1cm. This radiation concentrated in narrow, ~10%, energy interval around maximum [9, 52].

While using helical undulator, radiation (γ –quantas) is a circularly polarized, so it becomes possible to generate polarized positrons and electrons, as the polarization of γ –quanta is transferring to the secondary particles *if they are collected at the high edge of energy spectrum* [10].

The losses in efficiency, associated with non-full collection of the particles can be compensated by large amount of quantas generated in undulator.

Also, if there is no necessity for operation with polarized particles, the conversion coefficient can be made few times bigger.

The beams of e^- or e^+ after interaction are used as primary ones. They loss only 2% of theirs initial energy after passage the undulator. Degree of circular polarization can reach 70% with this method.

Then, after acceleration, the secondary particles injected in a damping ring, where they are cooled by synchrotron radiation. So, as the energy of the ring is fixed, it is easy to organize conservation of polarization.

After cooling and ejection from the damping ring, the bunch is shortened by linear modulation of energy correlated with longitudinal coordinate and transferring bunch through the optical system, in which the pass length depends on energy [25]. After that the necessary polarization is prepared and the bunch goes to the VLEPP linear accelerator.

In *First Chapter* the peculiarities of interaction of gamma-quantas with matter while polarization is transferring are considered. The number of the secondary particles with given polarization and energy is calculated here also.

In *Second Chapter* the properties of undulator radiation are considered under the scope of obtaining the highest amount of particles with polarization higher, than 60%. Here the requirements to the parameters of undulators are formulated too, together with

calculation of amount of radiation, brought to the elements of surrounding walls.

In *Third Chapter,* the problems associated with collection of particles after the target, preliminary acceleration and possible design of targets are considered. The general scheme of VLEPP conversion scheme is described there.

In *Fourth Chapter,* the problems associated with practical design of undulators with parameters required are considered together with results of testing the samples, manufactured for these purposes. The first undulator considered is the pulsed one with intense water-cooling system.

Considered separately, is a design of undulator with superconducting coils. Definitive conclusion done, that this type of undulator can be successfully used if the primary beam energy ≥ 200 *GeV*. Results of tests performed with manufactured sample are represented here.

Results of the job done are summarized in *Conclusion.*

CHAPTER 1. INTERACTION OF GAMMA-QUANTAS WITH MATTER

§1 Polarized states of the photon and electron[1]

For description of polarized states the polarized density matrix is broadly in use [12]

$$\hat{I} = \left|\overline{\vec{E}^2}\right| \cdot \hat{\rho}\,; \qquad \hat{\rho} = \tfrac{1}{2}\left(\hat{1} + \vec{\xi}\cdot\vec{\sigma}\right),$$

where $\sigma_1 = \begin{pmatrix} 0 & 1 \\ 1 & 0 \end{pmatrix}$, $\sigma_2 = \begin{pmatrix} 0 & -i \\ i & 0 \end{pmatrix}$, $\sigma_3 = \begin{pmatrix} 1 & 0 \\ 0 & 1 \end{pmatrix}$–Pauli matrices, $\vec{\sigma} = \{\sigma_1, \sigma_2, \sigma_3\}$,

$\hat{1} = \begin{pmatrix} 1 & 0 \\ 0 & 1 \end{pmatrix}$, $\vec{\xi} = \{\xi_1, \xi_2, \xi_3\}$, ξ_1, ξ_2, ξ_3 – Stokes parameters.

In general case, as the radiation is not a monochromatic one, $\left|\overline{\vec{E}}\right|$ means square of electric field in the wave averaged over frequency. The matrix of density in case of partial polarization can be represented as a linear combination of two matrices, representing non polarized state and fully polarized one [13]. Namely suggesting

$$\xi_i = P\eta_i$$

where $\left|\vec{\eta}\right|^2 = \eta_1^2 + \eta_2^2 + \eta_3^2 = 1$, $\left|\vec{\xi}\right|^2 = P^2$, expression for the matrix of polarization can be represented as the following

$$\hat{\rho} = \tfrac{1}{2}\cdot(1-P) + \tfrac{1}{2}\cdot(1 + \vec{\sigma}\cdot\vec{\eta})$$

[1] c=1 in this chapter.

Value P called degree of polarization of the photon beam.

Direction of polarization defined by Stokes parameters. We will consider circularly polarized states; for these states $\xi_1 = \xi_2 = 0$, $E_{02} = \pm iE_{01}$ and matrix of density has the form

$$\hat{\rho} = \frac{1}{2}\begin{pmatrix} 1 & \pm\xi_2 \\ \mp\xi_2 & 1 \end{pmatrix} = \frac{\hat{1} \mp \xi_2 \cdot \vec{\sigma}_2}{2}.$$

Sign "+" defined positive helicity and corresponds to the clockwise rotation of electric field polarization (if one looks towards direction of propagation).

Probability to have right or left polarization in the beam equates

$$W^+ = \frac{1+P}{2}, \quad W^- = \frac{1-P}{2}$$
$$W^+ + W^- = 1, \quad W^+ - W^- = P$$

In general case $P = \frac{N_\gamma^+ - N_\gamma^-}{N_\gamma^+ + N_\gamma^-}$, where N_γ^+ and N_γ^- are the numbers of the photons in the beam with right and left polarization respectively, and the Stokes parameter $\xi_2 = P$.

With other words, for example, for P=0.7, 70% of the photons have 100% polarization and the rest 30% divided in half between right and left polarization, i.e. there are 85% of right polarized and 15% of left polarized photons in the beam.

In contrast to the photon, polarized properties of electron defined in its rest system. The matrix of density becomes

$$\hat{\rho} = \tfrac{1}{2}\left(\hat{1} + \vec{\varsigma} \cdot \vec{\sigma}\right), \qquad Sp\hat{\rho} = 1$$

Vector $\vec{\varsigma}$ defines average value of electron spin as

$$\frac{1}{2}\langle\vec{\sigma}\rangle = \frac{1}{2}Sp(\hat{\rho}\hat{\vec{\sigma}}) = \frac{1}{2}\vec{\varsigma},$$

i.e. $|\vec{\varsigma}| \le 1$, and $\vec{\varsigma} = 0$ corresponds pure state.

For electron or positron with momentum *p* matrix of polarization is the following [12]

$$\hat{\rho}^{\pm}(p) = \frac{1}{2}(\hat{\not{p}} \pm m)(1 - \gamma^5 \cdot \hat{\not{a}})$$
$$\hat{\not{p}} = \gamma^{\mu} p_{\mu}, \quad a^{\mu} = (a^0, \vec{a}), \quad \gamma^5 = -i\gamma^0\gamma^1\gamma^2\gamma^3,$$

where "+" belongs to electrons, "– " belongs to positrons, and γ^{μ} – are the gamma matrices:

$$\gamma_0 = \begin{pmatrix} \hat{0} & \hat{1} \\ \hat{1} & \hat{0} \end{pmatrix}, \ \hat{\vec{\gamma}} = \begin{pmatrix} 0 & -\hat{\vec{\sigma}} \\ \hat{\vec{\sigma}} & 0 \end{pmatrix}.$$

In ultrarelativistic limit $|\vec{p}| \cong \varepsilon$

$$\hat{\rho} = \frac{1}{2}\hat{\not{p}} \cdot \left[1 + \gamma^5 \cdot \left(\pm|\vec{\varsigma}_{\parallel}| + \vec{\varsigma}_{\perp}\vec{\gamma}_{\perp}\right)\right]$$
$$\vec{\varsigma} = \vec{n}|\vec{\varsigma}_{\parallel}| + \vec{\varsigma}_{\perp}, \text{ and } \vec{n} = \frac{\vec{v}}{|\vec{v}|}.$$

For the state with certain helicity $|\vec{\varsigma}_{\parallel}| = 2\lambda = \pm 1$

$$\hat{\rho} = \frac{1}{2}\hat{\not{p}} \cdot [1 + 2\lambda\gamma^5].$$

4–vector of polarization a^{μ} defined as the following

$$a^{\mu} = \pm\frac{1}{2m}Sp\gamma^5\gamma^{\mu}\hat{\rho}^{\pm}(p),$$

or using the values in the rest frame

$$\vec{a} = \vec{\varsigma} + \frac{\vec{p}\cdot(\vec{\varsigma}\cdot\vec{p})}{m\cdot(\varepsilon + m)}, \qquad a^0 = \frac{\vec{p}\vec{\varsigma}}{m}, \quad |\vec{a}|^2 = |\vec{\varsigma}|^2 + \frac{(\vec{p}\cdot\vec{\varsigma})^2}{m^2}.$$

So one can see, that polarized states of the photon and electron (positron) defined in full by the values $\vec{\varsigma}$ and $\vec{\xi}$.

In external fields $\vec{H}$ and $\vec{E}$, $\vec{\varsigma}$ is precessing following the law [12]

$$\frac{d\vec{\varsigma}}{dt} = \frac{2\mu m + 2\mu'(\varepsilon - m)}{\varepsilon}\left[\vec{\varsigma}\times\vec{H}\right] + \frac{2\mu'\varepsilon}{\varepsilon + m}\left(\vec{v}\cdot\vec{H}\right)\left[\vec{v}\times\vec{\varsigma}\right] + \frac{2m\mu + 2\mu'\varepsilon}{\varepsilon + m}\left[\vec{\varsigma}\times\left[\vec{E}\times\vec{v}\right]\right]$$

For projection of the vector of polarization to the direction of motion one can obtain

$$\frac{d\vec{\varsigma}_{\parallel}}{dt} = 2\mu'\cdot\left(\vec{\varsigma}_{\perp}\cdot\left[\vec{H}\times\vec{n}\right]\right) + \frac{2}{|\vec{v}|}\left(\frac{\mu m^2}{\varepsilon^2} - \mu'\right)\left(\vec{\varsigma}_{\perp}\vec{E}\right),$$

where $\mu' = -\frac{e}{2m} + \mu$ is anomalous part of magnetic momentum.

In a transverse magnetic field the vector of polarization is rotating with respect to $\vec{v}$ with angular speed Ω as

$$\Omega = \nu_0\omega,$$

where $\nu_0 = \gamma\mu'/\mu$ and $\omega = v/R$, $1/R$ is the curvature of trajectory .
For electron (positron) the anomalous part of momentum is

$$\mu' = \frac{e}{2m}\cdot\left(\frac{\alpha}{2\pi} - 0.328\frac{\alpha^2}{\pi^2} - \right) = \mu - \mu_0 \equiv \frac{g-2}{2}, \quad g \cong 2.0023.$$

$\alpha = e^2/\hbar c = 1/137$ is the fine structure constant.

Existence of significant anomalous part in magnetic momentum yields a necessity to take it into account while building spin rotators as a part of preparation procedure for colliding beams (see Chapter 3 below).

So, for example, the energy of the storage ring was chosen 1.1 *GeV*, as during 180 degree bend the spin becomes directed on 90 degrees with respect to the direction of momentum, $\nu_0 = 2.5$.

§2. Interaction of γ- radiation with the matter in case of polarization.

Gamma-quantas, interacting with the media of target, initiate there a shower, developing as a result of beamstrahhlung and the pair creation. The maximal number of particles developing at the depth $\tau_{\max} \cong \ln(\varepsilon_0 / \varepsilon_{cr}) \cdot \frac{1}{\ln 2}$, measured in terms of radiational length. Here $\varepsilon_{cr} \cong 600 / Z\,[MeV]$ is so called critical energy. This number becomes $\varepsilon_0 / \varepsilon_{cr}$ per each initial particle [6]. The total number of the particles having energy $> \varepsilon$ becomes

$$N(>\varepsilon) = \int_0^{\tau(\varepsilon)} N d\tau = \int_0^{\tau(\varepsilon)} e^{\tau(\varepsilon)\ln 2} d\tau \cong \frac{e^{\tau(\varepsilon)\ln 2}}{\ln 2} = \frac{\varepsilon_0 / \varepsilon}{\ln 2}.$$

For the case of our interest, when the energy of gamma-quanta is of the order 15-30 *MeV*, the Compton effect is not giving significant input into the interaction process. Really the cross section of Compton effect for $\omega >> m$ goes [13]

$$\sigma_C = \pi r_e^2 \frac{m}{\omega}\left(\ln\left(\frac{2\omega}{m}\right) + \frac{1}{2}\right),$$

where $r_e = e^2 / m \cong 2.818 \cdot 10^{-13} cm$ is the classical electron radius.
Meanwhile the cross section for the pair creation (per nuclei) is

$$\sigma_p = r_e^2 Z^2 \alpha \cdot \left(\frac{28}{9}\ln\frac{183}{Z^{1/3}} - \frac{2}{27}\right) \quad \text{–full screening}$$

$$\sigma_p = r_e^2 Z^2 \alpha \cdot \left(\frac{28}{9}\ln\frac{2\omega}{Z^{1/3}} - \frac{218}{17}\right) \text{–without screening.}$$

So the ratio of these cross sections per g/cm^2 of media becomes

$$\frac{\sigma_C}{\sigma_p} \approx \frac{1}{\gamma Z \alpha} \sim 10\%.$$

Differential over energy cross section of the pair creation has the view

$$\frac{d\sigma(\varepsilon_\gamma, \varepsilon_+)}{d(\varepsilon_+ / \varepsilon_\gamma)} \cong 4\alpha Z^2 r_0^2 \ln(183 / Z^{1/3}) f(\varepsilon_+ / \varepsilon_\gamma) \cong \frac{A}{N_0 X_0} f(\varepsilon_+ / \varepsilon_\gamma),$$

where $f(x) = x^2 + (1-x)^2 + \frac{2}{3}x(1-x) - \frac{x(1-x)}{9\ln(183Z^{-1/3})}$,

$N_0 \cong 6.022 \cdot 10^{23}$ is the Avohadro number, A –is atomic weight of material, ε_γ is the photon energy, ε_+ is the full positron energy, $x = \varepsilon_+ / \varepsilon_\gamma$. X_0 stands for radiation length

$$X_0^{-1} \cong 4r_0^2 \alpha \frac{N_0}{A} Z^2 \ln(\frac{183}{Z^{1/3}})[cm^2 / gramm],$$

Z is atomic number of the media.

The graph of $f(x)$ is represented in Fig.1.

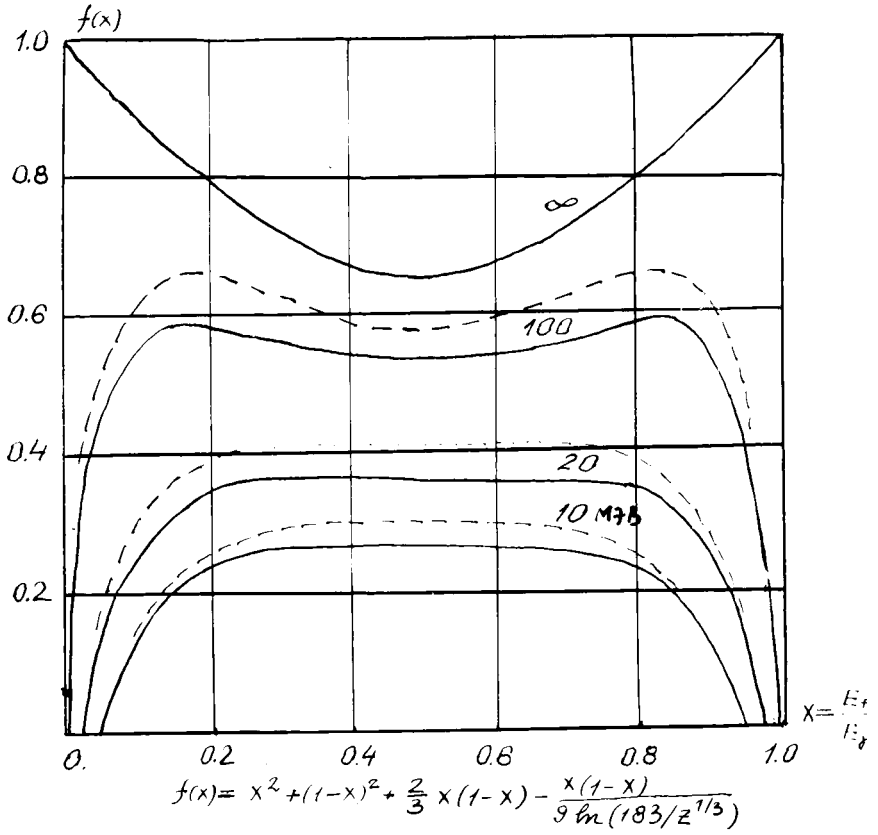

Fig.1 Differential over energy cross section of creation of e^+ and $\rho[g/cm^3]$ e^-. At the horizontal axis is the ratio $x = \varepsilon_+ / \varepsilon_\gamma$. Solid lines stand for Lead, dashed- for Air.

In Table 1 values for radiation length are represented together with corresponding distance X_0/ρ in media ($\rho[g/cm^3]$ is density of media) for some different materials with experimental corrections [48] .

Table 1.

Material	**A**	**Z**	$X_0[g/cm^3]$	**Length, *cm***
Lead	207.2	82	6.4	0.56
Mercury	200.6	80	6.5	0.48
Gold	196.9	79	6.6	0.34
Tungsten	183.8	74	6.8	0.35
Tin	118.7	50	8.5	1.18
Copper	63.55	29	13.0	1.45
Iron	55.84	26	13.8	1.75
Aluminium	26.98	13	24.3	9.0
Carbon	12.01	6	43.3	19.2
Beryllium	9.012	4	66.0	35.8
Lithium	6.939	3	83.3	156.0
Air			37.1	28700
Water			36.4	36.4

The mostly interesting property of interaction of the photon and the media – is a correlation between polarization of initial photon and final spins of secondary electron-positron pairs and Compton electrons however.

Dependence of the spin value on initial polarization of the photon for different positron energy has the form [10]

$$\vec{\varsigma} = \xi_2 \omega \frac{\left[(\varepsilon_+ - \varepsilon_-)(3+2\Gamma) + 2\varepsilon_-\left(1+4(\kappa-1)\kappa^{-2}\Gamma\right]\vec{n} + 4\varepsilon_- \dfrac{(\kappa-2)}{\kappa^2}\Gamma\vec{u}\right.}{\left(\varepsilon_+^2+\varepsilon_-^2\right)(3+2\Gamma) + 2\varepsilon_+\varepsilon_-\left(1+\dfrac{4(\kappa-1)\Gamma}{\kappa^2}\right)}$$

$\varepsilon_- = \omega - \varepsilon_+$, here $\vec{n}$ is an ort to the direction of initial photon, and $\vec{p}_+ / |\vec{p}_+|$ is an ort to the direction of propagation of secondary particle, $m\vec{u} = \vec{p}_+ - \vec{n}\cdot(\vec{n}\cdot\vec{p}_+)$, $\varepsilon_+, \varepsilon_-$ are the energy of positron and electron respectively. In its turn

$$\kappa = 2\varepsilon_+ p_+ / m^2,\ \Gamma = \ln\left(2\varepsilon_+\varepsilon_- / \omega m\right) - 2 - F(y)$$

and $F(y)$ has the form

$$F(y) = y^2 \sum_{n=1}^{\infty} \frac{1}{n(n^2+y^2)},\quad y = Z\alpha\,.$$

For $y \to 0$, $F(y) \to 0$; for $y >> 1$, $F(y) \to \ln y + 0.577$. So for $\varepsilon_+ \to \omega$, $\varepsilon_- \to m$ and

$$\vec{\varsigma} \to \xi_2 \cdot \vec{n}\,,$$

i.e. the photon polarization transferees to the secondary particle.
Graphically this dependence is represented in Fig.2. The graph itself is weakly dependent on the photon energy.

So one needs to arrange the *energy selection* of the secondary particles for arrangement of helicity transferring. The number of the particles around the maximum itself is small and defined by differential cross section over energy (Fig. 1).

The value of energy interval from which the particles are collected defined as a result of compromise between polarization value required and the total number of the particles collected.

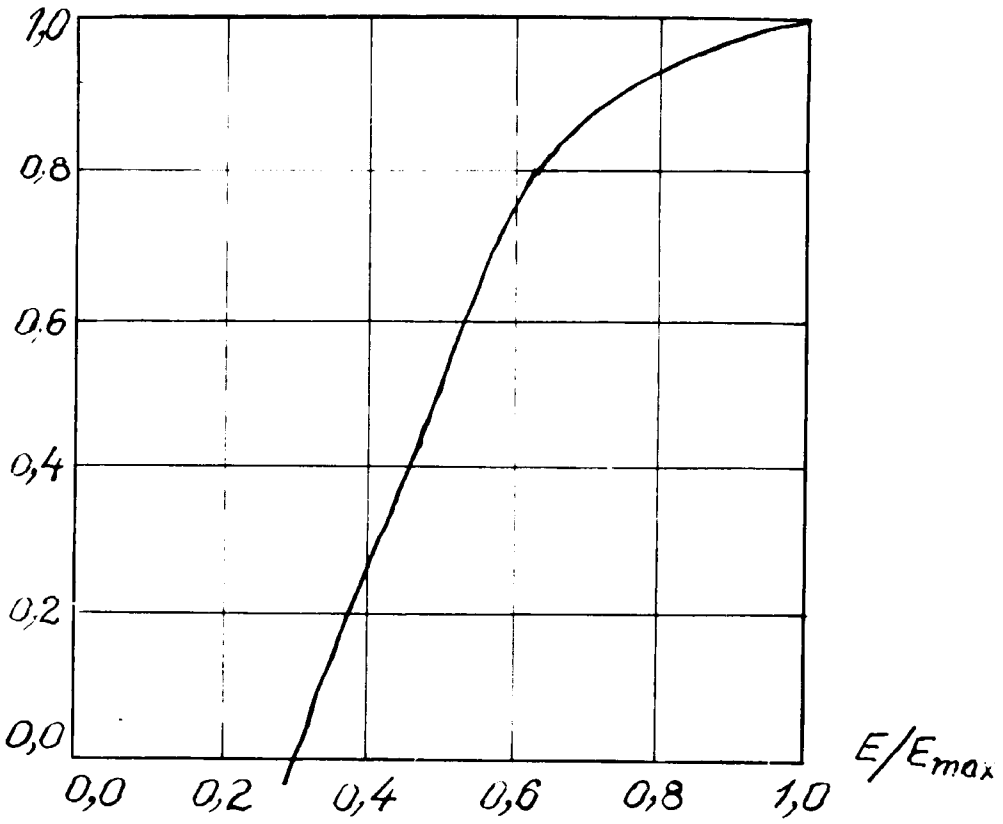

Fig.2. Longitudinal polarization of electron or positron as a function of its energy.

§3 The number of the particles with definite polarization as a function of particle's energy

To calculate the amount of the particles is a given energy interval, taken from the maxim possible energy for positron $\varepsilon_{\max}^{+} = \omega - 2m$, it is necessary to evaluate the integrals

$$\frac{\int_{\varepsilon}^{\varepsilon\max} \frac{d\sigma}{d\varepsilon_{+}} d\varepsilon_{+}}{\int_{0}^{\varepsilon\max} \frac{d\sigma}{d\varepsilon_{+}} d\varepsilon_{+}},$$

where differential cross section is represented in Fig.1 above.

To calculate the average polarization of particles, selected in such a way, one needs to evaluate

$$\frac{\int_{\varepsilon}^{\varepsilon\max} \varsigma(\varepsilon_{+}) \frac{d\sigma}{d\varepsilon_{+}} d\varepsilon_{+}}{\int_{0}^{\varepsilon\max} \frac{d\sigma}{d\varepsilon_{+}} d\varepsilon_{+}}.$$

In Fig.3 there is represented the average value of polarization as a function of variable $\varepsilon_{\max} - \varepsilon = \Delta\varepsilon$ - the energy interval, calculated from the maximal possible energy.

It was taken here $\omega / m = 10$; for higher photon energy average degree of polarization is higher for the same energy interval of collected particles.

If degree of polarization is chosen on curve 1, then using curve 2 one can estimate the fraction of particles from the total one, which can be collected using the energy separation in the limits defined by $\Delta\varepsilon$.

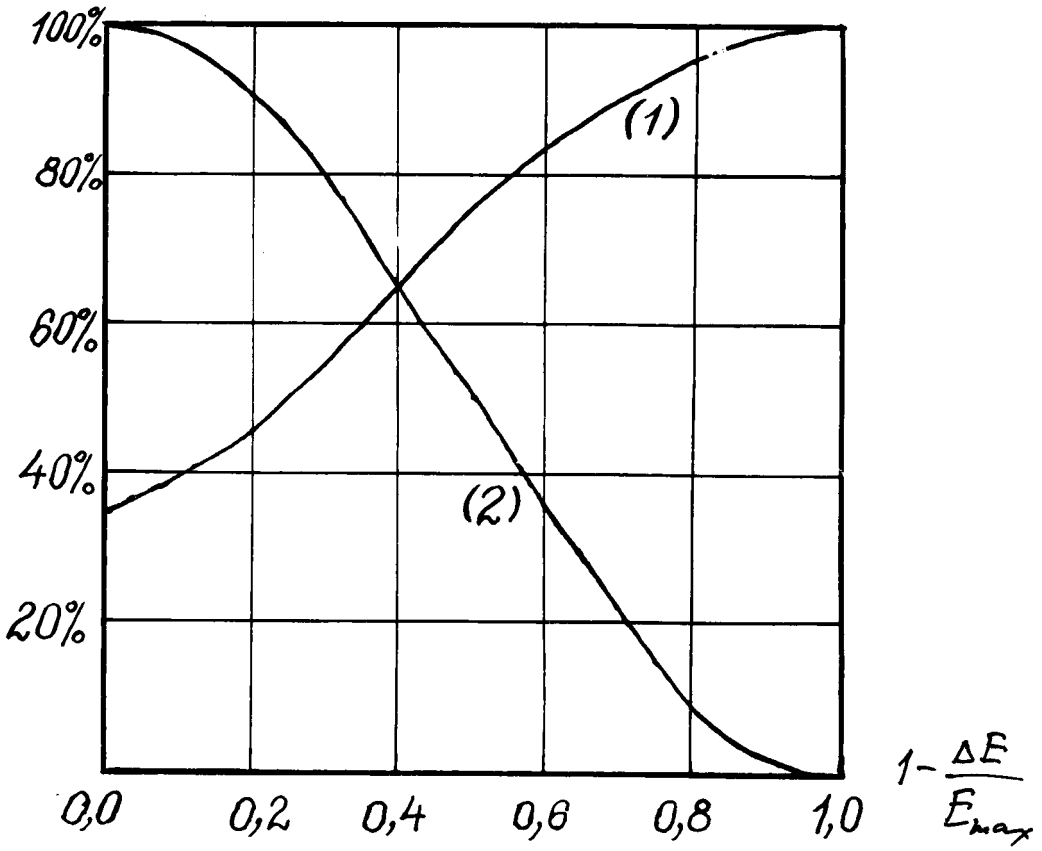

Fig.3 Average polarization (1) and the share of particles (2) as functions of energy interval, calculated from maximal possible value for $\omega / m = 10$.

So, for example, for obtaining 80% degree of polarization in the beam it is necessary collect the particles in 40% of energy interval from the maximum; the share of this particles will be ~40%. All this is valid under condition that initial photon beam has 100% polarization

and zero spread over frequencies. In reality, existing possibilities for obtaining such characteristics of the photon beams can diminish these limiting parameters.

As to the conversion system, it is necessary to satisfy the following characteristics:

Degree of circular polarization of the primary photon beam is the limiting number for created electrons and positrons, so it is desirable to have it as high as possible from the very beginning.

In addition, in the photon beam the highest density of radiation required for the purposes of selection of particles with necessary degree of polarization by using energy separation.

It is also necessary to have the number of the photons itself as high as possible to be able to compensate non full energy interval of collected particles; limited efficiency of conversion of gamma-quantas into the positrons and limited acceptance of transferring electro-optical system.

All these characteristics required, mentioned above in general has electromagnetic radiation generated by high-energy electrons or positrons passing through helical undulator. While the energy of initial particles runs in the region of 100 *GeV* and higher, the photon energy what can be expected here might fall in a diapason of tens *MeV* [52].

Next chapter is dedicated to investigation of characteristics of undulator radiation, in association with conversion.

CHAPTER 2. FORMATION OF CIRCULARLY POLARIZED RADIATION IN UNDULATOR

§1 General parameters tolerating to the properties of undulator radiation (UR).

Let us consider the problems associated with obtaining circularly polarized photons with the help of undulators. For these purposes the helical fields with minimal period are suitable [9,52,47]. The mostly interesting ways to generate such king of fields are usual static fields and the fields of electromagnetic waves. In perspective the method of obtaining circularly polarized quantas with the help of helical crystals will be possible in future [57].

Possibly, an interesting in a future can be bi–periodical structures, considered recently [47]. In the fields generated by such structure all maximums in radiation for all harmonics are coming to zero angle, i.e. straight forward; so the Stokes parameter $\xi_2 = 1$ in this direction. Let us mention also the possibility to rare out the spectrum of radiation by this method.

Below we shall consider the fields with sinusoidal distribution of the field at the axis [9].

The main parameters, tolerating to the properties of undulator radiation are

$$P_{\perp} = \frac{eH_{\perp}\lambda_0}{2\pi mc^2}, \quad \gamma^{-2} = 1 - \beta^2, \quad L, \qquad \Omega = \frac{2\pi\beta_{\parallel} c}{\lambda_0}$$

where $H_{\perp}$ –is the field amplitude in undulator, λ_0 –its period of variation, $L = N\lambda_0$ – is full length of undulator, N – is the number of it's elements of periodicity.

Under given angle ϑ, an observer can see a discrete lines of radiation having the width, defined by maximum between three values: $1/N$, $\Delta\gamma/\gamma$, and $\Delta\lambda/\lambda_0$. In our case $\Delta\omega/\omega$ defined by $\Delta\gamma/\gamma \sim 10^{-2}$, so the lines are overlapping here.

The value $P_\perp = \beta_\perp \gamma$ is the transverse normalized momentum of particle in undulator, also called *Undulatority factor*,

$$\beta_\parallel = \beta\sqrt{1-\left(\frac{\beta_\perp}{\beta}\right)^2}\,.$$

The length of formation of radiation in undulator depends on the trajectory angle and is [33]

$$l_f \cong \frac{\lambda_0}{\beta_\perp^2\gamma^2} = \frac{\lambda_0}{P_\perp^2},$$

and as at the length of formation α quantas are radiated, so the single quanta is radiated at the length $\lambda_0/\alpha P_\perp$ and N_γ quantas will be radiated on the length $\frac{N_\gamma\lambda_0}{P_\perp^2\alpha}$ i.e. after number of periods equal $\frac{N_\gamma}{\alpha P_\perp^2}$.

If we shall take for estimation the number of quantas required N_γ=50, so full length of undulator L=100m, period required goes to

$$\lambda_0 = \frac{P_\perp^2\alpha L}{N_\gamma} \cong \frac{P_\perp^2\cdot 2\cdot 10^4 cm}{137\cdot 10^2} \cong P_\perp^2\cdot 1.4cm\,.$$

For distribution of intensity of radiation over angles and energy, we have the formulas [9]

$$\frac{dI}{do} = I\frac{3}{4\pi\gamma^4}\cdot\frac{F(\vartheta)}{\left(1-\beta_\parallel Cos\vartheta\right)^3} = \sum_{k=1}^{\infty}\frac{dI_k}{do}$$

$$\frac{dI}{d\omega} = I\cdot\frac{3\omega}{2\beta_\parallel\Omega^2\gamma^4}F(\omega)$$

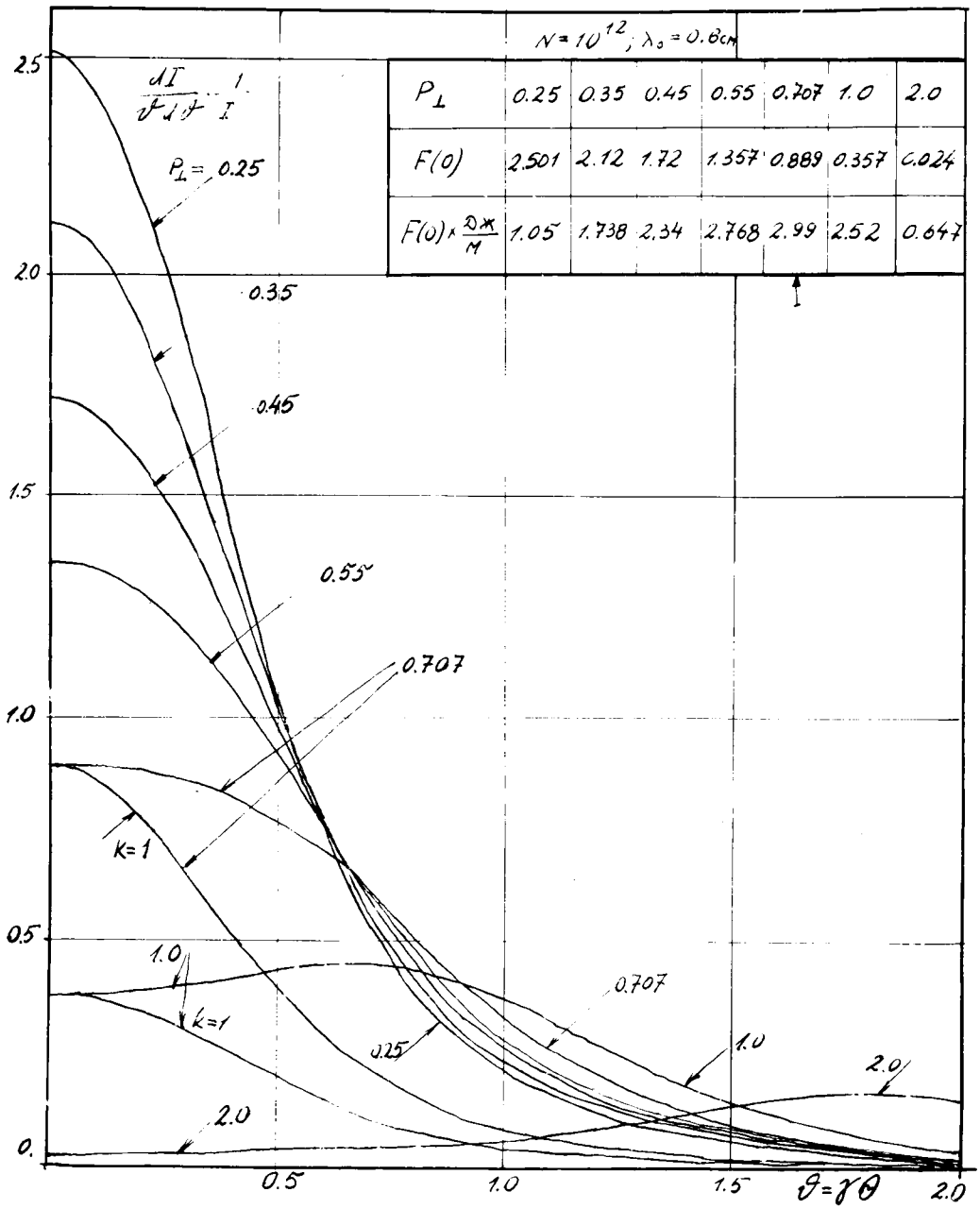

Fig.4 Angular distribution of intensity of radiation for different $P_\perp$.

where $F(\vartheta)=\sum_{k=1}^{\infty}k^2F_k(\vartheta)=\frac{4+3\kappa^2}{16(1-\kappa^2)^{5/2}}+\frac{4+\kappa^2}{16(1-\kappa^2)^{7/2}}\frac{Cos\vartheta-\beta_{\|}}{1-\beta_{\|}\,Cos\vartheta}$,

$$F_k(\vartheta)=J_k'^2(k\kappa)+\left(\frac{Cos\vartheta-\beta_{\|}}{\beta_{\perp}Sin\vartheta}\right)^2J_k^2(k\kappa)$$

$$F(\omega)=\sum_{k=1+k'}^{\infty}F_k\left(\vartheta_k(\omega)\right)$$

where $\kappa=\frac{\beta_{\perp}\sin\vartheta}{1-\beta_{\|}\cos\vartheta}$, k' is integer part of $\frac{\omega\cdot(1-\beta_{\|}}{\Omega}$, and

$$I=\frac{2}{3c}\Omega^2P_{\perp}^2\gamma^2$$

is full intensity of radiation.

For small angles, when $\gamma\vartheta\sim1$, expressions for intensity distribution can be simplified to the following

$$\frac{dI}{do}=I\frac{6\gamma^2}{\pi}\frac{F(\vartheta)}{1+P_{\perp}^2+\theta^2}\equiv I\cdot\Phi(\theta),$$

$$\frac{dI}{d\tilde{\omega}}=I\cdot6\tilde{\omega}F(\omega),\quad \tilde{\omega}=\frac{\omega}{2\Omega\gamma^2},\quad \theta=\gamma\vartheta.$$

It is evident existence here for the following normalization

$$\frac{3}{4\pi\gamma^4}\int\frac{F(\vartheta)do}{(1-\beta_{\|}\,Cos\vartheta)^3}=1.$$

If period of undulator λ_0 is fixed, then undulatority factor defines the properties of UR.

In Fig. 4, there is represented an angular distribution of intensity of

radiation for different values of undulatority factor $P_\perp$.

In upper corner of the picture, the density of radiation straightforward and linear density of energy deposition is represented in a Table. As one can see, for $P_\perp$ =0.7, the density of radiation in forward direction is maximal.

The formula for intensity can be represented as the following

$$I = \frac{8}{3}\pi^2 r_e c \cdot mc^2 \beta_\parallel \frac{\gamma^2 P_\perp^2}{\lambda_0^2},$$

$$mc^2 = 0.511\times 10^6 eV = 0.871\times 10^{13} J.$$

The value of full intensity calculated for the bunch population $N_0 = 10^{12}$.

§2 Number of photons as a function of energy and angle

In order to obtain angular and spectral distribution for the number of quantas, it is necessary to divide intensity by energy of the quanta. The last depends on the harmonics number, angle and undulatority factor

$$\varepsilon_\gamma = \frac{4\pi r_e nc^2}{\alpha} \frac{\gamma^2}{\lambda_0 \cdot (1 + P_\perp^2 + \theta^2)} = \hbar\omega,$$

$$\frac{d\dot{N}_\gamma}{do} = \frac{dI}{do\varepsilon_\gamma} = I\frac{\Phi(\theta)}{\varepsilon_\gamma}$$

$$\frac{d\dot{N}_\gamma}{d\tilde{\omega}} = \frac{dI}{d\tilde{\omega}\varepsilon_\gamma} = I\frac{6\tilde{\omega}}{\varepsilon_\gamma}F(\tilde{\omega}), \quad \frac{\hbar\tilde{\omega}}{\varepsilon_\gamma} = \frac{\omega}{2\Omega\gamma^2}.$$

Again, $r_e \cong 2.818\times 10^{-13} cm$, $1/\alpha \cong 137.04$.

In Fig.5 these distributions are represented for different $P_\perp$. In a Table in this figure there is also indicated the number of the quantas having right polarization (right threaded undulator) radiated per meter, total

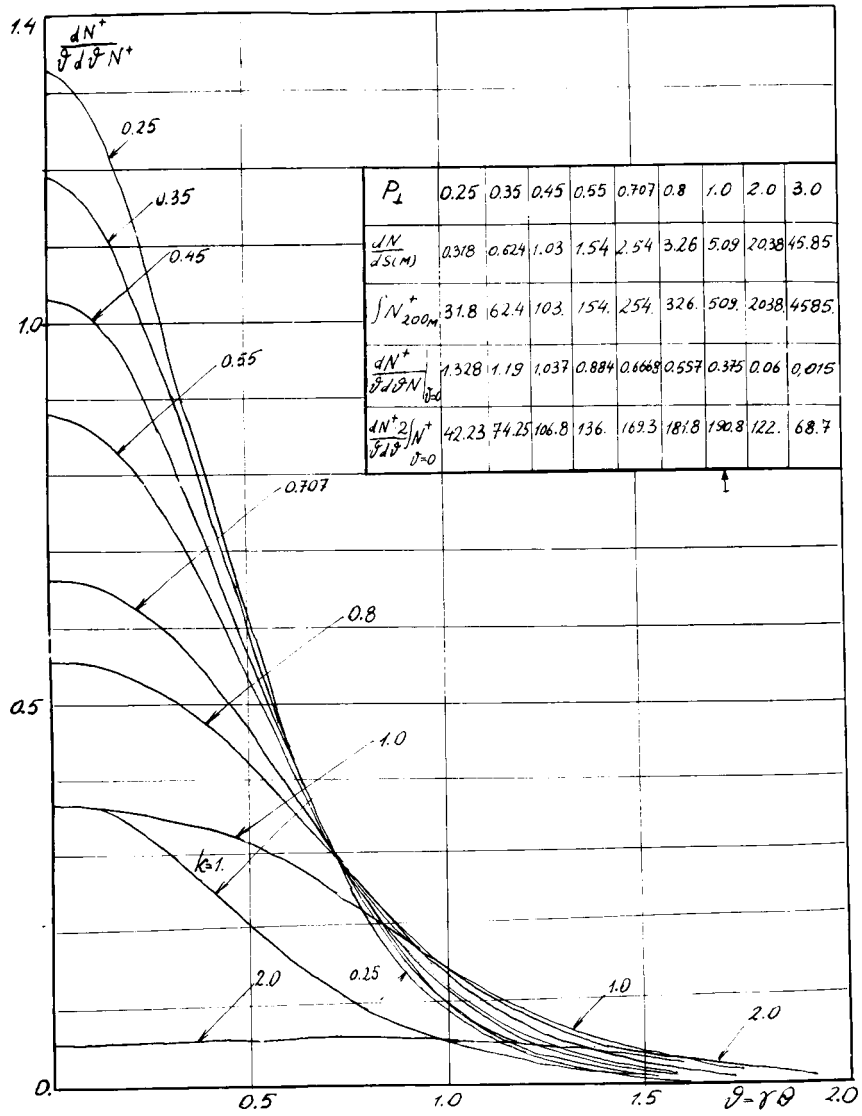

Fig.5 Angular distribution of the number of radiated photons for different $P_{\perp}$.

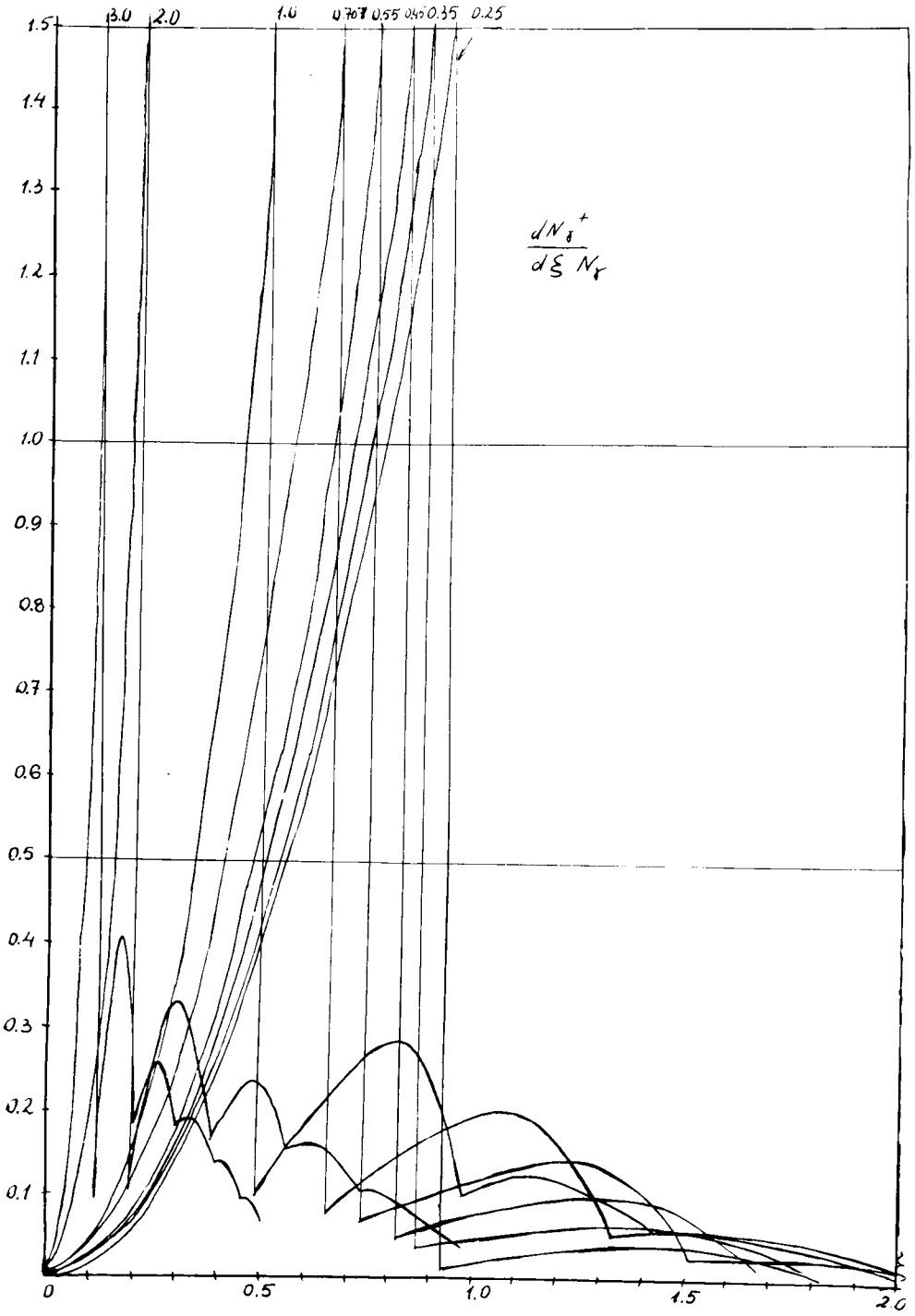

Fig.6. Spectral distribution of radiation.

$$\xi_2 = \frac{\frac{dN^+}{d\theta} - \frac{dN^-}{d\theta}}{\frac{dN^+}{d\theta} + \frac{dN^-}{d\theta}}$$

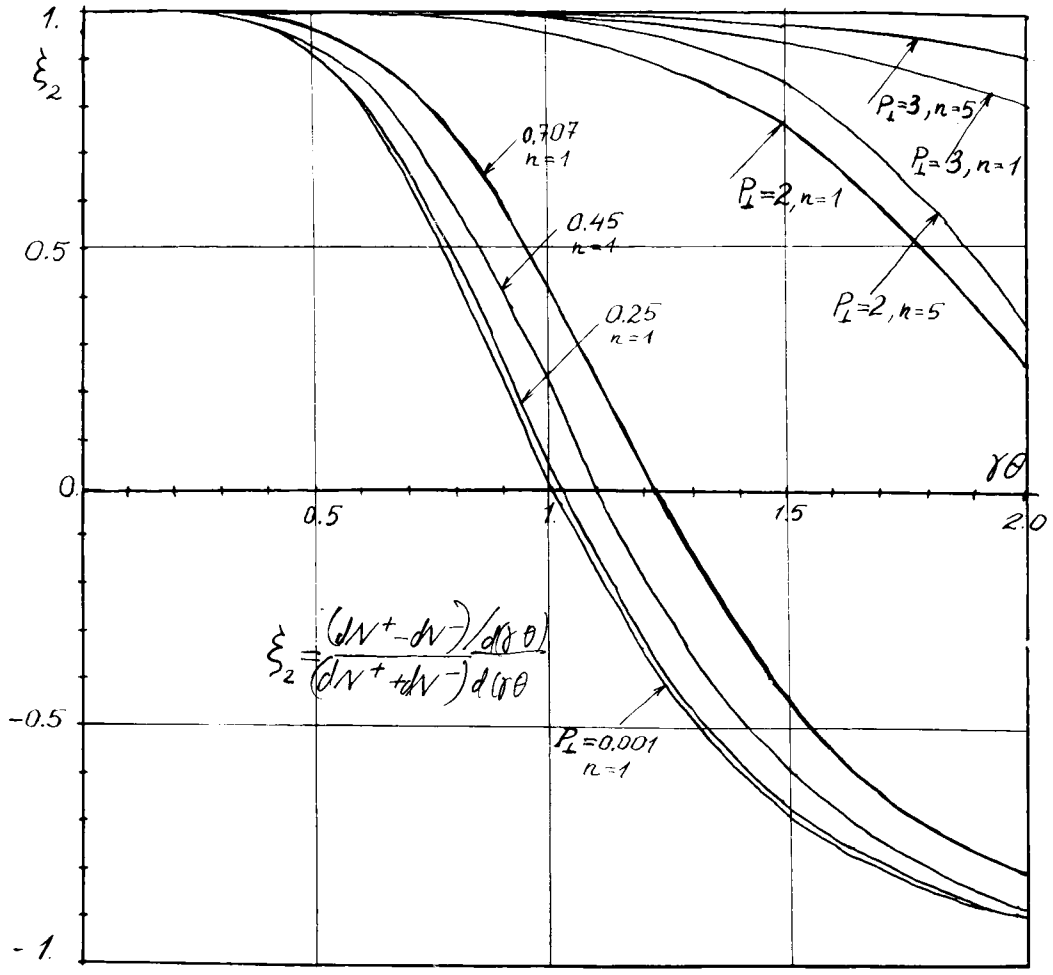

Fig.7. Angular distribution of degree of polarization.

$$\xi_2 = \frac{\dfrac{dN^+}{d\omega} - \dfrac{dN^-}{d\omega}}{\dfrac{dN^+}{d\omega} + \dfrac{dN^-}{d\omega}}$$

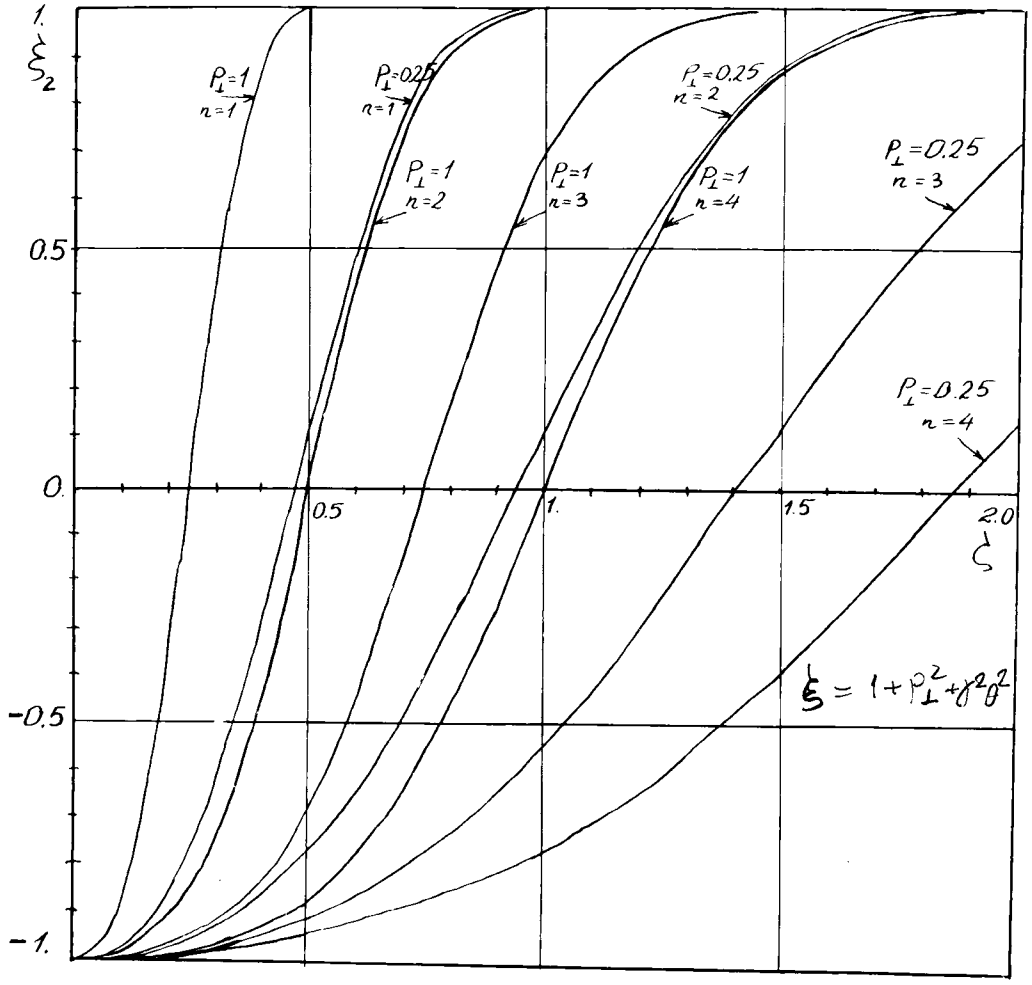

Fig.8. Spectral dependence of degree of polarization.

amount of quantas, radiated on 200 *m* trajectory, the value of photon density for zero angle, and density of right-polarized quantas.

Let us mention, that the maximum occurs here at $P_\perp = 1$, as a result of energy dependence from angle as $\sim 1/(1+P_\perp^2+\theta^2)$.

In Fig.6 the number of right-polarized quantas as a function of parameter $P_\perp$ is represented. In Figs. 7 and 8- polarization as function of angle and energy is represented respectively. Stokes parameter defined at the top of each figure.

It is interesting also to consider quantitatively ratios for the number of the photons radiated in 10% interval of energy around maximum and sum polarization of these quantas.

Interval of energy for photons defined by the limiting angle, measured relatively to the forward direction, $\theta_{\max}$, as the following

$$\varepsilon_\gamma^{\max} \cong \frac{1}{1+P_\perp^2+\theta^2}.$$

These distributions represented in Fig.9. These distributions show that polarization drops in half while undulatority factor changes from 0 to 3, and the number of the quantas, indeed, increases drastically. It also clear that even for fixed 10% energy interval, defined by corresponding angle, undulatority factor 0.5 defines resulting level of polarization only 90% and the number of quantas goes to20.

In Fig. 10 there is represented the density of the photons in 10% energy interval around maximum of the first harmonic.

Let us mention, though the quantas from second and higher harmonics also have required polarization in fixed solid angle, theirs energies are in integer number times bigger, than the energy of the first harmonic, radiated in the same solid angle. As it follows from materials, represented in Chapter 1, these quantas generate positrons and electrons with polarization, not higher than 50%.

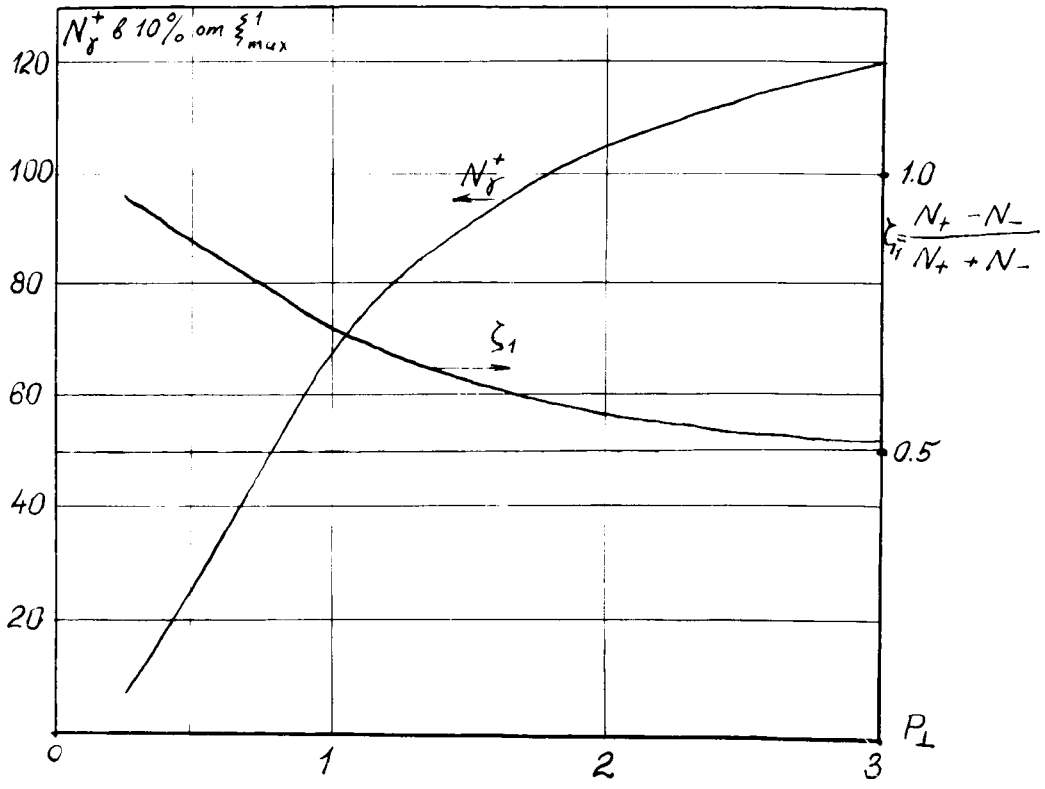

Fig.9. Number of right polarized quantas and degree of circular polarization as functions of $P_\perp$.

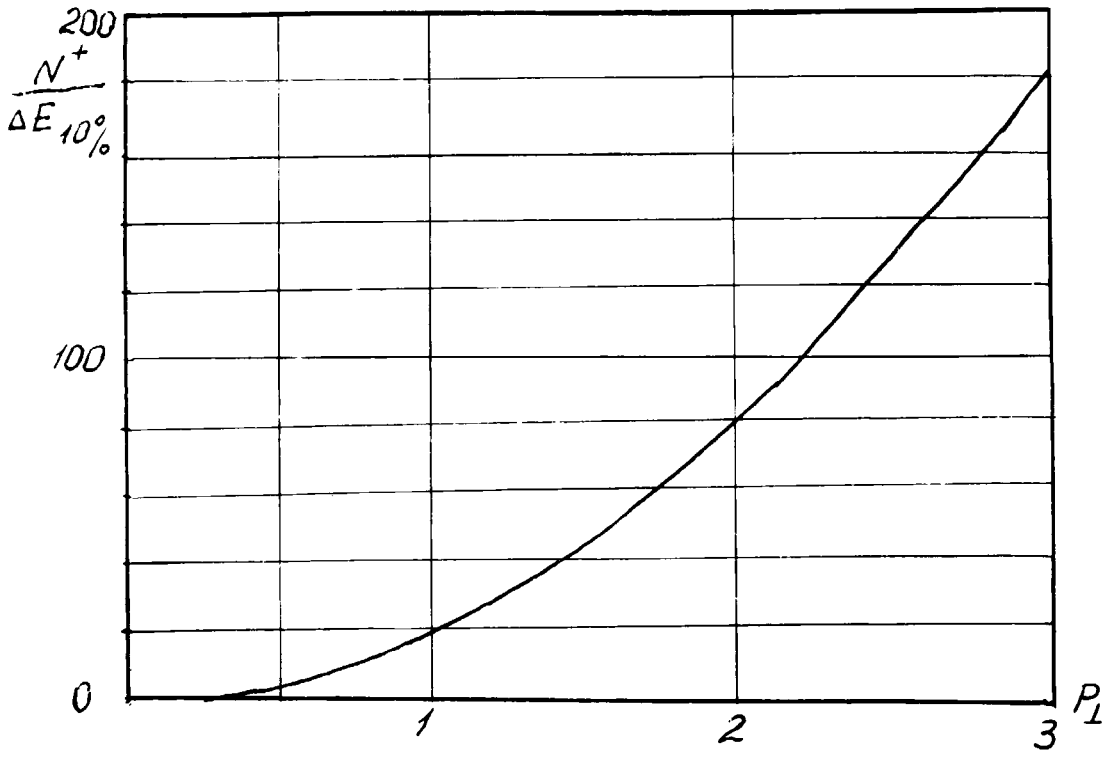

Fig.10. Density of the number of photons in 10% energy interval as a function of $P_\perp$.

Situation becomes worsen if there is no angle separation at converter. In Fig.11 the input from harmonics in total number of rightly polarized photons radiated in 10% energy interval is represented. Full share of radiated photons in all harmonics in margins of parameter $\tilde{\omega}$ from the value corresponding to the maximum of the first harmonics for fixed $P_\perp$, to the infinity and, separately, the input from the second and third harmonics respectively are represented here also.

It is clear from Fig.11, that for the undulatority factor value around 0.5, the share of the photons from the total flux radiated at first harmonic and from others is equal. This means that the undulatority factor value must be chosen even less. For $P_{\perp} = 0.25$ this ratio goes to 4.5 .

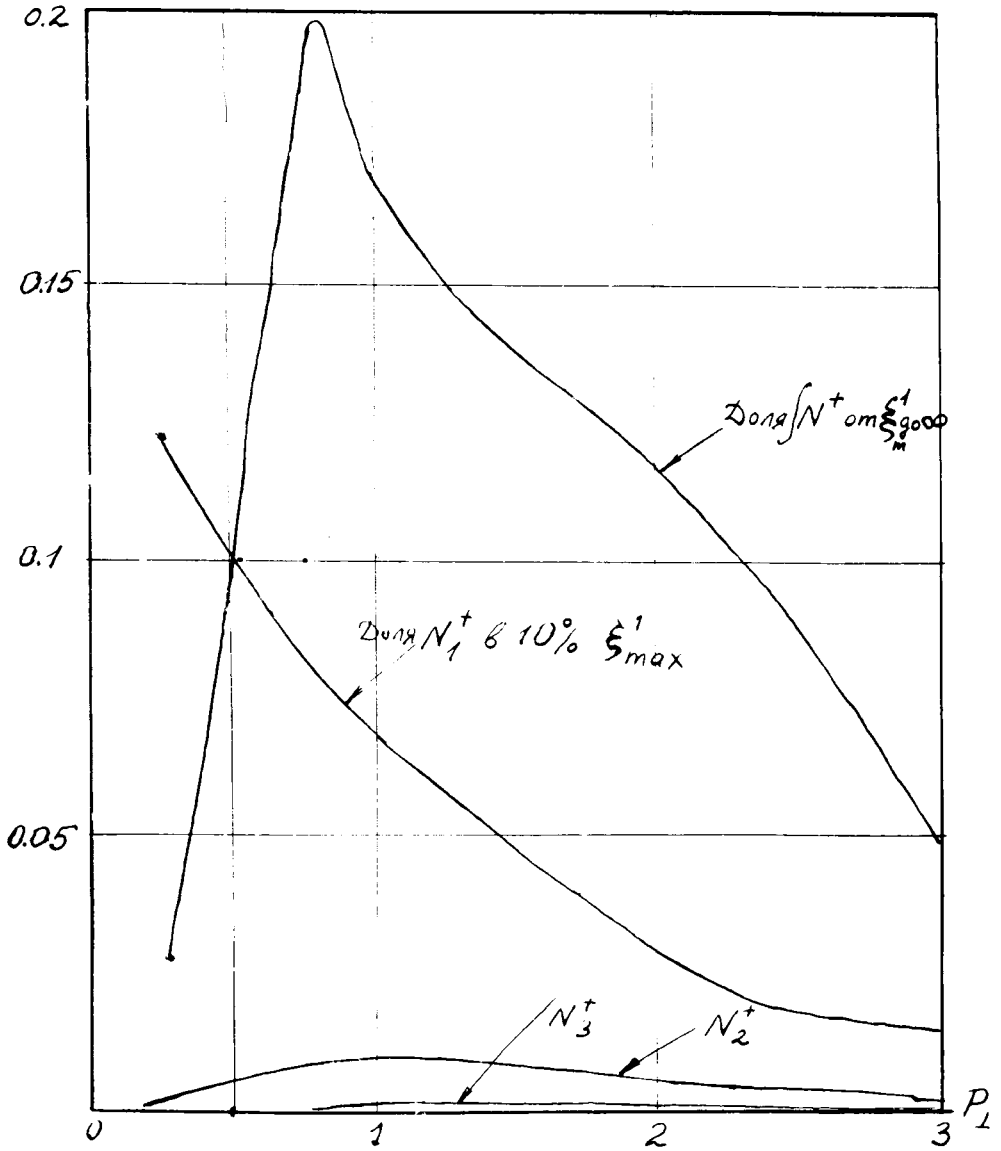

Fig. 11. Input from individual harmonics in 10% interval around maximum of the first harmonic.

To realize the possibility of angular separation, it is necessary to separate the angles of the order $0.5/\gamma$. For reasonable diameter of target-converter 5 *mm*, the distance from the end of undulator to the target must be ~500 *m*. The divergence of UR is of the order $P_\perp/\gamma$; the divergence of the beam defined [7] by $\sqrt{\varepsilon/\tilde{\beta}}$, where ε is emittance and $\tilde{\beta}$ is a beta-function of the order 400*m*.

It is possible to operate with variable undulatority factor, when initial parts of undulator have higher values of $P_\perp$. As the undulator itself serves for the length required for separation, it is possible to expect some relief for angular separation. For obtaining monochromaticity, it is necessary to change period in undulator in accordance with local value $P_\perp$ in order to prevent enlarging the energy spread in the flux.

In more detail conditions for optimal collection will be considered in Chapter 3.

Let us mention here, that the motion in varying field of undulator yields effective focusing with potential

$$U_{eff} \cong mc^2\gamma\beta_\perp^2 = mc^2\gamma\cdot\frac{P_\perp^2}{\gamma^2}.$$

Evidently one can neglect this effect for $\sim 100 GeV$.

§3. Amount of radiation to the walls of undulator

For estimation of heating the walls of undulator, let us use the formulas for distribution of intensity of undulator radiation over the angle. All harmonics need to be taken into account here.
As it will be seen, in our case the undulator has an aperture diameter ∅=4*mm*, $\lambda_0 = 6\,mm$. Let L again be the full length of undulator.

For the full energy deposited in the walls at the distance running from 0 to *x* meters, we have to evaluate the integral

$$\int f(\rho)d\rho \int d\varphi(\rho) \int_{\theta_{\min}(\varphi,\rho)}^{\theta_{\max}(\varphi,\rho)} \Phi(\theta)\theta d\theta ,$$

$$\theta_{\min} = \vartheta_{\min}\gamma , \qquad \theta_{\max} = \vartheta_{\max}\gamma ,$$

and multiply this integral by the full radiated energy, i.e. $I \cdot \frac{x}{c}$. Here $\int f(\rho)d\rho = N_0$, $f(\rho)$ –is the distribution of particles over the radius. Here practically, as a result of fast dropping of $\Phi(\theta)$, the real input is going from the angles $\theta \le 2$, so the integral can be extended to ∞.

In Fig.13 the geometry of radiation of the particle located at the radial distance ρ from the axis of undulator is represented.
The current angle θ depends on azimuth angle φ by the following way

$$\theta = \frac{z\gamma}{x},$$

where $z = \sqrt{d^2 + \rho^2 - 2d\rho Cos\,\psi}$,

$2d$ stands for diameter of aperture. In reality ratio $\frac{\rho}{d} \cong 0.1$

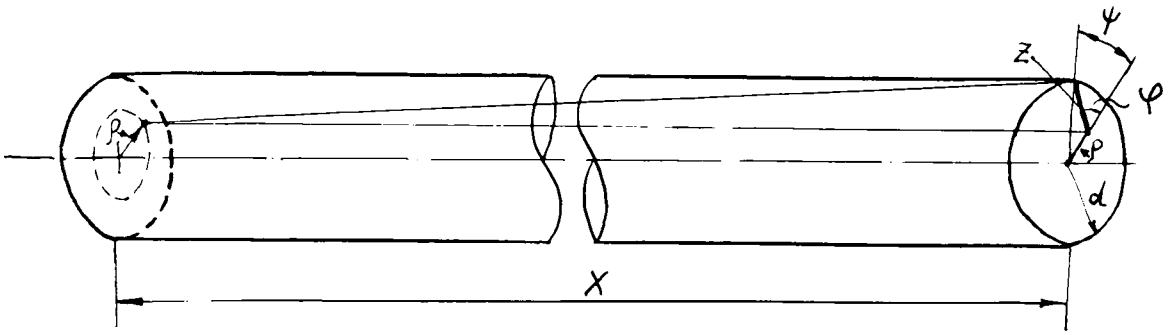

Fig.12. Geometry of the wall irradiation.

As the difference between φ and ψ manifests in the second order over $\frac{\rho}{d}$, one can write

$$\theta \cong \gamma \frac{d}{x} \cdot \left(1 - 2\frac{\rho}{d} Cos\,\psi\right)^{1/2} \cong \gamma \frac{d - \rho \cdot Cos\,\psi}{x}.$$

So for the amount of energy radiated into the walls, one can obtain

$$E(x) = I \frac{x}{c} \int_0^{\rho_{\max}} f(\rho) d\rho \int_0^{2\pi} d\varphi \int_{\frac{d-\rho Cos\varphi}{x}\gamma}^{\infty} \Phi(\theta) d\theta .$$

Integral over θ can be represented as the following

$$\int_{\frac{d-\rho Cos\varphi}{x}\gamma}^{\infty}\Phi(\theta)\theta d\theta=\int_{\frac{d\cdot\gamma}{x}}^{\infty}+\int_{\frac{d-\rho Cos\varphi}{x}\gamma}^{\frac{d\cdot\gamma}{x}}\cong\int_{\frac{d\cdot\gamma}{x}}^{\infty}+\Phi(\frac{d\cdot\gamma}{x})\cdot\frac{d\cdot\gamma}{x}\frac{\rho Cos\varphi}{x},$$

and the last term will give zero after integration over φ.
The angular spread in the beam yields an increase in the angular spread of radiation by the value

$$\vartheta_{efff}^2=\frac{1+P_\perp^2}{\gamma}+\frac{\varepsilon}{\tilde{\beta}}=\vartheta_{rad}^2+\vartheta_{beam}^2,$$

or

$$\theta_{eff}=\sqrt{1+P_\perp^2+\frac{\varepsilon\gamma^2}{\tilde{\beta}}}=\sqrt{\theta_{rad}^2+\gamma^2\vartheta_{beam}^2},$$

where $\tilde{\beta}$ is a beta—function on the beam in undulator with well-known dependence around crossover

$$\tilde{\beta}=\tilde{\beta}_0\cdot\left(1+\frac{s^2}{\tilde{\beta}_0^2}\right),$$

and ε here is the phase volume of the beam. Taking for estimation

$$\varepsilon=10^{-7}cm\cdot rad,\ \tilde{\beta}_0=400m,$$

(see [7,29]), one can obtain

$$\theta_{red}^2\cong1+P_\perp^2\le1.5$$

$$\vartheta_{beam}^2\gamma^2=\frac{\varepsilon\gamma^2}{\tilde{\beta}}\cong0.1\ .$$

So the input from angular spread in the beam at the length of undulator is small and is not considered below.
Results of calculation represented in the Tables below.

Table 2.

E=100 GeV, ($\gamma/10^5$=2), $E_{beam}=16kJ$

$x,\ m\rightarrow$	25	50	75	100	125	150	175	200
$\vartheta_{\min}\cdot 10^5$	8.	4.	2.67	2	1.6	1.33	1.14	1.
$\vartheta_{\min}$	16.	8.	5.4	4.	3.2	2.67	2.3	2.
$P_\perp=0.35$	$<10^{-5}$	$3.4\cdot10^{-4}$	$1.6\cdot10^{-3}$	$4.9\cdot10^{-3}$	1.1%	2.1%	3.36%	5.1%
	0.064	0.25	0.546	0.966	1.45	2.0	2.58	3.23
$P_\perp=0.707$	$<10^{-5}$	$3.4\cdot10^{-4}$	$1.7\cdot10^{-3}$	0.56%	1.3%	2.6%	4.4%	7%
	0.064	0.254	0.54	0.94	1.4	1.92	2.43	3.0
$P_\perp=1.0$	$<10^{-5}$	$3.5\cdot10^{-4}$	$1.9\cdot10^{-3}$	$6.6\cdot10^{-3}$	1.67%	3.55%	6.3%	10%
	0.064	0.254	0.53	0.92	1.35	1.8	2.26	2.75

Table 3.

E=200 GeV, ($\gamma/10^5$=4), $E_{beam}=32kJ$

$x,\ m\rightarrow$	25	50	75	100	125	150	175	200
$\vartheta_{\min}\cdot 10^5$	8.	4.	2.67	2	1.6	1.33	1.14	1.
$\vartheta_{\min}$	32.	16.	10.8	8.	6.4	5.4	4.6	4.
$P_\perp=0.35$	$8.\cdot10^{-7}$	$1.\cdot10^{-5}$	$1.\cdot10^{-4}$	$3.2\cdot10^{-4}$	$8.1\cdot10^{-4}$	$1.6\cdot10^{-3}$	$2.9\cdot10^{-3}$	$4.9\cdot10^{-3}$
	0.064	0.257	0.567	1.075	1.57	2.18	2.97	3.86
$P_\perp=0.707$	$8.4\cdot10^{-7}$	$1\cdot10^{-5}$	$1\cdot10^{-4}$	$3.3\cdot10^{-4}$	$8.5\cdot10^{-4}$	0.17%	0.32%	.56%
	0.064	0.257	0.56	1.01	1.56	2.16	2.91	3.78
$P_\perp=1.0$	$8.5\cdot10^{-7}$	$1.\cdot10^{-5}$	$1.\cdot10^{-4}$	$3.5\cdot10^{-4}$	$9.2\cdot10^{-4}$	$1.9\cdot10^{-3}$	0.36%	0.65%
	0.064	0.256	0.557	1.002	1.54	2.14	2.85	3.67

Table 4.

E=300 GeV, $(\gamma/10^5 = 6)$, $\quad E_{beam} = 48kJ$

x, $m\rightarrow$	25	50	75	100	125	150	175	200
$\vartheta_{\min}\cdot 10^5$	8.	4.	2.67	2	1.6	1.33	1.14	1.
$\vartheta_{\min}$	48.	24.	16	12.	9.6	8.	6.84	6.
$P_\perp = 0.35$	$<\cdot 10^{-8}$	$1.\cdot 10^{-6}$	$2.\cdot 10^{-5}$	$7\cdot 10^{-5}$	$1.4\cdot 10^{-4}$	$3.2\cdot 10^{-4}$	$6.2\cdot 10^{-4}$	$1.\cdot 10^{-3}$
	0.064	0.257	0.579	1.025	1.6	2.28	3.1	4.
$P_\perp = 0.707$	$8.4\cdot 10^{-7}$	$1.\cdot 10^{-6}$	$2.\cdot 10^{-5}$	$7\cdot 10^{-5}$	$1.5\cdot 10^{-4}$	$3.3\cdot 10^{-4}$	$6.5\cdot 10^{-4}$	$1.1\cdot 10^{-3}$
	0.064	0.257	0.578	1.023	1.59	2.27	3.08	3.96
$P_\perp = 1.0$	$8.5\cdot 10^{-7}$	$1.\cdot 10^{-6}$	$2.\cdot 10^{-5}$	$6\cdot 10^{-5}$	$1.5\cdot 10^{-4}$	$3.5\cdot 10^{-4}$	$6.9\cdot 10^{-4}$	$1.2\cdot 10^{-3}$
	0.064	0.257	0.576	1.02	1.58	2.25	3.05	3.91

In the columns of these Tables, for each $\theta_{\min}$, responsible for shown distance x, counted every 25 meters, the energy, radiated in the wall is represented for different undulatority factors as a fraction of full one E_{beam}. The energy of the gamma-quanta for the first harmonics is represented also. The energy calculated by the formula

$$\varepsilon_\gamma = \frac{2.48\cdot\left(\gamma/10^5\right)^2}{\left(1+P_\perp^2+\theta_{\min}^2\right)\cdot\lambda_0[cm]}[MeV]$$

(see page 27).

For the full energy radiated at the distance from 0 to x we have expression

$$\varepsilon(x) = I\frac{x}{c}N_0 = \frac{8\pi^2}{3}r_0 x\cdot mc^2\cdot\beta_\parallel\ \frac{\gamma^2 P_\perp^2}{\lambda_0^2}N_0\,.$$

For the number of the particles $N_0 = 10^{12}$ (e^+ or e^-) passing through undulator, we obtain

$$\varepsilon(x)[J] = 1.68\cdot\left(\frac{\gamma}{10^5}\right)^2 P_\perp^2\cdot x[m].$$

The full losses of energy for radiation and, particularly into the walls, are represented in tables 5-7 and corresponding graphics.

Table 5.

E=100 GeV, $((\gamma/10^5)$=2, $\quad E_{beam}=16kJ$

x, $m\rightarrow$	25	50	75	100	125	150	175	200
$P_\perp=0.35$	16.8	33.6	50.4	67.2	84.	100.8	117.6	134.4
	$1.7\cdot10^{-4}$	0.011	0.08	0.33	0.92	2.1	3.95	6.85
$P_\perp=0.707$	82.3	164.64	247.	329.	411.6	493.9	576.	658.5
	$8.2\cdot10^{-4}$	0.05	0.43	1.84	5.34	11.4	25.3	46.
$P_\perp=1.0$	168.	336.	504.	672.	840.	1008.	1176.	1344.
	$1.7\cdot10^{-3}$	0.12	0.947	4.43	14	35.8	74.1	134

Graph 1.

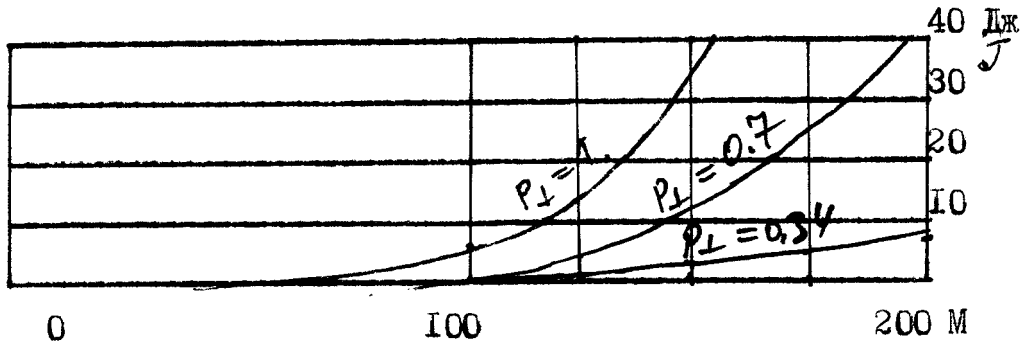

In Graph 1 the distributions of losses into the walls along the length are represented (so are the following).

Table 6.

E=200 GeV, ($\gamma/10^5$=4), $E_{beam}=32kJ$

x, $m\rightarrow$	25	50	75	100	125	150	175	200
$P_\perp = 0.35$	67.2	134.4	201.6	268.8	336.	403.0	470.	537.
	$6.4\cdot10^{-5}$	$1.3\cdot10^{-3}$	0.02	0.086	0.27	0.64	1.36	2.63
$P_\perp = 0.707$	329.	658.3	988.	1317.	1646.	1975.	2305.	2634.
	$3.3\cdot10^{-5}$	$6.6\cdot10^{-3}$	0.099	0.43	1.4	3.36	7.37	14.7
$P_\perp = 1.0$	672.	1344.	2016.	2688.	3360.	4032.	4704.	5376.
	$6.7\cdot10^{-5}$	$1.3\cdot10^{-3}$	0.2	0.94	3.1	7.66	16.9	34.9

Graph 2.

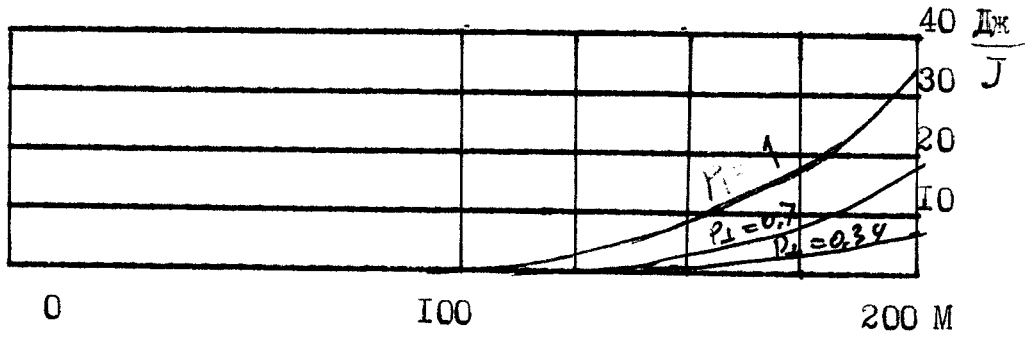

Table 7.

E=300 GeV, ($\gamma/10^5$=6), E_{beam} =48kJ

x, $m\rightarrow$	25	50	75	100	125	150	175	200
$P_\perp = 0.35$	151.2	302.	453.6	604.	756.	907.	1058.	1209..
	$1.5\cdot10^{-6}$	$3.4\cdot10^{-4}$	0.009	0.042	0.064	0.29	0.65	1.2
$P_\perp = 0.707$	740.	1482.	2223.	2963.	3704.	4445.	5186.	5927.
	$7.4\cdot10^{-6}$	$1.5\cdot10^{-3}$	0.044	0.21	0.55	1.46	3.4	6.5
$P_\perp = 1.0$	672.	1344.	2016.	2688.	3360.	4032.	4704.	5376.
	$1.5\cdot10^{-5}$	$3\cdot10^{-3}$	0.09	0.42	1.13	3.17	7.3	14.5

Graph 3.

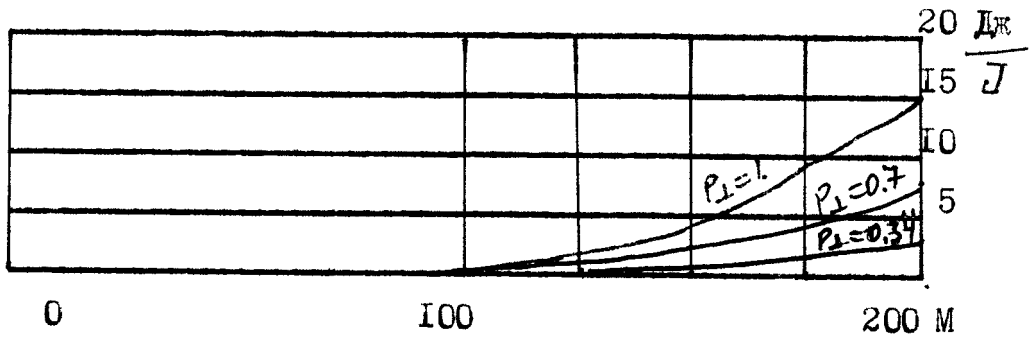

The losses in the wall at the end of 175 and 200 meters are represented in Fig.13 for repetition rate 1 *Hz*.

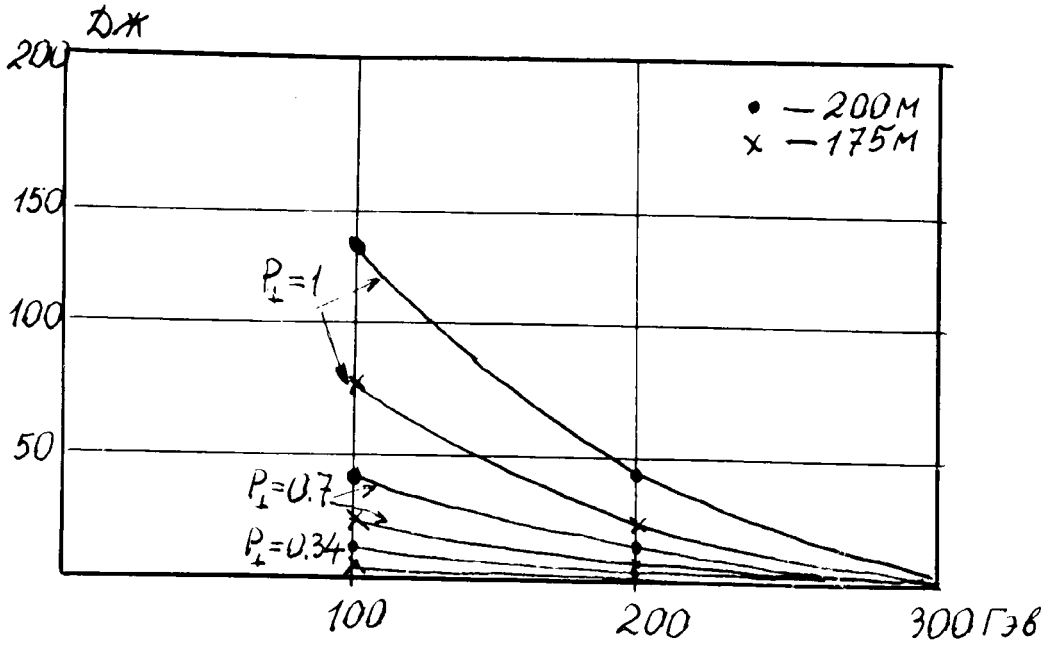

Fig.13. Full losses of the beam in the walls.

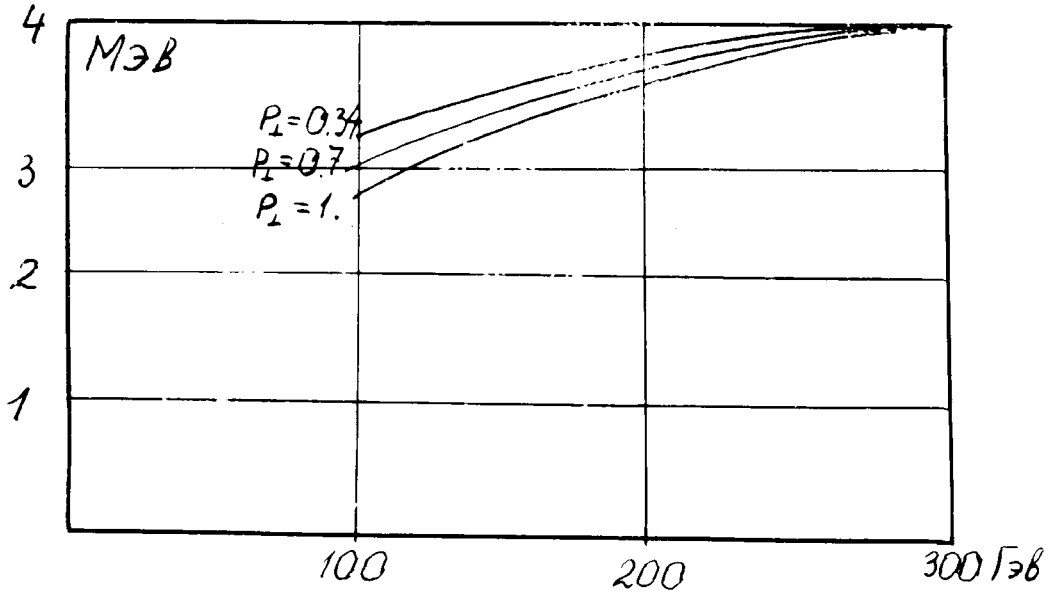

Fig.14. Maximal energy of γ-quanta, hitting the wall at the end of 200 *m*.

In Fig. 14 the maximal energy of the quanta hitting the wall at the end of 200 *m* is represented. In Fig. 15 the linear density of the losses at the last 25 of 200- *m* length of undulator are represented as functions of the beam energy.

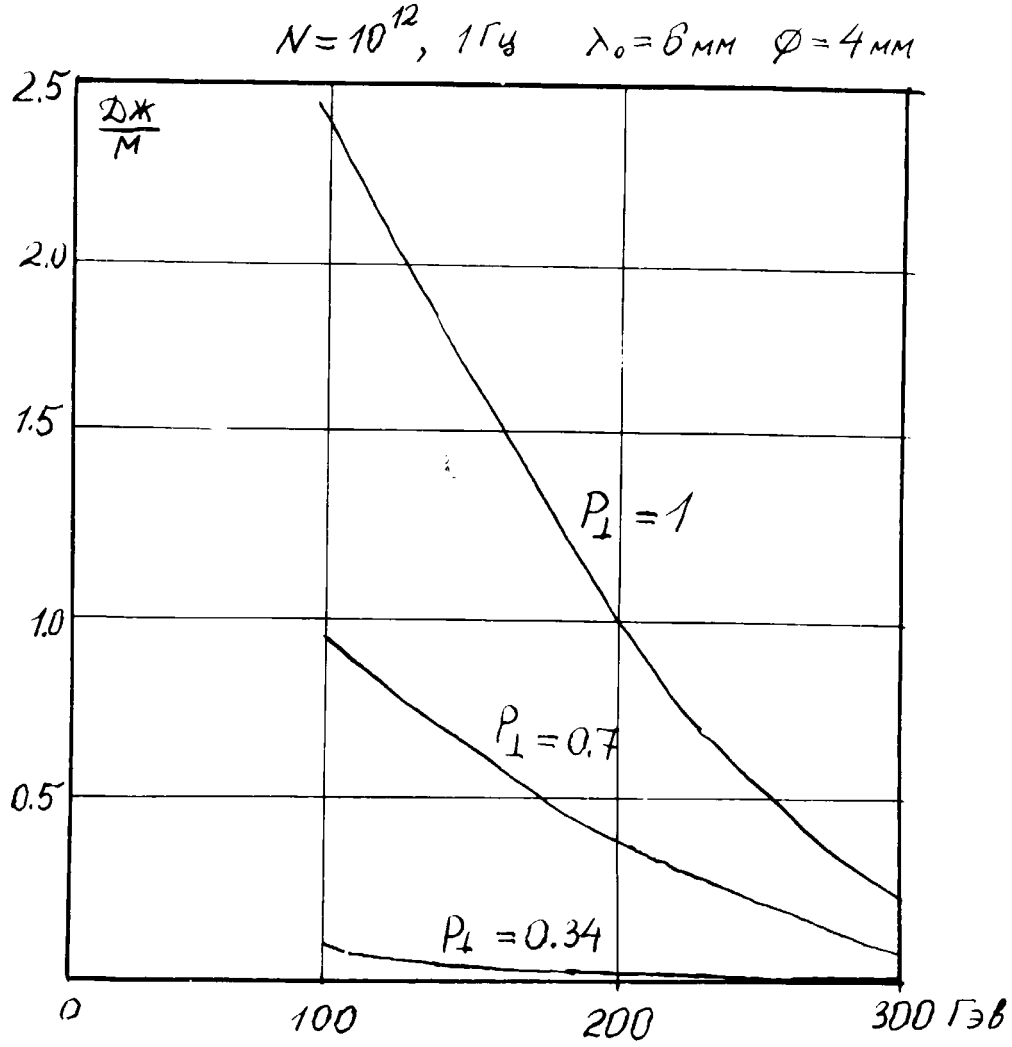

Fig.15. linear density of losses in the walls of undulator. $N_0 = 10^{12}$, $1Hz$, $\lambda_0 = 6mm$, $\varnothing$=$4mm$.

Table 8.

ε, GeV	100	200	300
$P_{\perp}$=0.34	0.11	0.051	0.025
$P_{\perp}$=0.7	0.828	0.29	0.124
$P_{\perp}$=1.0	2.4	0.72	0.268

For $\varepsilon \geq 300\ GeV$ the losses are negligible.

So one can see, so even for $P_{\perp}$=1, 100GeV beam going with repetition rate 10 Hz loses in the walls ~24 W/m. As the full length of section of undulator is ~1 meter, this gives additional 24 W (we will see lower, that for $P_{\perp}$=1 the active losses in conductors go to 9000 W and for $P_{\perp}$=0.4 , 10Hz losses are ~1500 W respectively).

The final conclusion is that for operation of undulator with parameters described above, the losses are not a problem to be mentioned.

For the higher energy, up to 500 *GeV*, the radiation to the walls drops even more significantly, as the angle of radiation drops as $1/\gamma$.

As it will be seen lower the operational value for the undulatority factor stays around 0.35 with full length of undulator ~150m, so the power of radiation to the wall at the end of undulator goes to 1-2 W limit.

The losses are optimistic for undulator with superconducting wiring also. For this SC undulator the heating by radiation emerges as a mostly serious factor tolerating the its successful operation.

The mostly perspective will be usage of this SC undulator at the energy higher than 200 GeV and for $P_{\perp}$=0.35 .

As one could see from the materials described above for the period of undulator ~6 mm and for undulatority factor higher than 0.3-0.4, the full losses by radiation are limiting successful operation (see Tables 5-7).

For successful functioning of conversion system it is necessary to shift to the longer undulator period.

In its turn this allows to make aperture diameter bigger too and, hence, reduction in the wall irradiation.

The losses in the number of the quantas radiated needs to be compensated the length of undulator however.

CHAPTER 3. COLLECTION OF PARTICLES AFTER THE TARGET

§1 Conditions for maximal yield of particles with definite polarization.

Conversion system must contain the following elements aligned behind undulator: the target, made from material with high atomic number where conversion occurs, short focusing lens for focusing and collecting the particles of the type selected (electrons or positrons).

The lens must be located as close to the target as possible with appropriate focusing distance.

Further on the separation system is going. It serves for energy differentiation and for passing by the particles with highest energy, accelerator providing to the particle selected the energy what is necessary for further injection into the damping ring. This ring lowers emittance of the beam captured. The are also some elements for spin operation at different points along trajectory.

We considered here the separation system combined with the focusing one, where short focusing lens and diaphragm sere for these purposes. Thus the particles with low energy (and polarization) becomes over- focusing and captured by diaphragm. As it will be seen lower, utilization of lithium lens instead of solenoidal one is principal from the point, that this lens separates electrons from positrons from the very beginning.

Indeed, the solenoidal lens is focusing the particles independently on its charge sign. In this case unnecessary particles penetrating into accelerator structure stimulating sparking when decelerated and touching the walls.

It is evident that with decreasing the diaphragm diameter, average degree of polarization is growing in accordance with the emittance lowering, all on expense of decreasing the number of the particles, however.

A desire to utilize as much photons from undulator as possible, yields a necessity to have the target as thick as possible.

Really, the cross section of the pair creation normalized to the length passed in terms of radiation length τ / X_0 goes (see Chapter 1)

$$\sigma_{pair} \cong 4Z^2 \alpha r_e^2 \cdot \left(\frac{7}{9} \ln \frac{183}{Z^{1/3}} - \frac{1}{54} \right) \sim \frac{7}{9} \frac{\tau}{X_0} \frac{N}{A},$$

$$\frac{d\sigma}{\varepsilon_+} \cong \frac{\sigma_{pair}}{\varepsilon_\gamma}.$$

So the number of created positrons goes to (N_γ stands for the number of the photons per particle)

$$N_+ \cong N_\gamma \cdot \frac{7}{9} \frac{\tau}{X_0}.$$

Energy distribution for the photons over spectrum defined by the formulas represented in the second Chapter

$$\frac{d\dot{N}_\gamma}{d\tilde{\omega}} = \frac{d\dot{N}}{d\varepsilon_\gamma} 2\Omega\gamma^2$$

$$\frac{dN_\gamma}{d\varepsilon_\gamma} = I \frac{6}{(2\Omega\gamma)^2} F(\varepsilon_\gamma),$$

so the energy distribution goes to

$$\frac{dN_+}{d\varepsilon_+} = \frac{\alpha P_\perp^2 L}{\gamma^2} \frac{7}{9} \int F(\varepsilon_\gamma) \frac{d\varepsilon_\gamma}{\varepsilon_\gamma}.$$

The number of the particles, having maximal energy, has a tendency to be a zero. So, for having maximal yield of particles, it is necessary to use the target of maximal thickness.

This requirement contradicts a desire to have the minimal energy and angular spread, however.

If $\tau[g/cm^2]$ stands for the thickness of the target, made from material with radiational length X_0, then the angular spread due to multiscattering goes to

$$\sqrt{\overline{\vartheta^2}} = \frac{21}{pv}\sqrt{\frac{\tau_{eff}}{X_0}} \ .$$

As one can see the angle is growing proportionally $\sqrt{\frac{\tau_{eff}}{X_0}}$, meanwhile the number of positrons grows proportionally to the thickness τ_{eff}/X_0.

The energy spread goes to

$$\frac{2\tau_{eff}}{\omega - 2m}[MeV], \qquad \tau_{eff} = \frac{\int_0^{\tau}(\tau - x)\cdot x \cdot dx}{\int_0^{\tau} x dx} \cong \frac{\tau}{3}.$$

So the choice of the thickness is the compromise between angular spread allowed by collection system and the full number of positrons desired.

In general, for obtaining the conversion coefficient N_+/N_0, it is necessary satisfy the following condition

$$N_\gamma \cdot \eta_p \eta_\varepsilon \eta_\varphi \geq \frac{N_+}{N_0},$$

where $\eta_p \cong \frac{7}{9}\frac{\tau}{X_0}$ is an efficiency to the pair conversion, $\eta_\varepsilon = \frac{\Delta\varepsilon}{\varepsilon}$ is

the share of the collected particles in energy space, η_φ is the phase volume collected. The particles leaving the target within angular spread $\sqrt{\overline{\vartheta^2}}$. Namely, for reduction of this spread the short focusing lens utilized here.

The combination of the target and short focusing length is a common block for any conversion system.

In particular, at SLC the solenoid with flux concentrator is planned for usage as a short focusing lens. This, as calculated, will give conversion efficiency ~2.5, while the accelerating gradient is 50 *MeV/m* [16].

The number of positrons and electrons behind the target is about the same (the difference defined by Compton effect, cross section for which $\sim \pi r_e^2 \frac{m}{\omega}\left(\ln\frac{2\omega}{m}+0.5\right)$ is small for $\frac{\omega}{m}\equiv\frac{\hbar\omega}{mc^2}=20-30$).

In accelerating structure the longitudinal magnetic field with the strength ~1-2 T is used for focusing. Some additional measures preventing interaction of the bunch with the structure is applied here, such as increase in diameter of diaphragm [17].

Accelerating gradient must be as high as a few hundreds *kV/cm*. At present, the gradient about 70-100 MeV/m is possible [18].

Spin direction for each particle defined by the process of creation. Multiple scattering does not diminish polarization, as the *length of depolarization* during scattering with radiation is [10]

$$L_{dep} \cong \frac{2X_0}{1-\frac{(\vec{\varsigma}\cdot\vec{v})^2}{3}} \approx 3X_0,$$

and in our case the thickness chosen to be $\sim\frac{X_0}{2}$. Effectively, the number of positrons created is growing linearly with the distance in the target.

So one can estimate the effective thickness for definition of depolarization to be

$$\tau_{eff} \cong \frac{t}{3} = \frac{X_0}{6}.$$

After acceleration, the phase volume decreases proportionally to the increase in momentum *p*, and average value of polarization still defined by the process of creation.

If one suggests the acceptance value $\eta_\varphi \sim 1$, share of energy acceptance $\eta_\varepsilon = 0.3$, efficiency to the pair conversion $\cong \frac{7}{18}$, then the number of the primary photons per each initial particle must be about $N_\lambda \cong 10$.

If this number of quantas with necessary polarization is fixed, i.e. for the fixed undulatority factor, then the full length of undulator can be defined from these numbers.

§2 The number of the particles with definite polarization

Results of detailed calculations carried out for the number of positrons N_+ obtained after conversion were represented in [49]. The modeling there was done numerically.

In the code, the radiation and number of quantas were calculated with the formulas represented in [9] (see Chapter 2.), calculations carried using Monte-Carlo method. Depolarization caused by radiation was taken into account too.

Following focusing, separation and acceleration up to 50 *MeV* were taken into account too. With the help of this code all parameters of conversion system were optimized for maximal yield with maximum polarization.

The same code used for calculations in [26].

As a result of optimization, it was found, that efficiency of conversion for the energy of primary beam $\varepsilon_0 \cong 150\,GeV$, λ_0=0.6 *cm*, *L*=150*m* and $P_\perp^2 = 0.1$ can be characterized by one single particle per each initial one in the energy interval $\Delta\varepsilon = 8MeV$, transverse emittance 2 *MeV/c* degree of polarization ς_1=0.65. The particles were collected from the target and accelerated up to 50 *MeV* level with gradient $\frac{d\varepsilon}{dz} = 0.5$ *MeV/m* in guiding solenoidal field $H_\parallel$ =2 *T*.

Gradient in the lens was ~150 *kG/cm*, diaphragming was carried by input iris having diameter 20 *mm*.

Spectrum of energy and distribution of polarization are shown in Fig. 16. As it was mention, collection of particles from the target was done with the help of short focusing Lithium lens, located close to the converter, Fig.17. The length of this lens was modeled to be 6.5 mm, diameter of Lithium rod 7 *mm*, flanges made from Beryllium having thickness 1 *mm* and 0.5 *mm* the input and output ones respectively.

The density of the particles at the out of converter goes o be 6 pairs per each initial one in the circle having diameter 0.5 mm.

Total number of initial particles in the bunch with population 10^{12} (i.e. for 10^{13} at the out of target) produces the energy deposition ~300 *J/g* per pulse, what inevitable case destruction of the target.

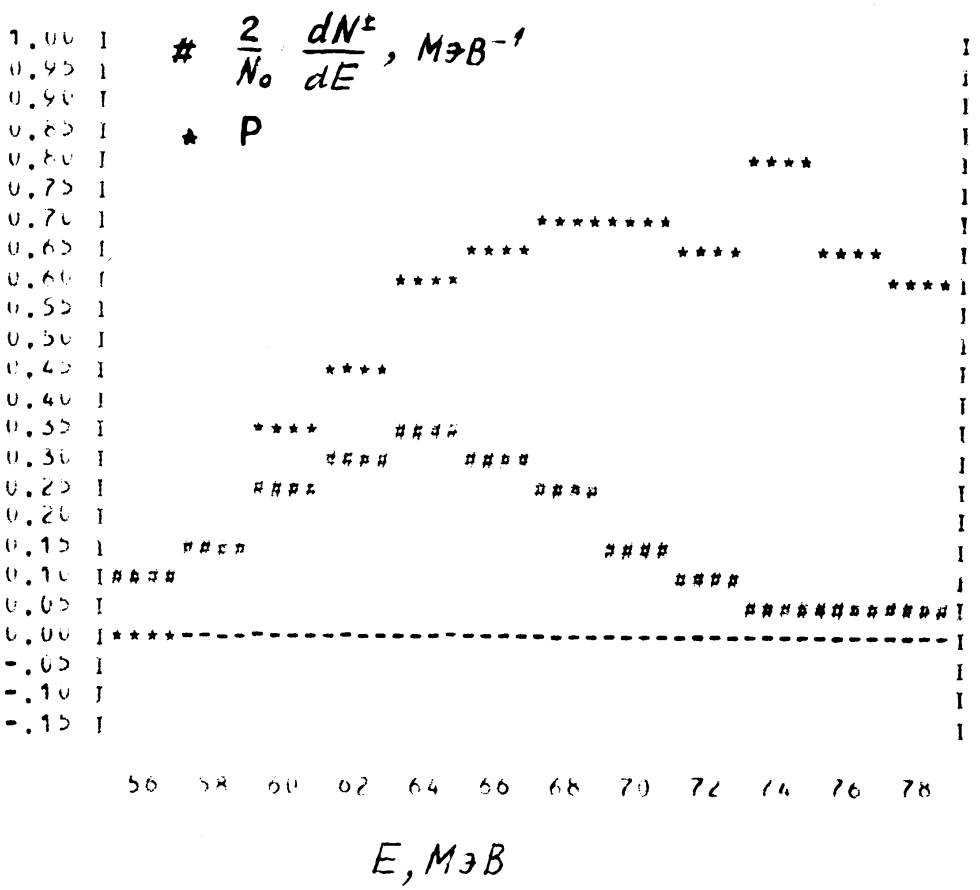

Fig.16 Spectrum and distribution of degree of polarization after collection from the target, acceleration up to 50 *MeV* with gradient 50 *MeV/m*. Geometry of capture is shown in Fig. 17.

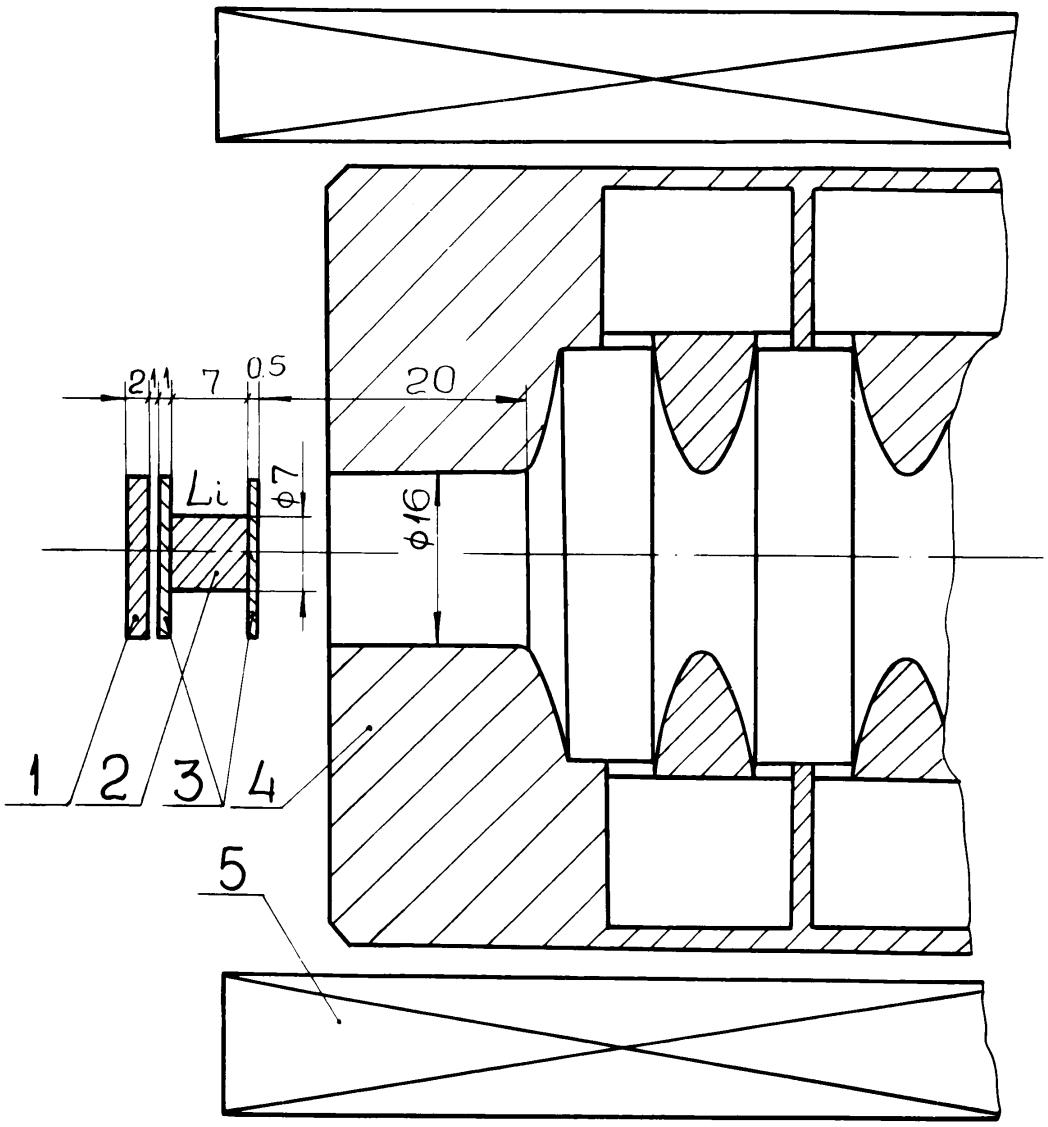

Fig.17. Conversion block. 1 is the target, 2 is the lens with liquid Lithium, 3 are the Beryllium flanges, 4 is accelerating structure, 5 is the focusing solenoid. (Dimensions are given in *mm*)

§3. Possible design of targets.

As it was shown above, for making the energy selection effective, it is necessary to have the number of positrons coming out directly from the target, few times (5-10) bigger than the initial number of particles entering the undulator.

By this way it is possible to reach the necessary level of polarization for positrons and electrons collected from the target,

All this yields extremely hard conditions for the target-converter.

So, if the area of the spot illuminated by quantas is *S*, then the temperature of the target goes to $\Delta T = \frac{2N_+ \cdot 2}{c_p S}$, and temperature difference between the front and back surfaces are about the same.

For the parameters under discussion, the temperature goes to

$$\Delta T = \frac{2 \cdot 2 \cdot 10^{13} \cdot 1.6 \cdot 10^{-19} \cdot 10^{6}}{c_p 10^{-2}} \sim 3000^{o}.$$

The average power however goes to 50 W for repetition rate 10 *Hz*.

For targets it is recommended to choose materials which are resistant to the pulse heating. Also there is no data in literature about properties of materials under this level of energy deposition, also there are few installations around the world operating (or planning to do this) with close parameters.

Promising circumstance is that the time of action of the load is extremely short (of the order of $\sim 10^{-11}$ *sec*) compared with the relaxation times for the target material.

This may allow operation during a single pulse, however.

Let us consider two possible variants –the liquid metal target with Mercury [20] and rotating disc target [16,21].

Rotating Tantalum-Tungsten target supposed to be in use for NLC installation [16].

At this installation, the conversion is going at the energy of primary beam ~ 33 GeV , with intensity ~10^{10} particles per pulse and repetition rate 180 Hz. The target has a thickness about 3 radiational lengths and the beam is focused onto the spot with diameter 1.2 *mm*.

The target represents by itself the round disc, rotating in vacuum, with the tubing for cool down inside the body of target. The beam falling onto peripheral part of the disc, creating about 60 pairs of particles in full spectra per each initial electron. Here the energy deposition occurs at the full length of the target as the secondary particles as well as by initial ones in addition to these first ones. The shower becomes wider during developing due to multiscattering process.

As a result, for the average energy deposition about few kilowatts, the heating per pulse developing to be ~380^{o} only.

For the focusing, the solenoidal field with flux concentrator used here. Maximal field value in this concentrator goes to 50 *kG*, dropping down as a square of distance from the target with the characteristic scale ~10 *cm*. Further on the field is continued with solenoid with accelerating structure inside giving the gradient ~50 *MeV/m*.

Similar design of rotating target is used in SACLE [21]. Here however, the gold used as a target material, as having much higher plasticity. The total mass of the gold ring, having dimensions $64\times0.4\times0.4$ cm^3, goes to be 0.67 kg. The ring brazed to the water-cooled disc, rotating with angular frequency 30 *rpm*, so the linear speed of the target goes to 1 *m/s*. So the average power deposition in the target by the beam having 1-2 *mm* in diameter, goes to be 25 *kW*.

The focusing of primary beam and collection of secondary particles is caring by multi-turn lenses.

In Fig.18, two variants of conversion block are represented. They can be used in VLEPP installation [20].

Variant 1 uses the Mercury target, variant 2 – rotating Tungsten target.

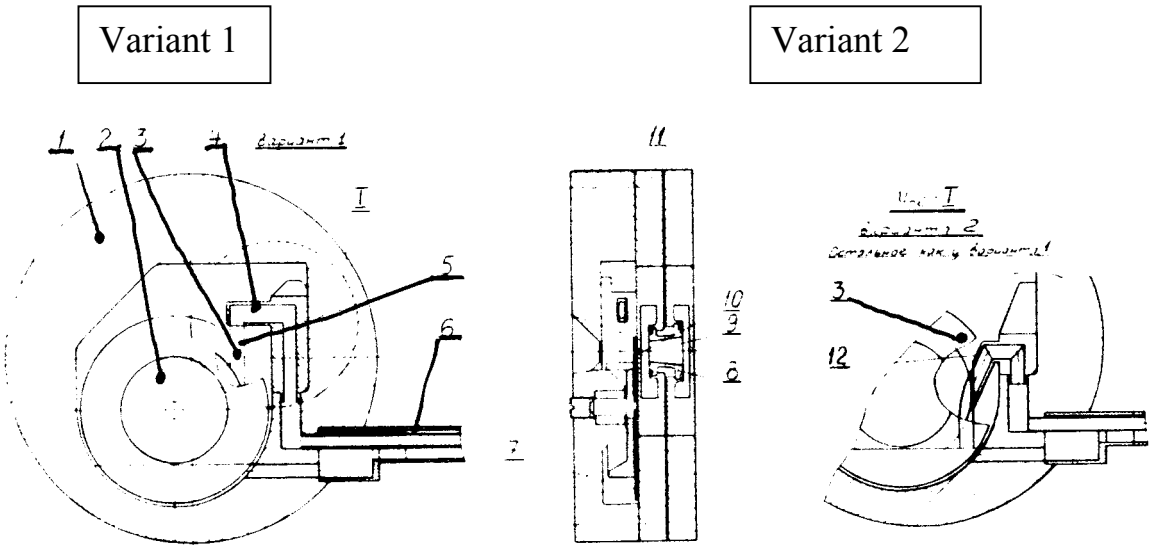

Fig.18. Conversion block with Lithium lens.

Variant 1. 1 is titanium corps, 2 is the teethed wheel, 3 is the target focusing point, 4 is the nozzle, 5 is the Mercury jet, 6 are the feeding tubes, 7 is secure titanium foil, 8 is the conically shaped lens, 9 is the volume with liquid Lithium, 10 is Beryllium made flange, 11 are the current leads made from Titanium.

Variant 2. 3 is the target focusing point, 12 is the nozzle.

The Mercury target represents by itself a jet, formed by flow from special nozzle 4, forming the shape of the jet. The Mercury circulation supported by magneto-dynamical pump [22]. The radiational length in the Mercury goes to be 4.8 mm, so the thickness of the jet in direction of the beam pass must be 2.4 mm. The same jet, falling to the teethed well, forcing rotation, which is also transferred to the disk 7 attached to the wheel. This disk 7 made from Titanium foil and serves for prevention of the lens end from destruction by the products of explosions at the out side of the jet.

As there is no any special requirements to the foil surface, it is possible to operate with this screen with significant damage of its surface.

It is required by focusing process, that the target must be located close to the focusing lens.

Variant 2 uses the target made from Tungsten where the jet just rotates the screen foil.

The focusing of secondary particles is done by Lithium lens. Usage of these lenses demonstrated theirs reliability when used at installation VEPP-2 and VEPP-3 [23, 24].

The focusing here is going by interaction with the current running inside the lens body. The focal distance f for this lens can reach for 20 MeV positrons the value

$$\frac{1}{f} = \sqrt{k}Sin(l\sqrt{k}), \qquad k[m^{-2}] = \frac{3G[kG/cm]}{p[GeV/c]},$$

$$G = \frac{8 \cdot 10^{-1} \times I[kA]}{d^2[cm^2]},$$

where I stands for the full current, d is diameter of Lithium rod, l its length. For example, for current 100 kA, the focal distance for the lens having diameter and the length about the same~1 cm, goes to be 0.8 cm for the beam energy ~18 MeV.

Radiation length of material of the lens is (see Chapter 1) 83 g/cm^2, what corresponds to the length 156 cm, so the scattering in material of the lenses goes to 0.06 rad for 20 MeV beam while it passes full distance inside lens. This angle must be compared with angle $\varnothing/f \cong 0.1$, where $\varnothing$ stands for the diameter of secondary particles beam, and f stands for the focal distance of the lens.

So scattering inside lens can be neglected.

For operation in the installation VLEPP the liquid Lithium usage is suggested similar to what was done for the similar purposes for linear accelerator in Kharkov [20].

Pumping of Lithium in closed loop allows an easy solution for cooling problem.

As one possible measure, the increase of the hot spot diameter on the target can be considered by introduction of the angular spread while the beam is passing through the different parts of undulator.

The increase in spot diameter three times yields an increase in phase volume three times also, but the temperature drops ten times. Resulting phase volume 6 MeV/c×cm or $6/1100 = 5.45 \cdot 10^{-3}\, cm \cdot rad$ at injection energy 1.1 GeV is inside the one can be captured into damping ring-cooler $\cong 10^{-2}\, cm \cdot rad$ [25].

§4. Conversion at complex VLEPP. Spin dynamics at complex.

A) General scheme of conversion system. Spin dynamics.

Let us consider the scheme of conversion system VLEPP, represented in Fig. 19 [4].

The beam after interaction in the collision point MB, deflected by kicker K1 vertically. Further on, with the help of two bending magnets M1 and M2 it is directed to the side and goes into undulator O, where the gammas are radiated. Further on with the help of weak magnet M3 it is deflected for usage in fixed-target experiments.

Design of bending magnets must guarantee reliable operation under exposure to the synchrotron radiation and provide achromatic bend for the beam [4].

Gamma quantas hitting the target MK where they generate positrons.

Right after the target the short focusing lens Л is located and further on an accelerating structure УС is located. This intermediate accelerator gains the energy to the level 1.1 GeV. At this energy the angle of the spin rotation is 2.5 times higher, than corresponding angle for momentum [31].

After passage through de-bunching magnet MP, spin becomes directed across the vector of momentum. Further on along the beam trajectory, the demodulator D and spin rotator CP are installed. Spin rotator transfers the spin vector into vertical direction. The last one is equilibrium in the damping ring HK.

Demodulator is the linear accelerator, phased so that the center of the bunch passes it at the moment of absence of accelerating voltage. By this way the energy spread becomes reduced, as by passing the de-bunching magnet the correlation of position along the bunch and the energy is established [28]. During this procedure the energy density

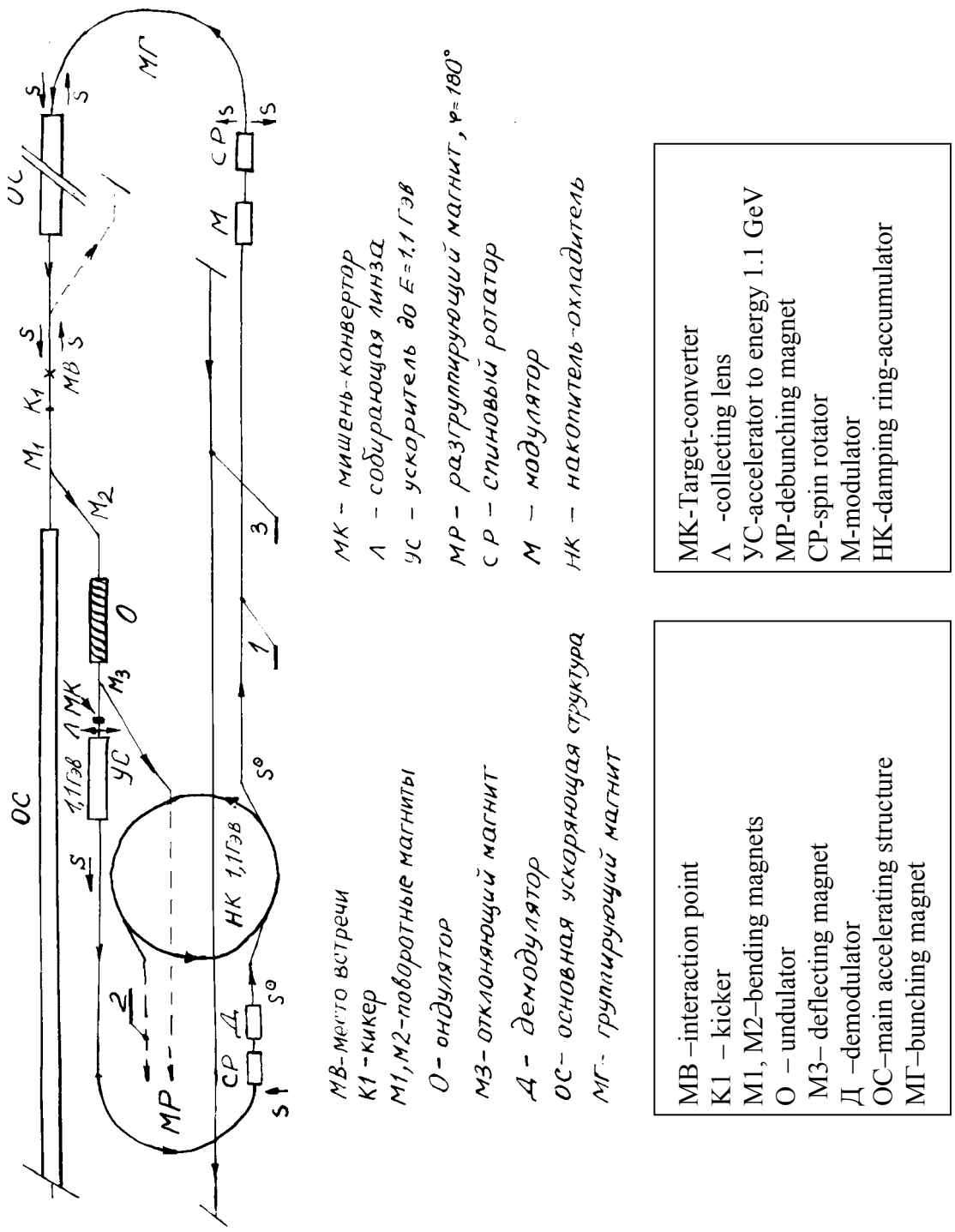

МВ- место встречи
К1 - кикер
М1, М2- поворотные магниты
О - ондулятор
М3- отклоняющий магнит
Д - демодулятор
ОС- основная ускоряющая структура
МГ- группирующий магнит

МК - мишень-конвертор
Λ - собирающая линза
УС - ускоритель до E=1,1 Гэв
МР - разгруппирующий магнит, φ=180°
СР - спиновый ротатор
М - модулятор
НК - накопитель-охладитель

МВ –interaction point	МК-Target-converter
К1 – kicker	Λ -collecting lens
М1, М2–bending magnets	УС-accelerator to energy 1.1 GeV
О – undulator	МР-debunching magnet
М3– deflecting magnet	СР-spin rotator
Д –demodulator	М-modulator
ОС–main accelerating structure	НК-damping ring-accumulator
МГ–bunching magnet	

Fig.19 . Detailed scheme of conversion system.

becomes increased, what is desirable for high operational energy of VLEPP.

As it was mentioned in paragraphs of previous Chapter, that the energy density of the particles is inversely proportional to the square of initial energy, so for the energy change from 250 to 500 *GeV*, it will be necessary to increase four times the energy, transferring to the edge particles.

According to calculations done above, this will go to ~50 *MeV* for the wavelength about one meter.

After injection to the damping ring, the beam decreases its emittance to the revel required for injection into the main structure of VLEPP.

Further on, the beam extracted either to the channel 1 or 2 to the beginning of main structure OC and passing by the spin rotator CP, which transfers spin direction into horizontal plane. After that, the modulator M is on the way (copy of demodulator).

For operation with opposite polarization at interaction point MB, the spin transferred from vertical direction (equilibrium in the ring) to the horizontal one with angles $\pm 90^{o}$ to the plane, which is rectangular to direction of propagation. Further on, after passage 180 –degree bend, spin becomes turned either to direction of propagation or in opposite direction. During this bend the bunch becomes compressed too.

For vertical polarization required, CP either is turned off or making 180^{o} - rotation in vertical plane, giving opposite polarization.

For spin rotation is possible to use longitudinal magnetic field. The field integral value required is 57.5-kG cm for electrons (positrons) at $\varepsilon = 1.1 GeV$. In reality the spin rotator has additional quadrupole lenses for elimination of coupling of transverse emittances [4].

As it was shown in [29], depolarization at interaction point due to

impact with incoming bunch, is about ~5%, and we'll neglect this effect.

Really, the field of incoming bunch can be evaluate by the following

$$E_x = E_0 \frac{x}{\sigma_x}, \qquad E_y = E_0 \frac{y}{\sigma_x}, \quad \vec{H} = \vec{\beta} \times \vec{E},$$

which for $\sigma_x = 20\mu m$, $\sigma_y = 0.1\mu m$ goes to $E_0 \sim H_0 \sim 1MG$. In these fields the momentum rotates by the angle

$$\Delta\varphi_P \cong eE_0\sigma_z / pc \cong E_0[kG] \cdot \sigma_z[\mu m]/15.$$

Vector of spin rotates by $\Delta\varphi_S \cong \mu'\gamma\Delta\varphi_P$ and depolarization goes to

$$D \cong \tfrac{1}{2}(\Delta\varphi_S)^2 \cong \tfrac{1}{2}(\mu'\gamma\Delta\varphi_P)^2.$$

Above, the so-called one side conversion system was described. In this scheme the generated positrons are going into the same main accelerating structure OC from which the primary bunch was obtained.

Other possibility deals with cross conversion, when the high-energy bunch is taken from opposing structure. In this case the bunch extracted from damping ring goes to direction 2 in Fig.19, with following spin rotation, energy modulation and bunching similar to how it was done for direction 1. Channel 3 transfers the bunch prepared in the second ring, not shown in the picture, where the bunch is prepared in simultaneously with the firs one.

New bunch appears in the damping ring by the time required for the bunch to pass the bunching system, main structure, undulator, de-bunching magnet, i.e. in ~10 microsecond. The bunch remains in the ring during the time defined by the damping time, i.e. about few milliseconds.

In [30] the model of damping ring of this kind described. This ring creates the bunch having the phase volume $\varepsilon_x \cong 10^{-6} cm \cdot rad$, $\varepsilon_y \cong 10^{-8} cm \cdot rad$ for radial and vertical directions respectively, with the bunch population 10^{12}.

B). Possible modifications

According to [31], there is a possibility for obtaining the longitudinal polarization at all length of straight section of a damping ring equipped with Siberian snake. When the damping ring of this kind is used, the injection becomes simplified, as they're no more necessity for spin rotators. From the other hand, all gravity is now transferred to the compensation of coupling of transverse emittances. The last one is strictly limited by value 10^{-2}. As a result of consideration of all possible variants, the scheme described above was chosen as more relaxed.

As it follows from §1, the probability of interaction of γ-s with the target goes to ~7/18 for the target having thickness $\sim\frac{1}{2}X_0$. As a result, after passage the first target there is a possibility direct the beam of γ-quantas to the second target and convert them into positrons there again. Each secondary bunch accelerated to the slightly different energy and combine these secondary bunches in the longitudinal phase space with the help of bending magnet [32]. Further on, the bunches are passing an accelerating structure, phased in such a way, that the bunches equalizing its energy. For successful operation of this scheme the energy spread must be small, compared with the energy difference. For the energy distribution considered above this goes to ~10 MeV, what is real.

This type of target split can be also used for reducing the temperature in each target, if the number of targets is fixed.

Evidently, the particles of opposite sign of charge can be collected from different targets also.
Modification of scheme for operation with few targets can be done in an evident way. Let us consider one of these possibilities, represented in Fig. 20.

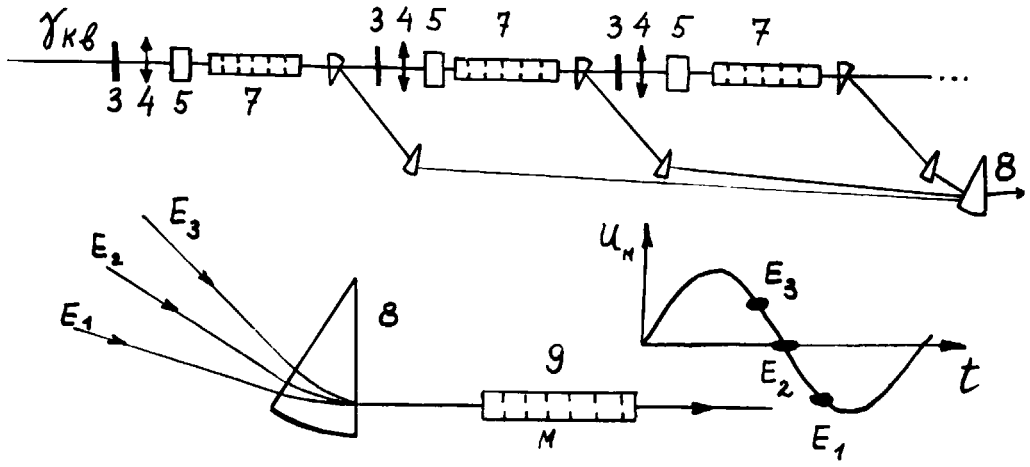

Fig.20. Operation with few targets. Comments are in the text.

In this figure it is shown, how the bunch of γ-quantas hits the first tharget, marked as 3. Behind this target, similar to operation with single target, the short focusing Lithium lens 4 and diaphragm 5 and so for all targets. The accelerating structures, marked by 7 accelerate secondary bunches to different energy, marked as E_1, E_2, E_3 as a sequence of descending values.

In the bending magnet 8 particles are running by equilibrium trajectories, corresponding to theirs energies and coming to accelerating structure 9.

This structure is phased so, that it equalizes the energy of these bunches.

C). Operation without polarization.

If there is no requirements for operation with polarized particles it is possible significantly increase the conversion efficiency for the same length of undulator, or decrease the length by increasing the undulatority factor value up to unity.

As a result the number of the photons radiated will be increased $\sim P_{\perp}^{2}$ and if the number is fixed, the length shrinkage goes in the same ratio coming to ~20 m.

Accordingly, the heat regime for the target-converter can be relaxed significantly, as the multiplication in particle's number at the outer side of the target now comes to about one pair of e^{+}, e^{-} per each initial photon only.

The number of secondary particles required for stationary operation can be adjusted in a simplest manner by tuning the field in undulator within small limits. It is possible, as the number of the particles is proportional to $\sim P_{\perp}^{2}$, while polarization practically does not change when $P_{\perp}$ changes within 3-5%.

So for the first stage undulator parameters come to the following numbers:

$$P_{\perp} = 0.33, \quad \text{L=150 } m, \quad \lambda_0 = 0.6cm .$$

Let us consider now some concrete variants for undulator design, which will be able to guarantee the operation with these numbers for the repetition rate not lower, than 10 *Hz*.

CHAPER 4. PRACTICAL DESIGNS OF UNDULATORS

§1. General questions associated with design of short period undulators.

Parameters of undulator have been chosen so that they give maximal number of quantas in fixed energy interval at the out of undulator.

Lowering period λ_0, while the fixed length of undulator is fixed, yields an increase in the number of radiated quantas. This lowering is limited, however, by the following factors:

First–by growing technological difficulties in manufacturing for small dimensions. Technology of assembling must provide the accuracy required for unperturbed passage through undulator, including small energy deposition by radiation to the large angle.

Second–by technical problems associated with exponential decrease of the field while approaching to the axis compared with the field value between the turns (for the fixed aperture). This forces to increase the current in the same proportion, this increase is limited, however by electro-mechanical destruction and melting.

Accuracy of alignment, mechanical tolerances and accuracy of passage inside chamber defined by the following parameters:

Field variation and its harmonics contest while shifting from the axis of undulator. This yields appearance of undesirable harmonics and widening of spectrum. This problem considered in [50]. As a result of considerations done there, it could be concluded, that for deviations in diameter and axial position of the order 0.1-0.2 mm this factors can be neglected.

Further on, while off axis passing the undulator, the particle can acquire angles in the fringe field of undulator forcing an increase in deflection and even hit of the walls. These questions can be answered after investigation the fringe fields out of regular part by measuring the field distributions in real construction.

As having mostly simple construction, an undulator with double helix with oppositely running currents was chosen as a basic one.

A). Modeling of dimensions and optimization.

The fields in undulator having the wires with rectangular cross section, can be calculated using scalar potential, created by thin helical tape as [34]

$$\psi(r,\kappa z-\varphi)=-\frac{8\pi\kappa r_0 I}{c}\sum_{n=1,3,5,\ldots}^{\infty}\frac{1}{\pi}\frac{Sin(\frac{n\kappa h}{2})}{\frac{n\kappa h}{2}}\begin{Bmatrix}K_n'(n\kappa r_0)\cdot I_n\\ I_n'(n\kappa r_0)\cdot K_n\end{Bmatrix}\times Sin[n(\kappa z-\varphi)]$$

where r,φ,z represent cylindrical coordinates, r_0 stands for the helix radius, $\kappa=2\pi/\lambda_0$, h is the gap between the wires, I is the current.

Potential for the thick layer calculated by summing the potentials from the thin ones. The fields can be found by the usual way

$$H_r=-\frac{\partial\psi}{\partial r};\ \ H_\varphi=-\frac{1}{r}\frac{\partial\psi}{\partial\varphi};\ H_z=-\frac{\partial\psi}{\partial z}.$$

For the field calculation with these formulas the computer code ONDJ was used [36]. In this code the losses, inductance and the voltage calculation were implemented also. The similar calculations were done in [49].

Results of calculations are represented in the figures below. In Fig. 21 it is shown the ratio H_0 / I –axis field to current ratio as a function feeding current –so called quality of undulator together with

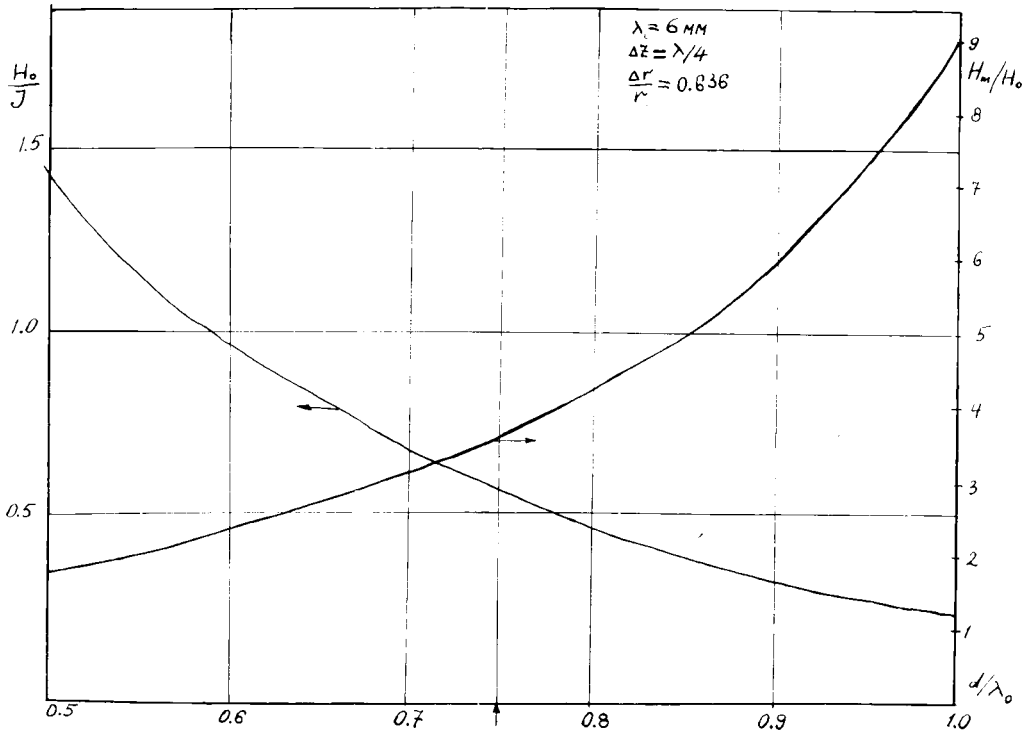

Fig.21. Characteristics of undulator as functions of the ratio of diameter to the period of the field variation.

H_m / H_0 –the field values between the turns to the field at the axis as a function of the ratio of diameter to period of undulator, d / λ_0. It was taken $\lambda_0 = 6mm$.

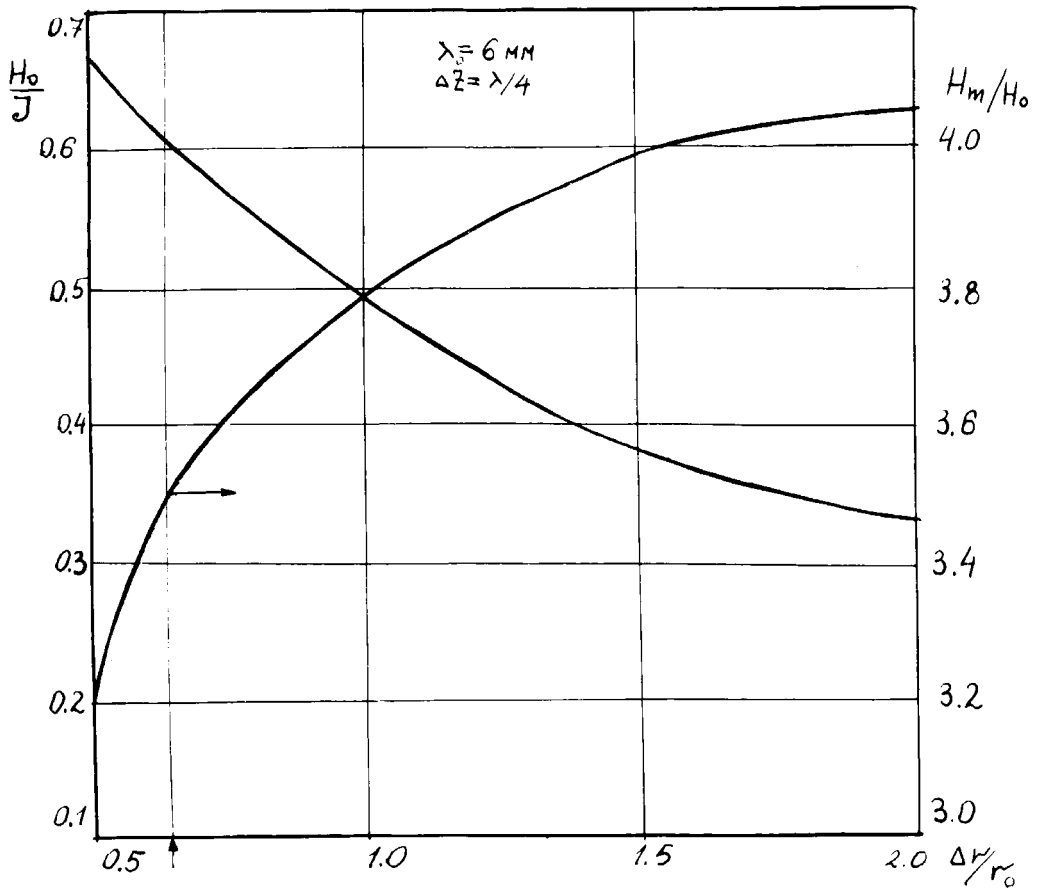

Fig.22. Characteristics of undulator as functions of ratio $\frac{\Delta r}{r}$.

In Fig. 22 the so called quality of undulator - H_0 / I and H_m / H_0 is represented as functions of ratio of radial thickness to the inner radius itself - $\Delta r / r_0$

The losses in the wire as a function of radial thickness for the fixed undulatority factor are represented in Figs. 23 and 24. It was taken for calculations, that d_0=4.5 *mm*, $\Delta z = \lambda_0 / 4 = \lambda_0 - h$ for the pulse duty time $t \cong 50 \mu s$.

One can see from the graphs, that the minimum of losses gives the conductor of rectangular cross section with side $\lambda_0 / 4$.

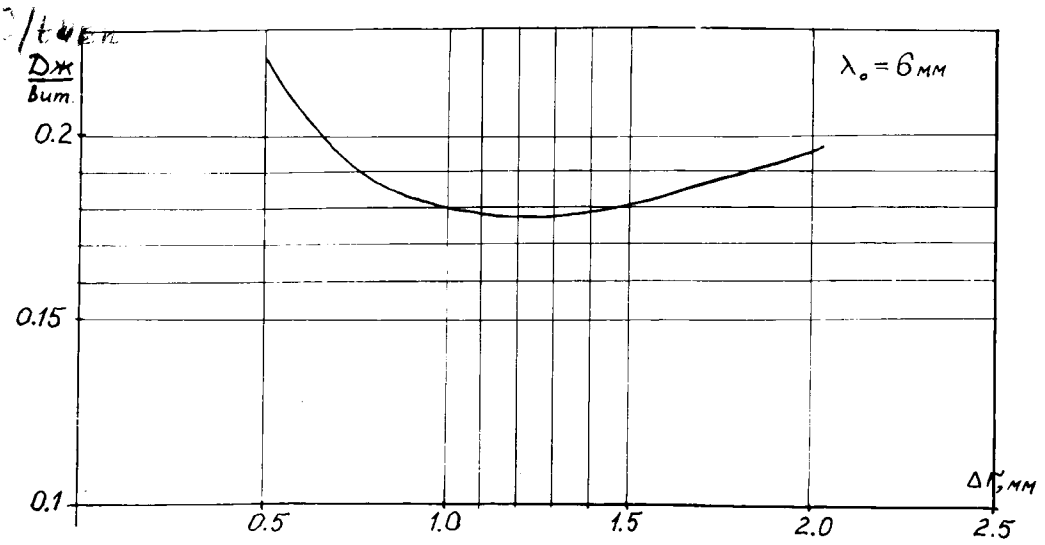

Fig.23. Active losses in turns for $\lambda_0 = 6mm$.

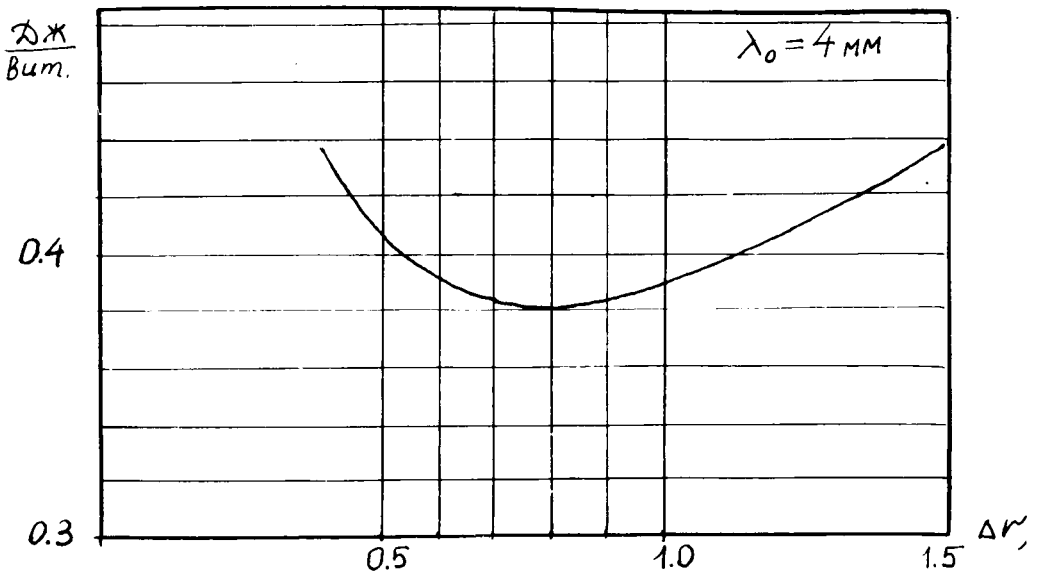

Fig.24. Active losses in turns for $\lambda_0 = 4mm$.

So one can see, that total losses per one linear meter going to be $\sim 2kW$ for the designed parameters. This power, by the way, dissipates in the wire having cross section $2 \times 2mm^2$, so the heating emerges as a serious problem here.

For investigation of correspondence of calculated fields to the measured ones, the scaled model in scale 7:1 was manufactured. With this model the way of end commutation were investigated also. The feeding of this model was done from high current power supply with current up to 200 A, entering the helix in the central part. The end commutation was done with the help of ring joint both conductors in a symmetrical way.

The measurements were carried with the Hall probe.

The probe motion, measurements and processing were carried automatically with the help of microcomputer “Odrenok” [35] made as a section in CAMAC crate. In this crate the other functional blocks, such as ADC, stepping motor controller, color monitors interface, DAC for the power supply operation were located too.

In Fig.25 there is represented for comparison the measured –1 and calculated-2 field distributions across the model.

In Figs. 26 and 27 there are represented the longitudinal axis field distributions for two rectangular orientations of the Hall probe. As one can see, the influence of the input current leads is negligible here.

Spectrum of longitudinal field was obtained as a sum of Fourier harmonics in longitudinal direction. The second harmonics runs below 2% level of the first one, the last-run below 0.5%.

The characteristic increase in the field value at the end caused by commutation. As the field integral over regular part equates to zero, so the resulting integral arises only at the ends, as a result the particle acquires the angle only at the ends.

With this model the integral was measured as a dependent of even or odd number of the turns and preference were given to the model with odd number of turns.

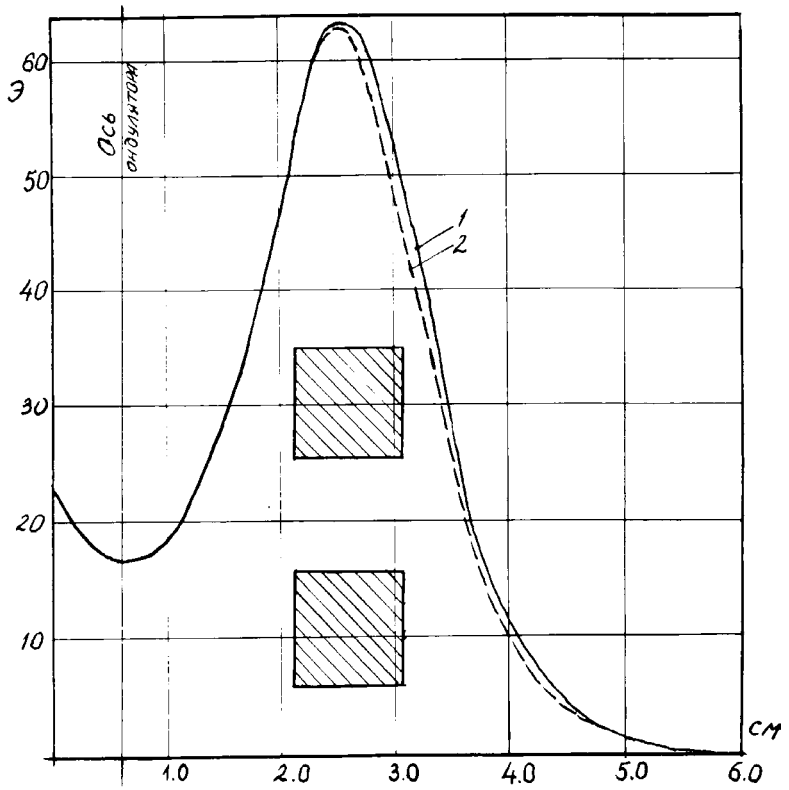

Fig.25. Field distribution in transverse cross section.

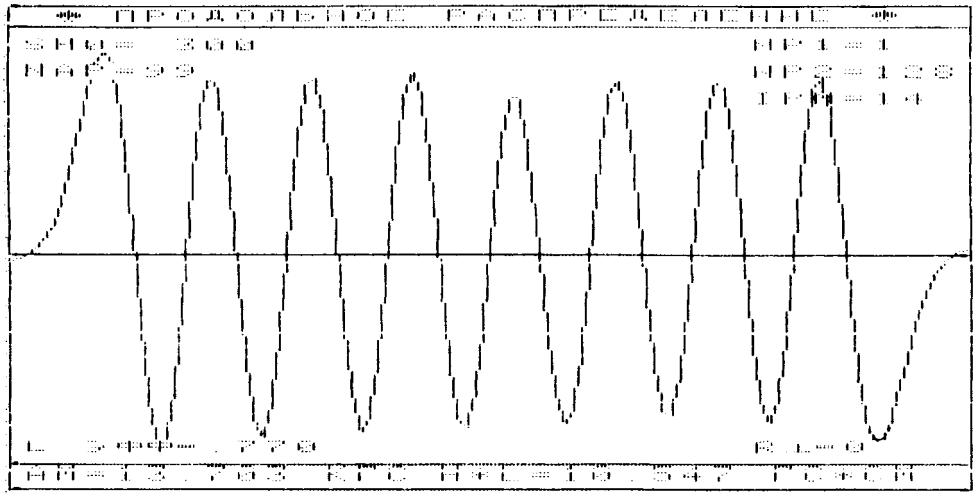

Fig.26. Field distribution at the axis of model, $\varphi = 0^o$.

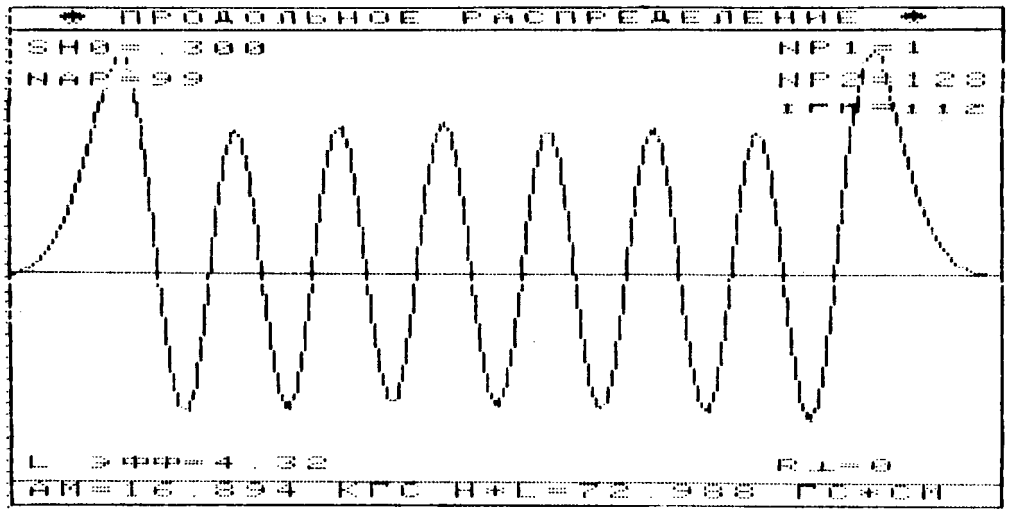

Fig.27. Field distribution at the axis of model, $\varphi = 90^o$.

Based on results of measurements the full-scale prototype was manufactured.

To satisfy designed parameters it is necessary to have $\lambda_0 = 6mm$, d=4.5mm, current, running in conductor with cross section $1.5 \times 1.5mm^2$, can reach 10 kA value.

The axis field 6000G must give the undulatority factor 0.34.

§2. Pulsed undulator.

A). Design of pulsed undulator.

Undulator (Fig.28) made as double helix 1 with period 6 mm, wounded with copper conductor having rectangular cross section $1.45 \times 1.45\, mm^2$. These helixes fixed between three rods 9,10 made from insulator, tightly squeezing the helixes.

The conductor was manufactured by rolling the annealed round wire of appropriate diameter between profiled rollers. Wounding was done around calibrated in diameter rod having diameter Ø=4.5 mm.

Two types of winding were investigated- first, the winding with necessary period of a single wire,- the second- winding four wires at the time with further usage only pair as a set. Both way were good four our purposes.

After the road was removed, diameter remained without change.

As the basing goes to the outer diameter of the helix, before removing the road, the helix windings were calibrated from outer radius between two metallic plates with fixed distance between them. Resulting spread in diameter at full length of the helixes was within 0.1 mm.

For fixation of period, in insulating rod 9 the grooves were milled, accommodating the wire.

These rods with squeezed helixes in between, were positioned in the corps 6, made with accuracy $\pm 0.05 mm$. The rod 9 squeezed to the helixes and further on to the rods 10 with the help of spring 11. Ceramic rods were fabricated. For make test of technology a bit simplified, G10 rods were used too.

Resulting basing of the helixes was done with accuracy not worse than 0.1 *mm*, what is enough for successful operation of the system.

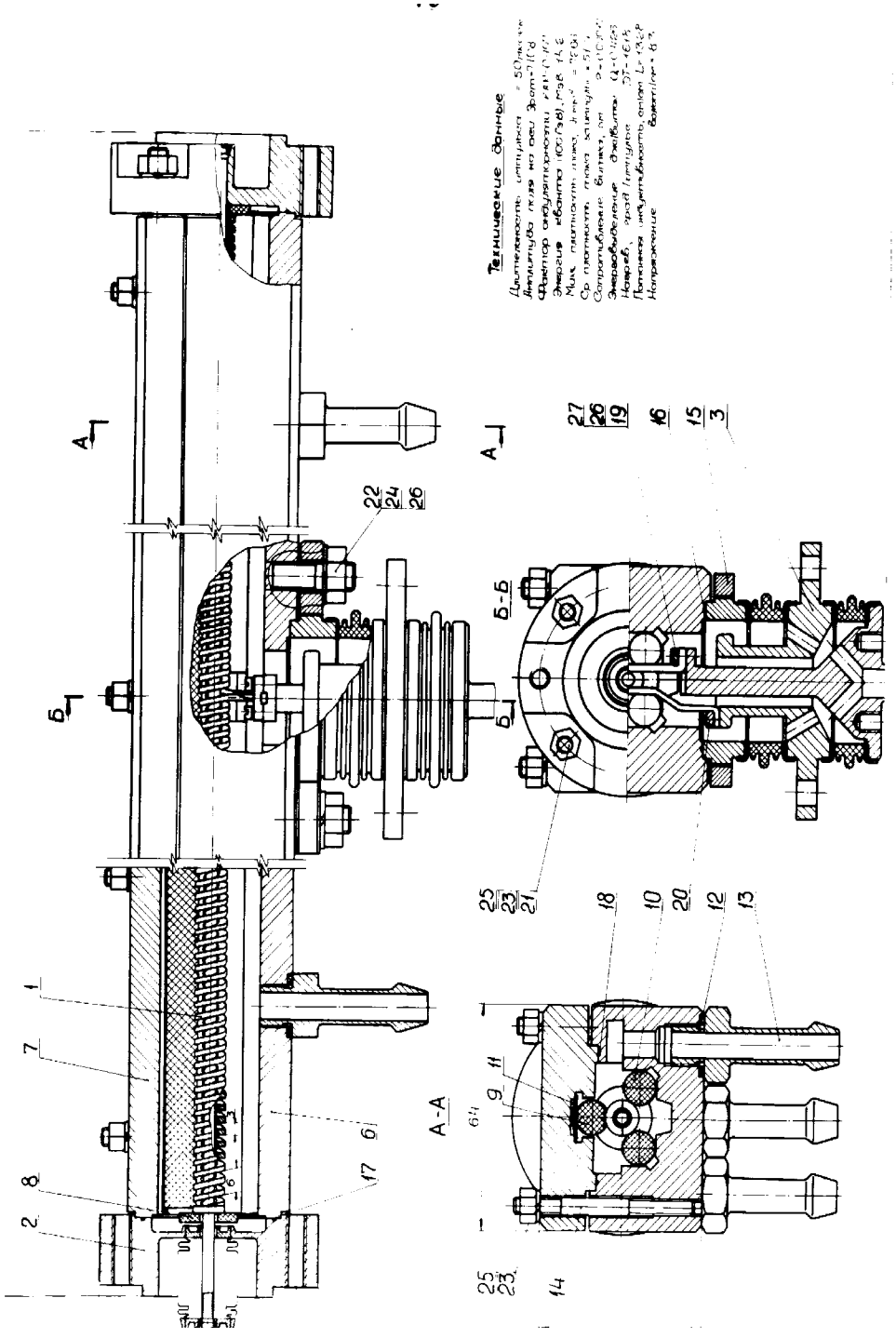

Fig. 28. Pulsed undulator design.

Inside helixes 1, the Stainless Steel thin wall tube with diameter 4*mm* is running for separation of the vacuum part, where the beam is going, from the inner part, where the water flows.

The water enters through the unions 13A, passing between the turns of the helix, and coming out symmetrically from both sides trough the unions 13.

Upper cover attached to the corps by threaded rods 14 with nuts with washes 23,24. These elements evenly distributed along the corps.

Indium wire 18 serves for sealing the inner volume of the corps. Flanges 2 also sealed with Indium wire 17.

The current, as it was mentioned, inserted into the helixes in the middle. It arranged as a coaxial 3 with transition into the break in one helix. Conductor is bend in the central part, and is attached to the contact places by the covers 26-27.

The feed-through attached to the corps 6 by studs 22,24,26 with rotatable flange 15.

Washes 8 made from insulating material serve for limitation of motion in longitudinal direction.

Attachment of flanges 2 to the corps done with studs, nuts, washers 21,23,25.

The Stainless Steel chamber has a thickness 0.2 mm, so it does not attenuate magnetic field. Insulation of chamber made with the polyamide film type Б[2] in four layers (the thickness of a single layer is 0.015mm.

When operated, the voltage between tube-chamber and the turns of helixes can reach 1.5 kV.

After assembling insulation was tested up to 2.5 *kV* with the help of high voltage Ohmmeter.

[2] Analog of Capton; comment added at translation.

The length of single section is 1010 mm.
Sections are mounted in pairs onto the common frame with intermediate station, as it is shown in Fig. 29.

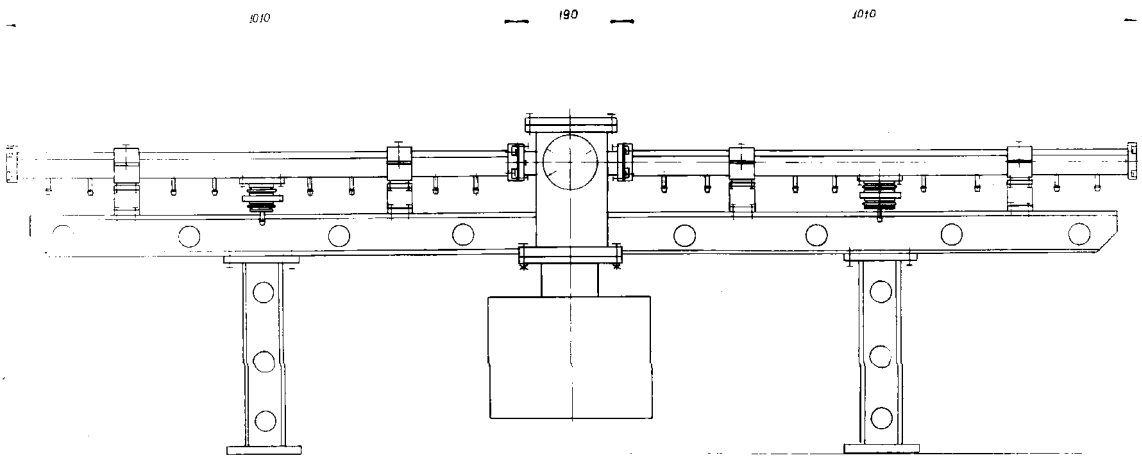

Fig. 29. Mounting of sections of undulator.

In Chapter 2, results of heating of undulator, providing by radiation of passing beam are represented for chosen geometry.

Among additional sources of radiation there are heating by imaging currents of passing beam and by eddy currents excited by magnetic field of helixes.

B). Wall heating by eddy currents and imaging currents of imaginary Currents of passing bunch.

For calculation of heating by image currents let us begin from expression for magnetic field value at the wall of the chamber having diameter *r*

$$J = \sum_m J_m \cdot Sin(m\omega t)$$

$$H_y(0,t) = \frac{1}{2\pi r}\sum_m J_m Sin(m\omega t).$$

Solution of diffusion equation one can obtain an expression for magnetic field inside the wall (*x* counted inside from surface, *y* –by tangent)

$$H_y(x,t) = \frac{1}{2\pi r}\sum_m J_m \cdot e^{-\frac{x}{\delta_m}} \cdot Sin\left(m\omega t - \frac{x}{\delta_m}\right)$$

$$\delta_m = \sqrt{\frac{2}{m\omega\sigma\mu}}.$$

Corresponding current density $j_s = \frac{\partial H_y}{\partial x}$ defines the loss [45]

$$\frac{dQ}{dl}[W/m] = \int \frac{j^2}{\sigma} 2\pi r dx = \frac{1}{4r}\sqrt{\frac{\mu}{2\pi\sigma}}\sum_m \sqrt{m\omega}\times J_m^2.$$

Taking for estimations $m\omega \approx \frac{2\pi c}{\sigma_z}$ one can obtain 100 *mW/m* (for the repetition rate 10 Hz), and this power can be neglected compared with the power of dissipation in wires, which is about 1500 W/m for the same repetition rate.

The losses associated with eddy currents are negligible too. Really, as a result of calculations, the field values at the places where

the chamber located, goes to ~16 *kG* for nominal field value at the axis. This field variation between wires is small (from 14.8 to 16.5 *kG*).

For the current running through the strip having width *a* ~equal to the distance between the wires, one can obtain

$$J = \frac{10^{-8}\omega H \delta a^2}{\rho},$$

where δ is the thickness of the chamber, $1/\rho$ is specific conductivity of material (Stainless Steel). Power of losses goes to

$$P = J^2 R = \frac{10^{-16}\omega^2 H^2 \delta a^3 L}{\rho} \sim 5 \text{ W}$$

where *L* is the length of the strip for one period

$$L = \sqrt{\pi d^2 + \lambda_0^2}.$$

So one can see, that main input in heat deposition is going from active losses in wires.

For circulation of water washing the turns of helixes, an autonomic system was used. This system includes hydro-pump and radiator acquired form serially fabricated UHF calorimeter M3-45. The system included also the thermo-pair, which was used for measurement of average heating. Double distilled water was used for cooling. Specific resistance of this coolant was ~1 Ohm cm. Maximal flow was measured as ~0.1 Liter/s defined by power of the pump.

B). Result of testing.

At the first stage the measurements were carried with DC current.

Usage of AC current provides some difference compared with feeding by AC, as the skin depth for 50 μs pulse goes to 0.6 mm. Taking into account, that conductor has rectangular cross section $1.45 \times 1.45 mm^2$, this effect was neglected.

With the help of power supply in hand it was possible to reach the current 90 *A*. i.e. the current density about 50 A/mm^2. The voltage was 5.75 *V* there. So the resistance was 0.064 *Ohm* and power –515 *W*, which is three times lower, than nominal for 10 *Hz* repetition rate.

Cooling system fully supports the operation of undulator there. Here the power meter was tested also. This was done for later measurements with pulsed current at nominal amplitude.

Longitudinal distribution was measured with Hall probe, moved inside chamber (3.6 *mm* in diameter) by long copper stock with help of stepping motor. That was basically the same equipment as used for measuring with models.

It was important to provide precise absolute movement of stock, as period of the field variation is small by itself. Keeping step not accurately when measuring spectral components of longitudinal distribution, it is possible to introduce unreal harmonics in spectrum. Variation of step within $\pm 0.01 mm$ was done for control.

The field distribution measured in 128 points along the length within two periods of field variation (with additional measurements in random places along undulator length) and automatically transformed with FFT into spectral distribution. That was operated under control of computer code.

As a result it was obtained that amplitude of second harmonic in regular part of undulator, averaged over its length, obtained there was

Less than 4% if normalized to the first one, the others not higher, than 1.5%.

Main attention was paid to the field distribution at irregular parts of

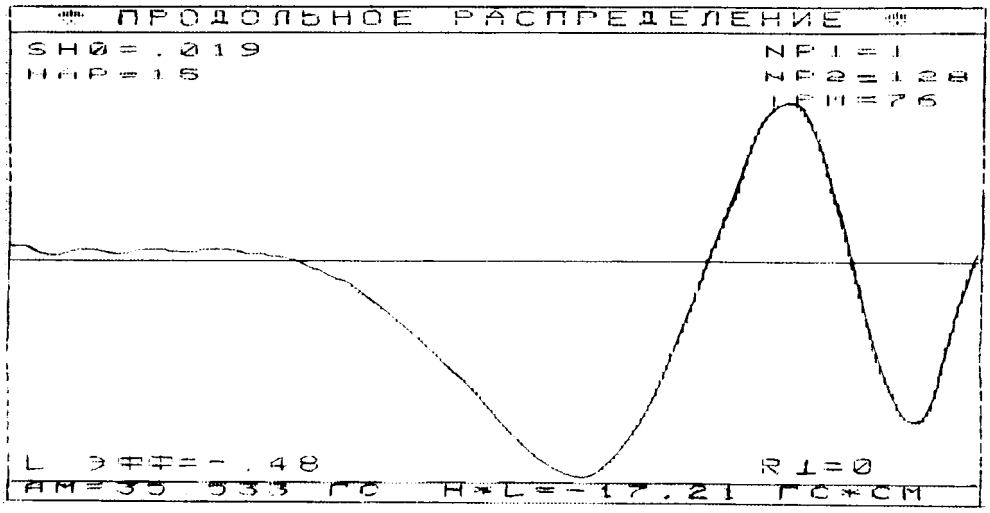

Fig 30. Field distribution at the end, $\varphi = 0^o$.

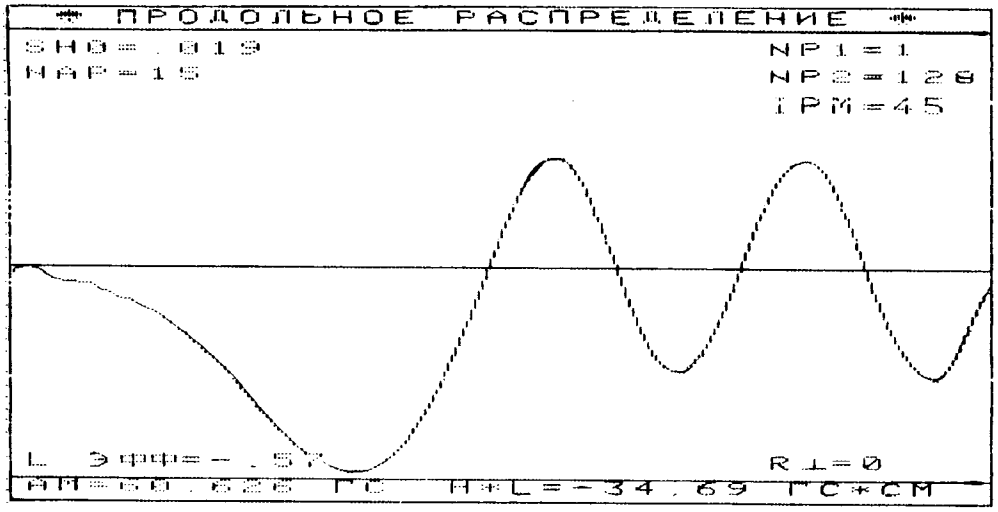

Fig 31. Field distribution at the end, $\varphi = 90^o$.

the helix, i.e. at the end and in the place where the current leads are attached to the coils.

In Figs. 30 and 31 there are represented the field distributions at the end of undulator for two rectangular orientations of the Hall probe. The feeding current was 52 A here. In Fig. 31 three half periods are represented; the same ones are present in Fig. 30.

Integrals for the first (negative) half wave go to –34.7 and –18.6 *G* respectively. The field amplitude in regular part is 31G, while calculated is 30 *G*. The ratio H_0 / I goes to 0.6, so for the field level 6000 *G* (giving undulatority factor =0.34) it is necessary to deliver the current value 10 *kA* in full agreement with calculation. Respectable field integrals at the ends will be about 200 times higher, i.e. 6.9 and 3.7 *kG cm*. The integral itself over half period in regular part goes to ~1150 *G cm*. The input into the angle is giving the difference between these two integrals, so the last value can be taken as 5.8 *kG* cm for estimation. The last gives for the beam having energy 100 *GeV* the angle $2 \cdot 10^{-5}$ *rad*. This angle can be reduced by optimal positioning of the sections so that the fields at the end have opposite signs.

In Figs. 32 and 33 the field distributions in central part for two rectangular components are represented. Here the current leads are attached to the double helix. One can see irregularities in field distribution.

Resulting value of the field integral is 2*kG* cm for the operational parameters, which induces the angle $6 \cdot 10^{-6}$ *rad* .

We would like to mention that this irregularity was caused by defect in assembling of central conductor and will be eliminated in the future.

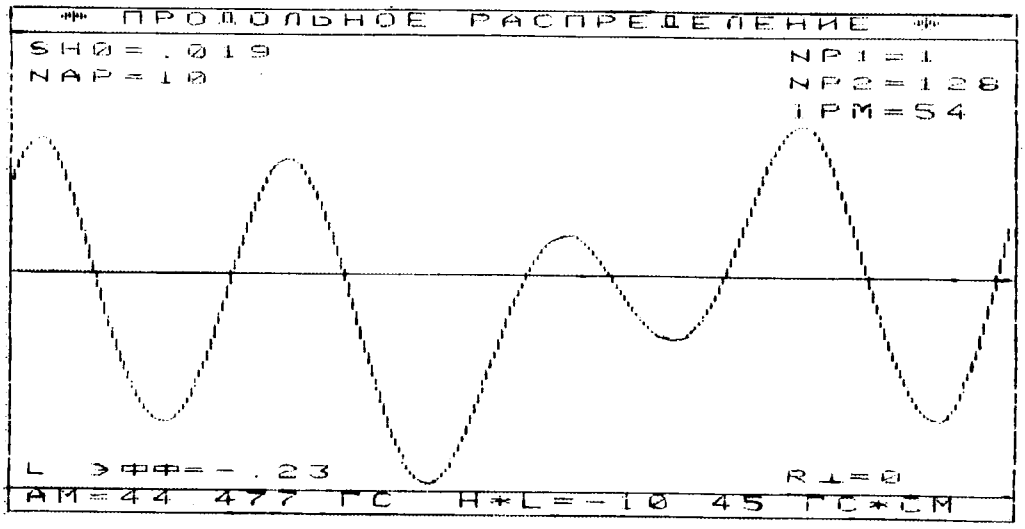

Fig.32. The field distribution in the region of input, $\varphi = 0^o$.

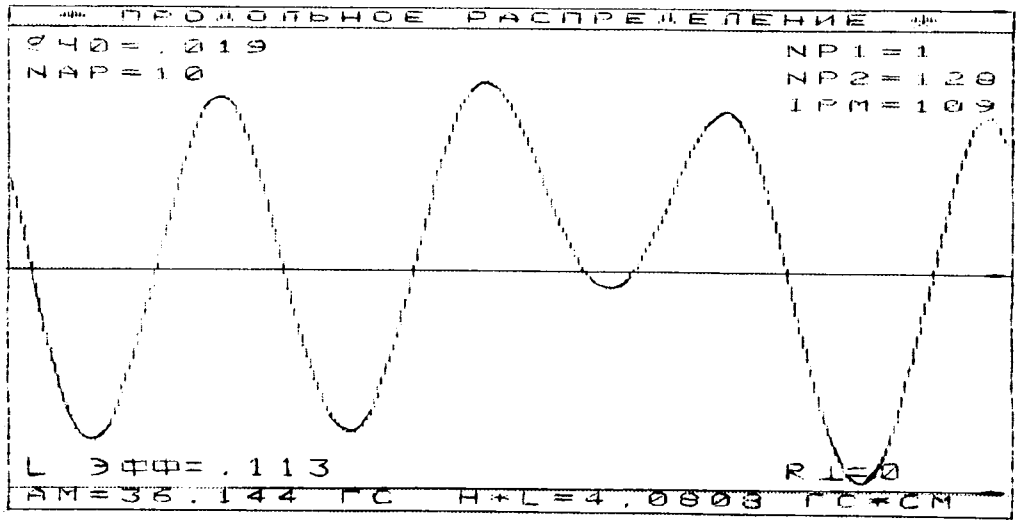

Fig.33. The field distribution in the region of input, $\varphi = 90^o$.

So, by results of measurements the field distribution at the central part we concluded, that design of the undulator is satisfied requirements (the angle $6 \cdot 10^{-6} rad$ is small itself).

Further job was associated with pulsed regime. For the feeding of this undulator thyristor switch was used with resonance charging [26]. Initially the feeding without transformer was used which allowed to reach the current 10 kA with time duration about 35 microseconds, i.e. designed parameters. Further on, for more stable operation the low inductance transformer was installed there.

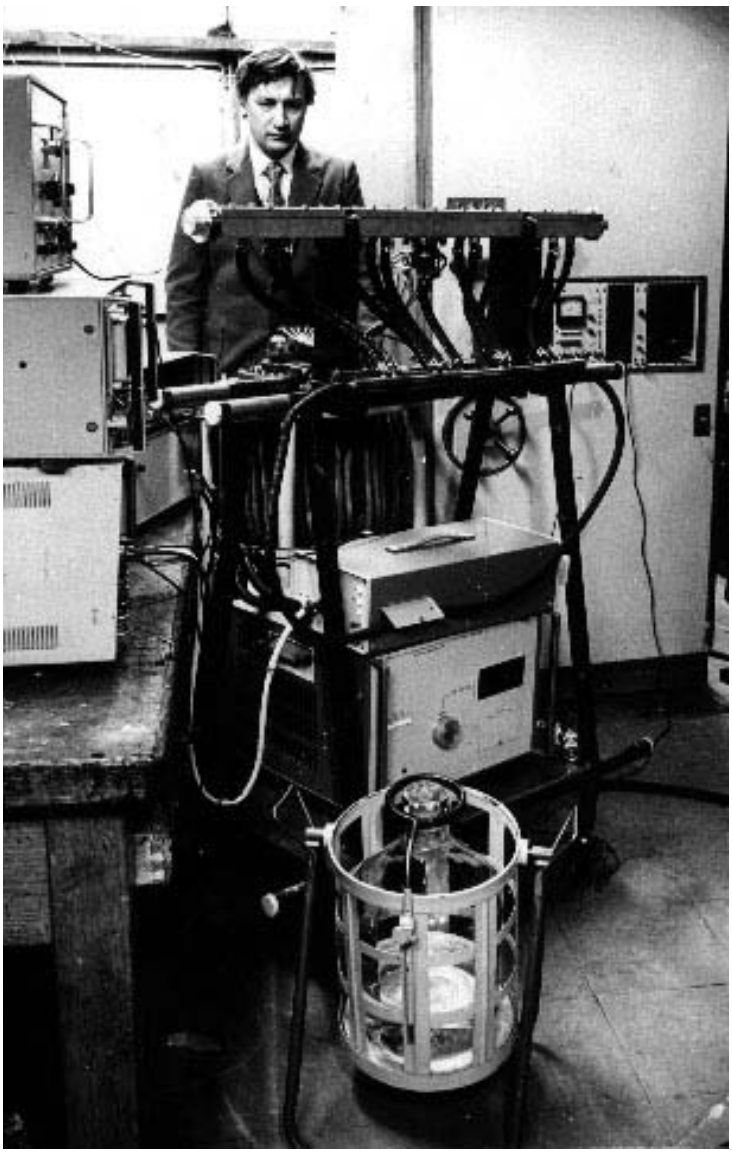

Fig.34. General view of undulator.

Transforming ratio was 5:1. With this transformer the operations were carried with repetition rate up to 25 Hz.

In final variant, one transformer will feed few sections in parallel.

General view of section is represented in Fig. 34. Transformer here can be seen at the second plane. The glass canister with bi-distillate can be see at the front. The generator can be seen here at the right. Number of pulses for test was around 10^5 .

General parameters of undulator are represented below.

Period	0.6 *cm*
Undulatority factor	0.35
Axis field	6100*G*
Current	≤ 10 *kA*
Pulse duration	50 μsec
Average power	1.5 kW/m
Inductance	.3 μH
Voltage	1.19 *kV*
Resistance	0.064 Ohm

As a result of the job fulfilled, we conclude, that pulsed undulator developed absolutely satisfies requirements for operation as a part of conversion system.

§3. General questions associated with design of undulator with superconducting coils.

In parallel to developments of pulsed undulator, the possibility for superconducting undulator was considered too.

One evident advantage of this kind of undulator is that it is not sensitive to repetition rate of operation.

Positive experience obtained while designing helical undulator at VEPP-2M installation [36].

The main concern, associated with the possibility of successful system operation with high intensity of the beam, is that the energy deposition in the walls by primary beam might be significant. The beam itself carries average power ~800 *kW* (for energy 500 *GeV* and repetition rate 10 *Hz*). This power is flowing only few millimeters apart from the cold surface.

The sources of energy deposition might be the following: Undulator radiation on big angles) considered in Chapter 2), Fraction of electron beam in the wings of Gaussian distribution behind few sigmas, and mainly, situation with direct hit by beam the walls. The last will cause the quench inevitably.

Estimations for this effect for undulator having aperture diameter 0.6 *cm*, period λ_0 =1 cm, for the beam with energy 200 *GeV* give the following results.

In Table 9 and in Graph 4, results of energy deposition by wall irradiation are represented for parameters indicated above.

From the Graph one can see, that for the length of undulator 200 m the energy deposition $4 \cdot 10^{-2} J.m$ can be expected at last 50 meters of the length.

For repetition rate 10 *Hz* this will generate 0.4 *W* of full power per meter, which will require the Helium supply ~0.56 *Liter/hour*.

When the illumination will happen under small slippage angle, the quantas will deposit theirs energy at the depth about 1-2 *mm*, i.e. in approximately 100 *g* of material per meter, what in its turn means, that the dose accumulation is about 100 rad/sec. So, the dose allowed for epoxy compounds ($1-3\times10^9$ *Rad*) will be accumulated in 2 years. The screening effect of wire (having 50% of Copper) and difference in specific weight of Copper and compound were taken into account.

Table 9.

ε=200 *GeV*, λ_0=1 *cm*, $\varnothing$=0.6 *cm*.

x, m	25	50	75	100	125	150	175	200
$\vartheta_{\min}\cdot10^5$	12.	6.	4.	3.	2.4	2.	1.7	1.5
$\theta_{\min}$	48.	24.	16.	12.	9.6	8.	6.8	6.
$P_\perp=0.35$	28 $4\cdot10^{-8}$ $1.1\cdot10^{-6}$	56 $2.7\cdot10^{-6}$ $1.5\cdot10^{-4}$	84 $2.\cdot10^{-5}$ $1.67\cdot10^{-3}$	112 $6\cdot10^{-5}$ $6.7\cdot10^{-3}$	140 $1.4\cdot10^{-4}$ $1.91\cdot10^{-2}$	168 $3.2\cdot10^{-4}$ 5.310^{-2}	196 $6.3\cdot10^{-4}$ 0.126	224 $1\cdot10^{-3}$ 0.224
$P_\perp=0.7$	119 $4.2\cdot10^{-8}$ $5\cdot10^{-6}$	238 $2.7\cdot10^{-6}$ $6.4\cdot10^{-4}$	357 $2.\cdot10^{-5}$ $7.1\cdot10^{-3}$	476 $6\cdot10^{-5}$ 0.0028	595 $1.5\cdot10^{-4}$ 0.089	714 $3.3\cdot10^{-4}$ 0.23	833 $6.6\cdot10^{-4}$ 0.55	952 $1.07\cdot10^{-3}$ 1.01
$P_\perp=1.0$	247.2 $4.2\cdot10^{-8}$ $1.2\cdot10^{-5}$	485.5 $2.7\cdot10^{-6}$ 0.0013	728. $2.\cdot10^{-5}$ 0.014	971 $6\cdot10^{-5}$ 0.058	1213 $1.4\cdot10^{-4}$ 0.18	1456 $3.5\cdot10^{-4}$ 0.51	1699 $7.1\cdot10^{-4}$ 1.2	1941.6 $1.16\cdot10^{-3}$ 2.02

In the colons of this Table the full losses are represented for three different undulatority factors together with the fraction of losses and full losses in the walls.

Graph 4.

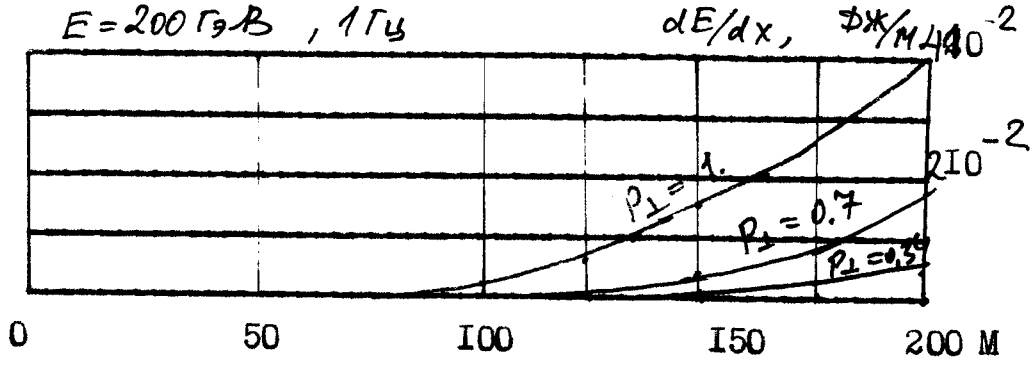

In [4] the factors defining the beam size were considered and the conclusion was made, that the beam with r.m.s. size $2\sqrt{< r^2 >} = 0.4mm$ deposits by its tail extremely small amount of energy. This energy deposition can be mentioned if diameter of aperture less than 4 mm, or when the beam trajectory is shifted from axial, while tuning.

For prevention of direct hits by beam the walls when more radical, especially front collisions happen (which made irreversibly damage the undulator [51]), the careful collimating required at the entrance of system.

For required diameter of collimator 2-3*mm*, the main part of the wing in distribution, will hit the inner surface of collimator, giving significant radiational load and energy deposition into front sections of undulator.

In superconducting variant of undulator, this may yield an increase in Helium losses.

For cut of electrons scattered with large angles, the system of collimators must be installed in few places along undulator.

§4. Undulatior with superconducting coils
A). Design of undulator.

Superconducting undulator has period 10 *mm*, aperture diameter 6 *mm*, radial thickness of windings 5 *mm*, in z direction –3 *mm*.

The windings look like double helix, located in grooves in the yoke, acting for the field profile formation. The number of the turns in the coil came to 15. The wire with 0.7 *mm* in diameter was used here. For improvement of field distribution, the yoke has closed by special halves made from soft steel (see Fig.35). The windings impregnated with epoxy compound filled with Barium Titanate and cured.

The yoke with windings inside represents a core 1, Fig.35, surrounded by these two cylindrical halves inserted into cylindrical tube made from Stainless Steel and fixed there with screw 21, which deforms the tube in specially thinned places without braking its hermiticity. The central core (yoke, two halves and tube) fixed in corps 2 with the help of rods 11, made from Pyrex.

For alignment, the same method was used as described above-deformation of the walls of corps by the screw 24, fixed later by nut 22.

Thermal insulated wrapping 14, made with 25 layers of super insulation surrounds central core. In its turn it is made with Lavsan films covered by Aluminum and thin glass veils.

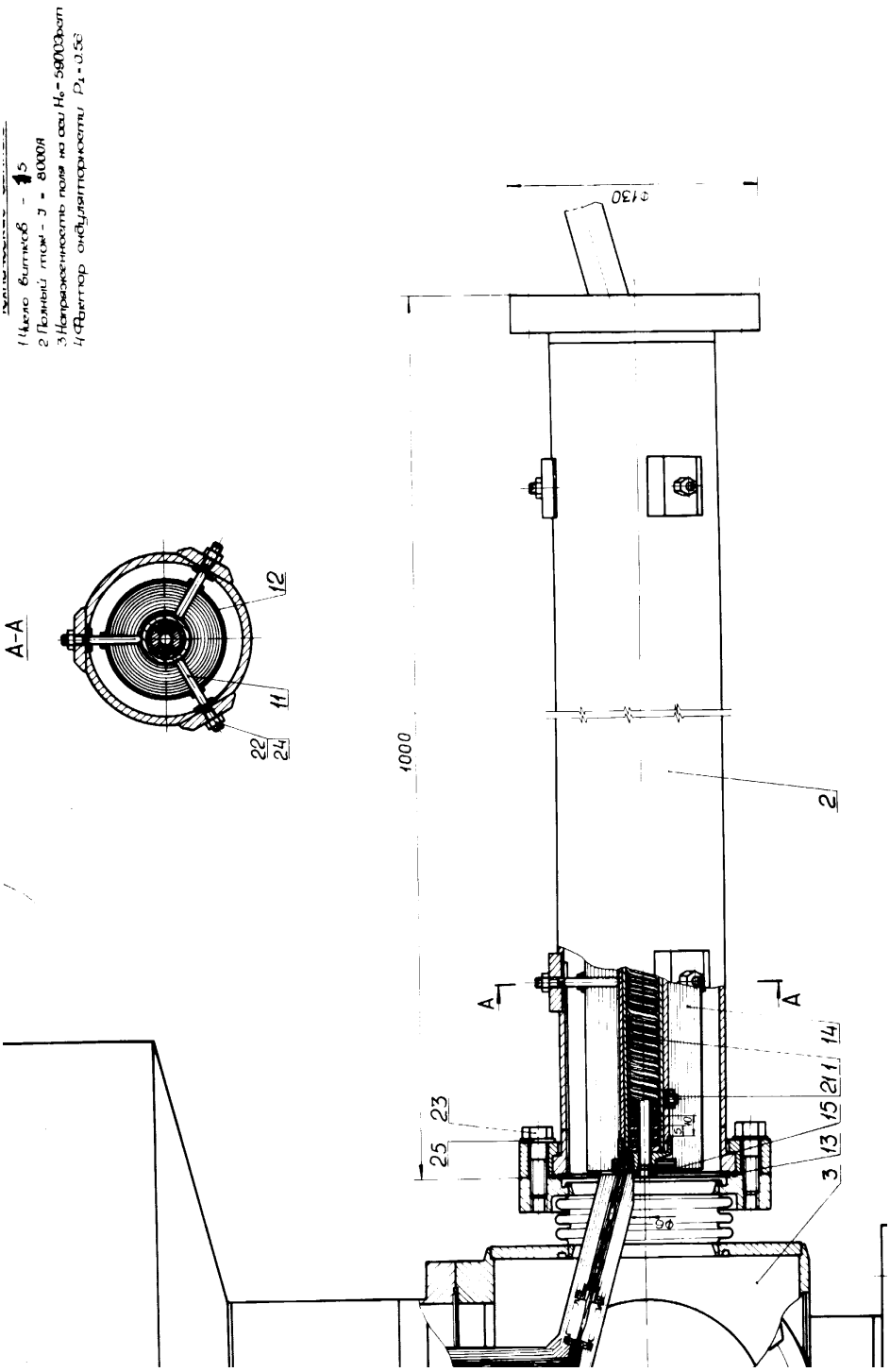

Fig.35. Design of undulator with superconducting coils.

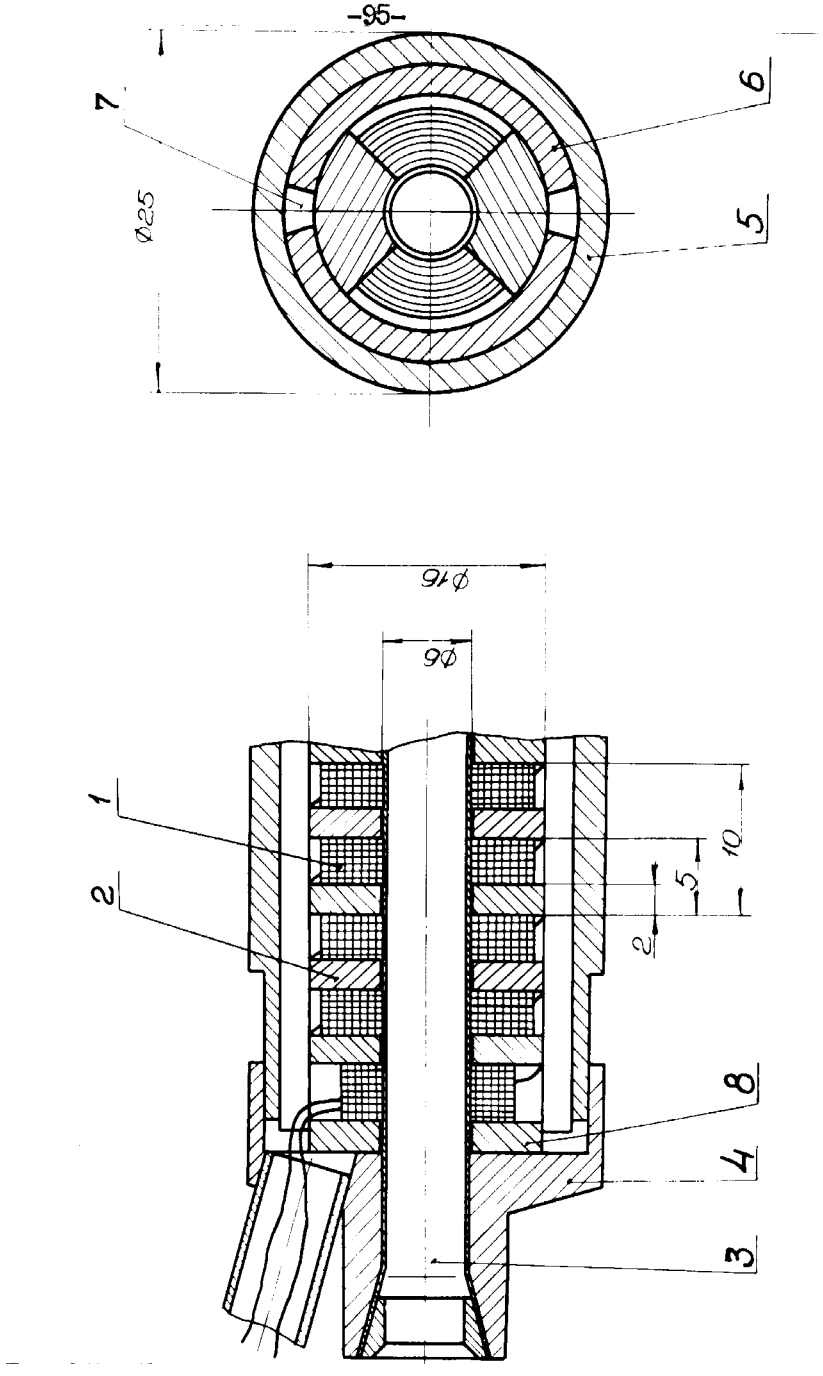

Fig.36. Central core detailed view.

In addition, a thin wall polished Stainless Steel cylinder 12 serves at the same time for fixation of the rods 11.

All sections are joint with pumping stations 3 by stud-bolts and grooves 23, 25 with metallic gasket 13.

Detailed view of core is represented in Fig. 36. In this figure, 1 are the windings, 2 is iron made helical core, 6 is a yoke, 7 is the channels for Helium passage, 5 is cylindrical corps made from Stainless Steel, ended with part 4 and welded to it camera, marked as 3.

Let us mention here the Iron made ring 8, serving for fringe fields elimination (an analog of mirror plate in magnets).

The field dependence as a function of total feeding current is represented in Fig. 37.

As one can see from this figure 37, up to undulatority factor value 0.42 there is no saturation in the yoke. The feeding current at this point is about 200 *A*.

For the total current equal to ~8000 *A* the ratio of the saturated current to the full one goes to 0.38, so the additional current of 4931 *A* adds to the axis field 1405 *G* only.

The field calculations were carried with computer code ONDJ, which was successfully used for calculations for undulator, installed into storage ring VEPP-2M [36].

The points on the graph marked the measured field values (see § 3).

The field between turns at the maximal current goes to 5*T*.

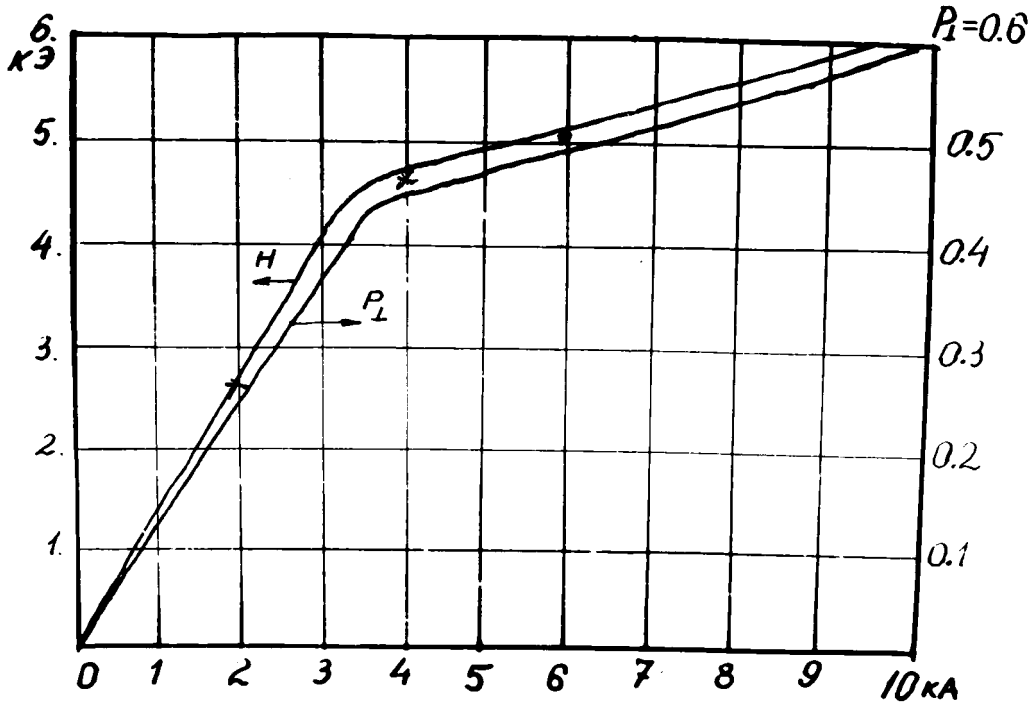

Fig.37. The field dependence at the undulator axis and undulatority factor, as functions of total current in the coil.

Filling with Helium arranged through the heat-insulated thin-wall tubes made from Stainless Steel. The wiring for feeding the coils runs inside. Liquid Helium with gas phase runs along the core in grooves between two halves of yoke and special longitudinal cuts (position 7 in Fig. 36).

Truly perspective the forced pumping with pressurized Helium might be here [38].

The length of each separate section between the flanges is about $1m$. The sections linked into elements by pairs and installed on common frame similarly to how it was done for pulsed undulator (Fig.29).

Compensation of the trajectory kick caused by fringe fields done with the help of azimuthal rotation of neighboring sections in the plane perpendicular to the axis of undulator.

Resistive warm up of the walls by passing beam is small, it can be decreased even more by using intermediate vacuum chamber made from Copper or by copper covering, however.

As the temperature of surface of chamber is equal to the liquid Helium one, electric conductivity of copper cover is two orders of magnitude lower, that it is at room temperature.

Intermediate station having the length 190 mm (Fig.29) between the flanges serves for positioning the pick up electrodes for orbit measurements there and for vacuum pumps serving for initial pumping the channel.

By passing the station, the bunch can radiate into inside cavities. Let us estimate the maximal possible amount of radiation leaven by the bunch there, suggesting the point-like shape of the bunch.

For radiation in all modes by single pass we have as expression [39]

$$W = \frac{l}{4\pi\varepsilon_0}\frac{Q^2}{d}, \qquad Q = eN_0,$$

where *d* stands for diameter of the chamber.
Substitute here values of parameters, one can obtain

$$W = 5\cdot 10^{-3}\ J,$$

and for repetition rate 10 Hz this is ten times higher, $W = 5\cdot 10^{-2}\ J$. In all joints (199 ones) the losses will be ~10 *J/s* or 10*W*. This value can be lowered even more by arranging extensions for the chamber in sections as perforated tubes, similar to how it is done for BEP [3].

So the heating due to radiation into the station is negligible.

B).Vacuum conditions.

The pressure which it is necessary support inside the corps 2 for getting the heat flow to the intermediate shield 12 (Fig.35) at the level of Q [*J*], can be defined from expression

$$Q[W] = k\cdot p\cdot \alpha_1 \times (T_2 - T_1)\times S,$$

where $k=0.016$ (for air), α_1=0.5 accommodation coefficient, which depends on the properties of gas and roughness of the walls. $T_2 = 300\ ^oK$, $T_1 = 4.2\ ^oK$, *S* stands for the area, cm^2. For the walls having radius 2 cm, for given heat flow 0.1W, one can find that the vacuum pressure must be not higher, than $1.7\times 10^{-5}\,Torr$. Obviously it will be not a problem to reach the vacuum better in order of magnitude. During pumping the vacuum chamber from both ends, the value of equilibrium pressure established inside could be calculated by formula

$$P_{av}[Torr] = q \cdot l \cdot \left(\frac{1}{S_{pump}} + \frac{1}{3u_{1/2}} \right),$$

where q [*Liter Torr/cm/ s*] is desorbtion caused by undulator radiation, l =100 *cm* is the length of the vacuum chamber, $S_{pump}[Liter/s]$ is a productivity of the pump, $u_{1/2}$ is a vacuum conductance of the half of the vacuum chamber. Desorbtion q can be calculated as the following

$$q = \frac{\dot{N}_{phot}\eta}{3.3 \times 10^{19}},$$

where $\dot{N}_{phot}$ measured in *Photons/sec*, η is desorbtion coefficient *Mol/photon* or $\beta = \frac{1}{\Phi}$, where Φ stands for quantum yield.

For molecular flow the conductivity of cylindrical tube of round shape can be calculated as the following

$$u_{1/2}[Liter/s] = 38.1 \frac{d^3}{l/2} \sqrt{\frac{T}{\mu}},$$

where $d[m]$ is the tube diameter, $l/2[m]$ is a half of the tube length, T is a temperature, μ stands for molecular mass.
For air

$$u_{1/2}[Liter/s] = 1.21 \cdot 10^5 \frac{d^3}{l/2}.$$

Substitute here values of parameters, one can obtain

$$u_{1/2} = 1.21 \cdot 10^5 \frac{4 \cdot 1.6 \cdot 10^{-9}}{0.5} = 1.5 \cdot 10^{-2} [Liter / s].$$

The quantum yield runs $\Phi \cong 0.1 - 0.2$ *photoelectron/photon* for small angles of illumination.

Taking for estimations $P_{av} = 10^{-6} Torr$, $S_{pump} = 100$ $Liter / s$, one can find

$$q = \frac{10^{-6}}{100 \cdot 0.21} = 5 \cdot 10^{-8}.$$

In its turn

$$5 \cdot 10^{-8} = \frac{\dot{N}_{phot}}{3.31 \cdot 10^{19}}.$$

For the number of photons (10 *Hz*)

$$28.3 \cdot 10^{12} \cdot 10 = 2.8 \cdot 10^{12} \cdot 10 = 2.8 \cdot 10^{14} \text{ photons/sec.}$$

Finally we can obtain the value of desorbtion coefficient required

$$\eta = 5.9 \cdot 10^{-3} \ Mol / photon,$$

and

$$\beta = \frac{5.9}{0.1} \cdot 10^{-3} = 5.9 \cdot 10^{-2} \frac{Mol}{photon / electron},$$

it will be no problem to reach this value (for BEP is planned to have $\eta = 2 \cdot 10^{-6}$ *Mol/electron*) [30].
For calculation of heat exchange between walls of corps 2 and wall 12 (Fig.35) one can write

$$\frac{Q}{S_1} = \frac{\sigma \cdot \left(T_2^4 - T_1^4\right)}{\frac{1}{\varepsilon_1} + \left(\frac{1}{\varepsilon_2} - 1\right) \cdot \frac{S_1}{S_2}} = \sigma \bar{\varepsilon} \cdot \left(T_2^4 - T_1^4\right),$$

where $\bar{\varepsilon} = \frac{1}{\frac{1}{\varepsilon_1} + \left(\frac{1}{\varepsilon_2} - 1\right) \cdot \frac{S_1}{S_2}}$ is effective coefficient of blackness, $\frac{S_1}{S_2} \cong 1$ stands for ratio of the areas of inner wall of corps and the intermediate shield. Taking as example $\varepsilon_1 = \varepsilon_2 = 0.025$ (polished Stainless Steel) one can obtain

$$\frac{1}{\bar{\varepsilon}} \cong \frac{1}{\varepsilon_1} + \frac{1}{\varepsilon_2} \approx 80.$$

and, sequentially, Q=1.4 W.
This flow can be reduced by system of multi layer screens [46], 14 to the level 0.06 W (25 layers).

The heat flow over pivots can be calculated by the following formula [46]

$$Q[W] = \bar{\lambda}\left[\frac{W}{cm \cdot \deg}\right] \cdot S[cm^2] \cdot \frac{\Delta T}{l[cm]},$$

where λ stands for the heat conductance coefficient, $\lambda \cong 1.1 \cdot 10^{-2} \frac{W}{cm \cdot \deg}$, and for the dimensions and material chosen (Pyrex pivot with 4mm in diameter, having length 37 *mm*), this flow goes to 11 *mW*, what gives for all six supporting pivots 0.07 W.
So the sum power of heat losses goes to from 0.4 to 0.5 *W*, which in its turn will require the Helium flow ~0.7 *Liter/hour* per one meter. For all 100 meters the Helium losses goes to 70 *Liters/hour*. The Helium losses caused by current leads can be estimated as 0.7 *Liter/hour* for 250 *A*.

So, the full amount of heat losses together with uncounted, which supposed to be in 30% margins, goes to ~100 *Liters/hour* or 2400 *Liters/per 24 hours*. For generation of such amounts of Helium it is necessary to build a special cryo-plant.

As it was mentioned above, it is a rational arrangement of Helium supply for few sections connected in series. By this way the cost of watt of losses becomes lowered drastically.

In this case the refrigerators are used here, what drastically reduces the amount of Helium required for operation.

Possible quenches caused by direct hit by primary beam is included in this 30% as the full energy stored in 1 meter long section of undulator is low and comes to 100 Joules.

The energy what shower deposits into one meter long section comes to 1.1-0.1 *J/m* on the distance 60-100 meters for beam population 10^{12}, incoming angle ~10^{-4} and primary beam energy 100 *GeV*.

Without developing a shower and multi scattering, the beam could pass about 5 meters depositing in Copper and Iron about 600 J, i.e. 600/5=120 *J/m* [51]. The losses of Helium is 0.4 *L/kJ*.

We would like to attract attention that this design does not contain of Nitrogen shields of any kind as the main heat losses associated with the beam radiation.

C). Thermal relaxations of construction.

For calculation the cooling time and parameters, characterizing transition processes, let us use the equations of heat transfer. For the part of cold mass having the length Δz one can write

$$\frac{\Delta Q}{\Delta t} = \alpha_T \cdot S \cdot \left(T_C(z,t) - T_H(z,t)\right),$$

where α_T stands for heat transferring coefficient, $\alpha = \frac{4S_\perp}{\mathrm{P}}$ is so called

hydraulic parameter (P is perimeter of the channel , $S_{\perp}$ cross section area, T_C is the temperature of the core T_H stands for temperature of Helium.

The temperature change in Helium and in core can be expressed as

$$\Delta T_H = \frac{\Delta Q}{\Delta m c_p}, \quad \Delta T_C = \frac{\Delta Q}{\Delta M_C c_C}$$

respectively. Here $\Delta m = \dot{m}\Delta T$, $\dot{m}$ defined by Helium losses, $\Delta M_C = M' \cdot \Delta z$, $c_p(T_H)$ and $c_C(T_C)$ are heat capacity of Helium and core respectively. As a result for temperature change of Helium and the core can be described by equations [41]

$$\frac{\partial T_H}{\partial z} = \frac{\alpha_T \pi d}{\dot{m} c_p}\left(T_C(z,t) - T_H(z,t)\right)$$

$$\frac{\partial T_C}{\partial z} = -\frac{\alpha_T \pi d}{M' c_C}\left(T_C(z,t) - T_H(z,t)\right).$$

So parameters $\tilde{\kappa} = \frac{\dot{m} c_p}{\alpha_T \pi d}$ and $\tau_r = \frac{M' c_C}{\alpha_T \pi d}$ introduced define characteristic length and time respectively.

For turbulent flow α_T defined from the following relations

$$\alpha_T = \frac{Nu \lambda_T}{d}, \quad Nu = 0.023 \cdot \mathrm{Re}^{0.8}\,\mathrm{Pr}^{0.48}.$$

For laminar flow

$$Nu = 1.68 \cdot \left(\mathrm{Re}^{0.33}\frac{d}{l}\right)^{0.33}$$

where Nu stands for Nusselt number, $\mathrm{Re} = \frac{\rho v d}{\eta}$ is a Reynolds number, $\mathrm{Pr} = \frac{\eta C_p}{\lambda_T}$ is a Prandtl number, λ_T is a heat conductivity, η is viscosity of Helium. For boiling Helium Pr=0.59, $\mathrm{Re}=3.5\cdot 10^3$, $\eta = 3.56\cdot 10^{-5}\frac{g}{cm\cdot s}$, $\lambda_T = 2.71\cdot 10^{-4}\frac{W}{cm^o K}$ (under the pressure 0.4 MN/m^2 the same parameters become Pr=0.28, $\mathrm{Re}=4\cdot 10^3$, $\eta = 4.5\cdot 10^{-5}\frac{g}{cm\cdot s}$, $\lambda_T = 3.5\cdot 10^{-4}\frac{W}{cm^o K}$).

The equivalent diameter for this shape of core is 0.2*cm*. The Reynolds number goes in our case to

$$\mathrm{Re}=4\cdot 10^{-3}$$

So the flow, according to Reynolds criteria is turbulent.

$$\text{For } \alpha_T \text{ we have } \alpha_T = 1.75\cdot 10^{-3}\frac{W}{cm^o K}$$

and for characteristic parameters we obtain, taking into account, that the mass is about 2.4*kg,*

$$\tau_r \cong 22.4\ s$$
$$\tilde{\kappa}^{-1} \cong 10\ cm,$$

i.e. this construction relaxing pretty fast.

For protection of the coil against quenches, the well-known techniques can be used here (external resistor, thyristor keys [44]).

Power supply design and fabrication for 400 feeding current with

necessary stability 10^{-3} will be not a problem. In a future the operation with capture flux is suggested. The feeding in this case is going with the help of superconducting transformer. In this case the losses associated with feed through current leads are eliminated.

Fig.38. General view to the equipment under preparation for test of superconducting undulator.

For testing of technology and methods of exploitation, central part of undulator (see Fig. 33) having the length of 300 *mm*, was fabricated.

The helix of the yoke was turned out from solid rod made from soft steel Armco on lathe.

By requirements of technology two helixes were turned by time. After the helixes were turned, the central part was drilled off. The length of each part was 100 *mm*. Further on this yoke was mounted on the thin-wall Stainless Steel tube having diameter 6*mm*. This tube serves as a vacuum chamber.

The yoke was fixed on this tube by soldering in numbered places with soft Tin alloy. Separate parts of the yoke were trimmed so the resulting helix-yoke became practically homogeneous. The tube wall thickness runs on 0.2 *mm*.

The mostly difficult part in winding was associated with turning back the wire at the end of the undulator. To make this operation successful it was necessary to cure each layer in specially designed fixtures, which were removed after curing.

For monolithing, in regular parts and at the ends the filler as Barium Titillate was used here.

As a result of difficulties described above, the number of turns which could be positioned in the grooves were 15 instead of 18, what yield proportional increase in the feeding current.

The winding was done in five layers having three turns in each one. Each layer was cured one by one; the glass tape impregnated by epoxy separated the layers.

After curing of each layer, the places were cleaned and the layer was wounded. As a result the filling coefficient came to ~50%.

In Fig.39 the view of central part is represented in detail.

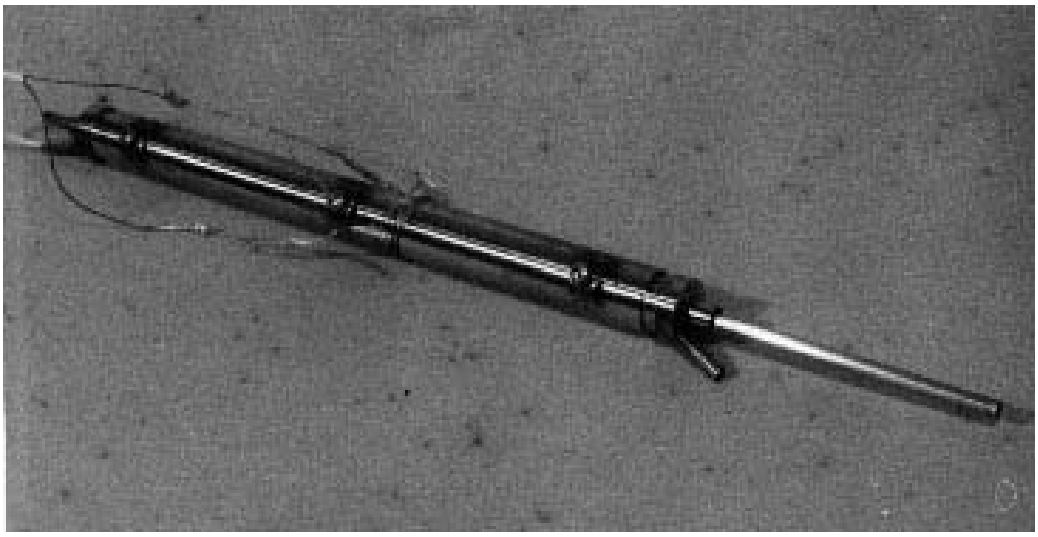

Fig.39. View on central part of superconducting undulator.

D). Results of testing.

Tests of section fabricated were carried in a Dewar. In Fig.38, the moment of tuning the mechanism for Hall probe motion is shown. With the help of this Hall probe the field distribution was measured in liquid Helium. Similar to the warm undulator it was measured the longitudinal field distribution. Based on these measurements, spectral components of longitudinal harmonics were identified together with accounting the fringe fields.

Section was powered from high current power supply with thyristor's switched rectifier with manual level control. The current was controlled with the help of shunt with the readings done with digital voltmeter.

The Hall probe was carried by shaft, made from Stainless Steel and sealed hermetically at the flange end for prevention of gaseous Helium escape from Dewar here. The Hall probe was located at the end of tube-like stock. The four wires from the probe were running inside this stock. The wall thickness was about 0.2 *mm*, the length was~1200 *mm*, diameter—5 *mm*.

Measurements of longitudinal field distribution along the axis of undulator confirmed result of calculation in full.

The axis field reached 5000 *G* with feeding current in single wire 400 *A*, i.e. with total current 6000 *kA*.

Spectral analyzes showed, that the second harmonics in longitudinal distribution is about 1.1% from the first one, the third one is 0.23% only, the rest have negligible amplitudes.

The measurements were carried with the current running in single wire 200 *A* ($P_{\perp}$=0.4).

The integral of the field along all length was measured also. Results of these measurements are represented in Table 10.

Table 10.

Current per turn, A	$\int, G \cdot cm$
100.	130.
200.	260.
250.	330.
260.	280.
280.	150.
300.	60.

One can see from this Table, that while the iron becomes more saturated, the field integral value is lowering down. This caused, more likely by lowering input from the end commutation.

Let us mention here, that the current was limited by 400 A, and the measurements were not carried there as the current leads became overheated. So that is why the integral was not measured here also

E). Electric supply with superconducting transformer.

Later on, a transformer with superconducting coils was manufactured for the purposes of work with captured flux. The primary coil has 150 turns of superconducting wire of 0.7 *mm* in diameter, the secondary was a single turn one with the wire 0.7 *mm* also. The windings were made from Aluminum made carcass having longitudinal cut. The windings impregnated by epoxy filled by a mixture of Aluminum oxide and cured to monolith.

Inside the carcass there is a yoke having cross section of 15×40 square millimeters.

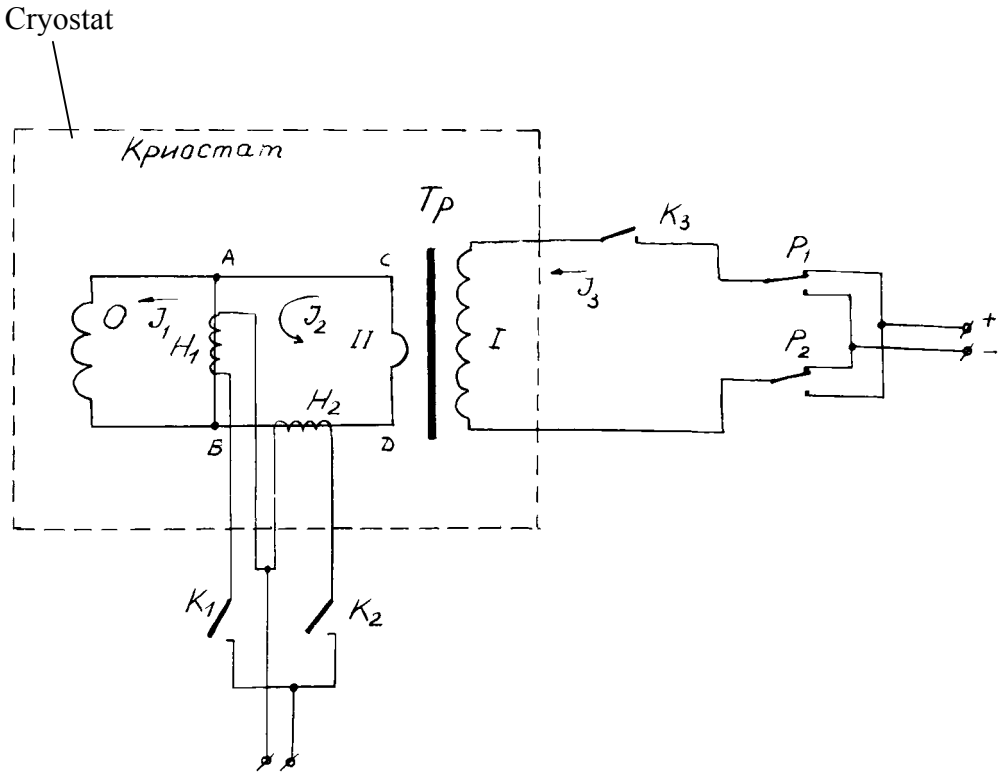

Fig.40. Scheme of feeding the section with the help of superconducting transformer.

For feeding, the scheme represented in Fig. 40 was used [43]. Computer “Odrenok” type with the help of special code operated the switches.

The scheme represented in Fig.40 operates as the following.

When the switch K2 closed the heating of element in region H2 starts. This yields the loss of superconductivity. After that the contact K3 forced to be closed and the power supply through contacts of relay P1 and P2 (with the help of these contacts the polarity can be changed) excites the flux in contour I of transformer (current J3). After that the contact K2 opens and contour ABCD becomes a superconducting one. After that the contact K3 opens what creates the current J2 in secondary contour 9the input in current J1 still small as the difference in the inductance value between undulator and contour ABCD). After the contact K1 became closed, the superconductivity at the region AB is broken and the flux captured increases the current I. Again the contact K1 becomes open, contact K2 –closed and so on.

For fabrication of superconducting switches (regions H2 and AB) the copper matrix was removed with the help of acid at the distance ~ 12 *mm*. Above this region without Copper, the heating made from Constantine wire with 0.15 *mm* in diameter was wrapped around. The DC resistance was found to be ~5Ohm.

The time during which the heater was turned on could be changed by code remotely. The peak power could reach ~2 W and was tuned for fixed operating time around minimal possible, which triggered the quenching. For the optimal time of heating the single circle of flux feeding took ~ 1 second.

At initial stage the magnetic field, measured by special command, gained in its value ~ 100 *G* with the primary current from the power supply 5A. I.e. the current grow was numerically the same 5A per single circle.

Some discrepancy in the ratio of currents calculated with given transformation ratio can be explained by the stray flux in transformer.

In regime with captured flux, the decay time for the field was about 4 hours.

It was possible to reach the axis field here 3300 *G*. Further field grows was limited by stray field for selected power supply.

No doubt, that in future the systems with superconducting transformers can be used successfully.

Let us represent main parameters of superconducting undulator

Period ……. 1.0*cm*

Undulatority factor ……. 0.35

Axis field …… 3710 *G*

Current …… 2800 *A* (/15)

Helium losses ……. 0.7 *Liters/hour/m*

So as a result of testing of superconducting undulator in is possible conclude, that it has suitable design for satisfactory operation in the second stage of VLEPP installations, when the background conditions caused by imperfect aim at IP will became more clear and when high repetition rate will be required.

CONCLUSION

In conclusion let us represent general parameters which characterize conversion system.

Beam energy …….	150-200 *GeV*
Bunch population……...	10^{12}
Period of undulator……	0.6-1 *cm*
Undulatority factor ……	0.35
Length of undulator ……...	150 *m*
Number of quantas per particle …..……...	10-20
Energy of quanta ……	25-35
Thickness of the target ……...	0.3-0.5 X_0
Average polarization ……..	0.65
Conversion efficiency …….……...	≥ 1

Let us summarize in brief main results of the job done.

1. Proposed principally new type of conversion system for obtaining polarized e^+ and e^-, using undulator radiation from particles after interaction.
2. It was shown that conversion efficiency could be not less, than unity with degree of polarization 60% in the energy range 100-500 *GeV*.
3. Considered design of undulators, satisfying the undulatority factor required with minimal period. In particular, designed fabricated and tested model of pulsed undulator with period 6 *mm*, field at the axis 6000 *G* with repetition rate 10 *Hz*.

4. It was shown that it is possible to use an undulator with superconducting wiring when the energy is higher than 200 GeV.
5. Manufactured and tested in practice an undulator with superconducting wiring.
6. It was shown that conversion system is closed for spin motion for all VLEPP installation.

Main results of the job were represented at the session of International Committee for Future Accelerators (ICFA) CERN, Geneva; at VII All Union Conference on Accelerators (Dubna, 1980); at International Symposium on Polarized phenomena in nuclear Physics (Dubna, 1981); at XIII International Conference on Charged particles Accelerators (Batavia, USA); at XIII International Conference on Charged particles Accelerators (Novosibirsk, 1986) and published in [8, 26, 32, 53, 54].

Taking a chance, I express my thanks to V.E.Balakin, with whom the conversion system was proposed and G.I.Sil'vestrov for Scientific supervision of the job; to T.A.Vsevolojskaja from who Author learn much. Thanks to E.A. Perevedentsev from all my hart for permission to use his codes.

My special thanks to Yu.M.Shatunov for his support; the job could not be completed without this support; to L.M.Shegolev for designing developments; to M.A.Timoshenkov and N.I. Chuprikov for theirs job on assembling of undulators. My sincere thanks to A.D. Cherniakin for his developments of pulsed generator and joint work while testing pulsed undulator. A lot of new things Author learned from talks with G.A. Blinov and C.V. Sukhanov. To them and to all other members of Cryogenic Group Author brings his thanks.

LITERATURE.

[1] Plans for Polarized Beams at SLC, Charles Prescott, Slac-PUB-3728, July 1985.

[2] H.Frischoltz, Generation and distribution of Radio frequency Power in LEP, CERN-LEP/RF/85-18.

[3] SLC Design Handbook, December 1984.

[4] VLEPP, Physical foundation, INP, 1982.

[5] E.L. Garwin, R.E. Kibry, C.K. Simclair, et al., Oxide effects on Photoemission from high Current GaAs photocathodes, Vacuum, 1981, vol.31, pp.553-556.

[6] D. Perkins, *Introduction into High Energy Physics*, translated from English, ed. by Yu.A. Budanov, Mir, Moscow, 1975.

[7] V.E.Balakin, G.I. Budker, A.N. Skrinsky, *On the possibility to create a Super High Energy Electron Positron Colliding Beams Installation*, G.I.Budker Selected woks, Nauka, M., 1982. p. 419.

[8] V.E.Balakin, A.A. Mikhailichenko, *The Conversion System for Obtaining highly polarized Electrons and Positrons*, Preprint INP79-85, September 1979.

[9] D.F. Alferov, et al., *The Undulator as a Source of Electromagnetic Radiation*, Part. Acc. 1979, vol.9, pp. 223-236.

[10] V.N. Bayer, V.N.Katkov, V.S. Fadin, *Radiation of Relativistic Electrons*, AtomIzdat, M., 1973.

[11] V.M. Aul'chenko et al., Proceedings of V International simp. On High Energy Physics, Warsaw, 1975; Selected Works of G.I. Budker, p. 539.

[12] V.B. Besrestetsky, E.M. Lifshits L.P.Pitaevsky, *Quantum Electrodynamics,* M., Nauka, 1980.

[13] A.I. Akhiezer,V.B. Besrestetsky, *Quantum Electrodynamics,* M., Nauka, 1969.

[14] L.M. Kurdadze, et al., Radiation Polarization of the Beams in the VEPP-2M storage ring, pr. INP 75-66, Novosibirsk, 1975.

[15] A.D. Bukin, *The Method of Absolute calibration of Energy of the Beams in the storage ring, the measurements of φ meson mass*, pr. INP 75-64, Novosibirsk, 1975.

[16] F. Bulos, H.de Staebler et al., *Design of a High Yield Positron Source,* Part. Acc. Conf. Vancouver, B.C. Canada, May 13-16 1985.

[17] A.V. Novokhatsky, *the Beam dynamics in a Linear Collider VLEPP*, Dissertation, Novosibirsk, INP, 1985.

[18] V.E. Balakin, A.A. Mikhailichenko et al., *Test of acceleration section of the VLEPP,* Proc. Of VIII All Union Conference on Charged Particle Accelerators, vol. 2, p.410, Dubna, 1983.

[19] A.A. Sokolov, I.I. Ternov, JETF. 698 (1953).

[20] G.I. Silvestrov, *The problems in obtaining of Intense beams of Secondary particles,* a talk on XIII International conference on high Energy Accelerators, Novosibirsk, 1986.

[21] F. Netter, L' accélérateur Linéare èlectrons SACLAY, agrand cycle utile et forte intensite, B.I.S.T. Commisariat à Energie Atomic N 179, Mars 1973.

[22] B.V. Bayanov, T.A. Vsevolojskaya, G.I.Silvestrov, *Investigation of Mechanical Stress and design of Cylindrical Lithium Lenses*, preprint INP 84-168, 1984.

[23] G.I. Budker, Selected Works, Nauka, M., p. 387.

[24] B.V. Bayanov, G.I.Budker et al., Proceedings of X International Conference on High Energy Charged Particles, Protvino, 1977, Serpukhov, 1977, vol. 2, p. 103.

[25] V.V. Anashin, A.A. Mikhailichenko, et al., injector Prototype for VLEPP, a Talk on XII International Conf on High Energy Accelerators, Novosibirsk, INP, 1986.

[26] T.A. Vsevolojskaja, A.A. Mikhailichenko, E.A.Perevedentsev, G.I.Silvestrov, A.D. Cherniakin, *Helical Undulator for the*

VLEPP conversion System, a Talk on XII International Conf. On high Energy Accelerators, Novosibirsk, INP, 1986.

[27] Second ICFA Workshop, 4-10 October 10979, CERN, Geneva.

[28] N.G. Afanasiev et al., *the System for Energy Compression on LUE-300,* Proc. Of VIII All Union Conference on Accelerators, vol. 2, Dubna, 1983.

[29] V.E.Balakin, N.A. Soliak, *Effects of Collision on VLEPP*, preprint INP 82-123, Novosibirsk 1982.

[30] V.V.Anashin, A.A. Mikhailichenko et al., *Electron-Positron Storage ring BEP*, Preprint INP 84-114, Novosibirsk 1984.

[31] A.M. kondratenko, *polarized beams in Storage Rings and Cyclic Accelerators*, Dissertation on Doctor of Ph.-M. Science Degree, Novosibirsk, 1982.

[32] V.E. Balakin, A.A. Mikhailichenko, *Conversion System for obtaining Polarized Electrons and Positrons*, a Talk on International Symposium on polarized Phenomena in Nuclear Physics, Dubna, 1980.

[33] V.N. Bayer, V.M. Katkov, V.S. Fadin, JETF, 63, 2121, 1972.

[34] H. Buchhotz, *Electrische und Magnetische Potentiafelder*, Springer-Verlag, 1957.

[35] G.S. Piskunov, Distributed Control System for VEPP-4 Installation, Dissertation, novosibirsk, INP, 1985.

[36] V.V. Anashin et al., *Superconducting Helical Undulator for measurement of radiational Polarization of Colliding Beams at VEPP-2M installation*, Preprint INP 84-111, 1984.

[37] A.I. Vorob'ev, *Precision measurements of masses of ρ and ω Mesons,* Dissertation, INP Novosibirsl, 1986.

[38] M. Uilson, *Superconducting Magnets,* Trans. from English, ed. A.I. Pipko, Mir, M., 1985.

[39] O.A. Kolpakov, V.I. Kotov, JTF, vol. XXXIV, ser. 8, p. 1387, 1965.

[40] A.I. Pipko, *The Vacuum Techniques Foundation,* Energoizdat, M., 1981.

[41] H. Lierl, P.Shmüser, *Cooldown of a HERA Octant Equipped cold Dipoles,* DESY, HERA, 84/16, 1984.

[42] C. Bovet et al., *Polarization of Beams in LEP*, CERN/LEP-BI/85-17, 1985.

[43] Laquer, *Cryogéniques,* 1963, vol. 3, № 1,p. 27.

[44] K. Koepke et al., IEEE Trans. on Magnets, MAG-15, 658(1979).

[45] G. Knopfel, *Superstrong Pulsed Magnetic Fields,* trans. from English, ed. by B.I. Samsonova, Mir, M., 1972.

[46] G. Brechna, *Superconducting Systems*, trans. from English, ed. by V.P. Karasik, Mir, M., 1976.

[47] V.I. Alexeev, E.G.Bessonov, *On the ways of generation ...,*Proc. SR-84, Novosibirsk, 1985, p. 92.

[48] O.I. Dovjenko, A.A. Pomansky, JETF, 45, 268(1963).

[49] A.D. Cherniakin et al., *Development of the Conversion System for VLEPP project*, Proc XII Int. Conf. On High Energy Acc., Batavia, USA, 1983, 0.131.

[50] E.G. Bessonov, Proc. FIAN, 105, 1985.

[51] A.D. Bukin, *a private communication*.

[52] D.F.Alferov, E.G. Bessonov, Yu.A. Bashmakov, B.B. Govorkov, YaF, 27, 971(1978).

[53] V.E.Balakin, A.A. Mikhailichenko, *Conversion system for obtaining Polarized Positrons and Electrons,* a Talk on VII All Union Conference on Charged Particle Accelerators, Dubna, 1980.

[54] V.E.Balakin, A.A. Mikhailichenko, *VLEPP, The Conversion system,* XII Int. Conference on High Energy Accelerators, Batavia, USA, 1983.

[55] *The Sources of Polarized Electrons (Review of Contemporary Methods)*, Review/V.L. Agranovich et al., CNIIAtomInform. 1984.

[56] A.A. Polunin, Yu.M. Shatunov, *Spin Flip of Particles in a Storage Ring by a high Frequency Electromagnetic Field,* Preprint INP 82-16, 1982.

[57] D.F. Alferov et al., Proceedings of VIII All Union Conference on the Physics of Interaction of Charged Particles with Monocrystalls, Moscow, MGU, 1976, p. 65.

[58] Ugo Amaldi, *Colliding Linacs,*CERN –EP/79-136, November 6, 1979, 13 pp. In 9th Int. Symposium on Lepton and Proton interaction at High Energies-Lepton-Photon Symposium, Fermilab, Batavia, IL, USA, 23-29Aug. 1979, Proc. pp. 314-32.